MODELING OF POLYMER-BASED SELF-COMPACTING CONCRETE USING RHEOLOGICAL INDEXING

BY

NAEEM SOHAIL SALEEM SALEEM

A Dissertation Presented to the

DEANSHIP OF GRADUATE STUDIES

KING FAHD UNIVERSITY OF PETROLEUM & MINERALS

DHAHRAN, SAUDI ARABIA

In Partial Fulfillment of the

Requirements for the Degree of

DOCTOR OF PHILOSOPHY

In

CIVIL ENGINEERING

DECEMBER 2014

KING FAHD UNIVERSITY OF PETROLEUM & MINERALS

DHAHRAN- 31261, SAUDI ARABIA

DEANSHIP OF GRADUATE STUDIES

This thesis, written by **Naeem Sohail Saleem Saleem** under the direction of his thesis advisor and approved by his thesis committee, has been presented and accepted by the Dean of Graduate Studies, in partial fulfillment of the requirements for the degree of **DOCTOR OF PHILOSOPHY IN CIVIL ENGINEERING.**

Prof. Mohammed H. Baluch
(Advisor)

Dr. Omar Abdullah Al-Swailem
Department Chairman (A)

Dr. Muhammad K. Rahman
(Co-Advisor)

Prof. Salam A. Zummo
Dean of Graduate Studies

Prof. Shamsad Ahmad
(Member)

19/5/15
Date

Dr. Ali H. Al-Gadhib
(Member)

Dr. Salah U. Al-Dulaijan
(Member)

Dedicated to

My Beloved Late Father, Mother, Wife, Sisters, Brothers and My son Omar

May Almighty ALLAH Bless Them All

ACKNOWLEDGMENTS

All praises and thanks to Almighty Allah (SWT), the Most Gracious, the Most Merciful, who gave me the knowledge, courage and patience to accomplish this research. May the peace and blessings of Allah be upon Prophet Muhammad (PBUH).

I acknowledge, with deep gratitude and appreciation, the inspiration, encouragement and guidance given to me by Prof. M.H.Baluch, who served as my thesis advisor. This work was completed due to his guidance and personal involvement in both the experimental and the numerical components of this thesis. I am deeply indebted and grateful to Dr. Mohammed Kalimur Rahman, my co-advisor who did not stop helping me since the day I joined KFUPM and for his personal involvement in all phases of this research, Dr. Mohammed Al-Osta, Dr. Shamsad Ahmad, Dr. Ali Gadhib and Dr. Salah Al-Dulaijan for their extensive guidance and continuous support. Their valuable suggestions and useful discussions made this work interesting and satisfying for me. I would have never accomplished this work without their valuable suggestions and support.

Acknowledgement is due to King Fahd University of Petroleum & Minerals represented by the Department of Civil and Environmental Engineering and the Deanship of Scientific Research (Project IN101036), for the support and the excellent facilities given for this research, and for granting me the opportunity to pursue my graduate studies with financial support.

I highly acknowledge the help of Saudi Ready Mix Concrete Company and Prainsa Precast Company for their amazing support during all the experimental tests.

TABLE OF CONTENTS

LIST OF TABLES

LIST OF FIGURES

ABSTRACT

Full Name : [Naeem Sohail Saleem Saleem]

Thesis Title : [Modeling of Polymer-Based Self-Compacting Concrete Using Rheological Indexing]

Major Field : [Civil Engineering]

Date of Degree : [December 2014]

This work was targeted to experimentally investigate and numerically model the behavior of self-compacting concrete (SCC) using rheological indexing. Two major areas were investigated, which includes lateral pressure exerted by SCC on formwork and pumping aspects of SCC. Influence of yield stress, viscosity and thixotropy on the rheological behavior of SCC were also studied.

Four mixes with different mineral admixtures, fly ash (SCC – FA), silica fume (SCC – SF), ground granulated blast furnace slag (SCC - GGBFS) and the control mix (SCC – C) were used with a water-cement ratio of 0.35. The lateral pressure exerted by SCC mixes were experimentally investigated by pouring the concrete in a steel formwork of a 3.1 m height, 3 m in length and 200 mm thickness. The variation of pressure across the height was measured using pressure transducers at different heights and the evolution of pressure on the formwork was measured for 12 hours. Rheological parameters including the yield stress, relative viscosity, and thixotropy were obtained for each mix at the time of measurement. A finite element model for the prediction of the lateral pressure exerted by SCC was correlated to the experimental data was also used to simulated experimental data as reported elsewhere using ANSYS.

The pressure variation during pumping of SCC was also experimentally investigated. Two arrangements of pipes were studied, one with a total length of 60 m including 13 bends and another one of 22 m including 2 bends. Three mixtures with different mineral admixtures were studied in each arrangement, SCC – C, SCC – FA and SCC – SF. Pressure sensors were placed on different locations along the pipeline, pressure readings were taken every 2 seconds for a period of 10 minutes. Pressure drop per linear meter and the pressure drop due to bends were found and correlated to the viscosity and yield stress values. A constituve model for the prediction of pressure drop using the values of viscosity and yield stress was developed. The pressure variation along the pipeline was also compared to a finite element model using ABAQUS/CFD.Derivation of the equation of velocity of concrete while pumping was discussed here, estimation of the slip layer thickness was made and validated by comparing the actual flow with the calculated one.

ملخص الرسالة

الاسم الكامل: نعيم سهيل سليم سليم

عنوان الرسالة : نمذجة الخرسانة ذاتية الدمك ذات الاساس البوليمري بإستخدام المعايير الريولوجية

التخصص: الهندسة المدنية

تاريخ الدرجة العلمية: كانون اول ٢٠١٤

هذا العمل كان موجهاً لدراسة سلوك الخرسانة ذاتية الدمك (SCC) بالاستعانة بالمفاهيم الريولوجية وذالك بإجرا اختبار عملي بالاضافة الى اجرا محاكاة باستعمال الحاسوب. لقد تم دراسة موضوعين رئيسين في هذه الرسالة, الضغط الافقي الجانبي الناتج عن هذه الخرسانة وذالك على قوالب الخرسانة في مواقع الصب, والموضوع الآخر يتحدث عن ضخ هذا النوع من الخرسانات. وقد تم دراسة تأثير إجهاد الخضوع واللزوجة وتسييل القوام على السلوك الريولوجية لهذا النوع من الخرسانات.

لقد تم اعتماد اربعة خلطات لهذة الدراسة والمحتوية على انواع مختلفة من الإضافات المعدنية والتي تشمل, الرماد المتطاير (SCC - FA) و غبار السيليكا (SCC - SF) و حبيبات خبث الفرن المطحونة (SCC - GGBFS) بالإضافة الى مزيج التحكم (SCC – C) وكانت نسبه الماء الى الاسمنت ٠,٣٥. ولقد تم اجراء إختبار الضغط الجانبي عملياً وذالك بصب الخرسانة في قالب حديدي بإرتفاع ٣,١ م وطول ٣ م وسمك ٢٠٠ مم. لقد تم قياس التغيرات في الضغط عبر الارتفاع وذالك بإستخدام أجهزة استشعار الضغط المثبتة على ارتفاعات مختلفة وقد تم قياس ومراقبة تطور الضغط على القالب لمدة ١٢ ساعة وقد تم الحصول على المعايير الريولوجية بما في ذلك إجهاد الخضوع و اللزوجة النسبية و تسييل القوام لكل مزيج وذالك في نفس وقت الصب وقياس الضغط. لقد تم ربط نموذج عناصر محدودة للتنبؤ بالضغط الجانبي لهذه الخرسانة مع البيانات والنتائج التجريبية كم استخدم هذا النموذج لمحكاه بيانات تجريبية من مصادر اخرى وذالك بإستخدام ANSYS.

لقد تم ايضاً دراسة تباين الضغط خلال عملية ضخ الخرسانة ذاتية الدمك عملياً وقد تم ذالك لمجموعتين من الانابيب, الاولى بطول إجمالي يبلغ ٦٠ م بالإضافة الى ١٣ من الانحناءات والثانية بطول إجمالي يبلغ ٢٢ م بالإضافة الى وجود انحنائين. تمت دراسة ثلاثة من الخلطات المحتوية على الإضافات المعدنية وذالك لكل مجموعة من الانابيب وهي كاالتالي, SCC – C و SCC - F وSCC - SF. وضعت أجهزة استشعار الضغط على مواقع مختلفة على طول خط الأنبوب، وكانت قراءات الضغط تسجل كل ثانيتين لمدة ١٠ دقائق. تم إيجاد انخفاض الضغط لكل متر طولي بالإضافة الى انخفاض الضغط بسبب الانحناءات وتم وربطها باللزوجة قيم إجهاد الخضوع. اعتماداً على النتائج التي تم الحصول عليها فقد تم تطوير نموذج وذالك للتنبؤ بهبوط الضغط باستخدام قيم اللزوجة و إجهاد الخضوع و في النهاية تم مقارنة تباين الضغط على طول خط الأنبوب مع نموذج عناصر محدودة وذالك باستخدام ABAQUS/CFD. لقد تم مناقشة اشتقاق معادلة سرعة الخرسانة اثناء الضخ , كما تم تقدير سمك طبقة الإنزلاق والتحقق من صحتها بمقارنة التدفق الفعلي مع التدفق المحسوب.

CHAPTER 1

INTRODUCTION

1.1 General

Concrete is a stone-like structural material made by mixing a carefully designed mixture of cement, sand, and aggregates with water to harden into a specially made forms of a particular shape and dimensions. Cement and water react chemically to bind the aggregate particles into a solid mass. A water-cement ratio of 0.25 is required to obtain full hydration of all cement particles. Additional water, over and above that ratio is necessary to give the mixture the required workability that enables it to move and fill the forms and surround the reinforcing steel prior to hardening. Concrete with a wide range of properties can be obtained by appropriate adjustment of the proportions of the constituent materials. Special cements (such as high early strength cements), special aggregates (such as various lightweight or heavyweight aggregates), admixtures (such as plasticizers, air-entraining agents, silica fume, and fly ash), and special curing methods (such as steam curing) permit an even wider variety of properties to be obtained (Nilson et al. 2003).

The greatest breakthroughs in concrete technology in the past 30 years were made through the use of superplasticizers (Collepardi 2005). One of the most important breakthroughs is development of self- consolidating (compacting) concrete (SCC).

SCC is considered one of the most revolutionary and important breakthroughs in concrete technology, and due to its characteristic fresh properties, it has the potential to alter, change and improve the future of concrete placement and construction process (Daczko 2012).

The benefits of SCC over the conventional concrete have been summarized by many concrete technology books and many researchers, below are some of the important points summarized by Omran (2009):

- Reduction in construction cost and time;
- Simplifying the casting process by eliminating vibration;
- Improve working conditions by reducing the noise;
- Possibility of casting complex irregular structural shapes;
- Possibility of casing congested steel elements without vibration;
- Improve the final surface of concrete by reducing honeycombing and bug holes'
- Producing highly durable concrete;
- Reducing the required pumping pressure which will extend the life time of pumping setup;
- Possibility of producing any architectural shape.

Since the initial development of SCC in the late 80's by Ozawa et al. (1989), concrete researchers have diverted their research towards SCC in order to understand their behavior. Three new areas in this field were opened lately; rheology of SCC, formwork pressure exerted by SCC and pumping process of SCC. This research will concentrate on these areas concerning the SCC and will be discussed in details in the coming chapter.

1.2 Need for Research

This is needed in order to have a broader understanding of fresh properties of self-compacting concrete; industry still treats SCC as normal concrete in mixing, transporting, pumping, placing and in formwork design. SCC has special characteristics that are not found in normal concrete such as the low yield stress that allows it to spread with almost no external vibration efforts, hence, the flow of such concretes needs to be thoroughly investigated to have a fundamental understanding of the flow chrematistics of SCC in pipes while it is being pumped aiming to suggest some ideas that may solve part of the problems occurring in actual pumping process such as segregation and the high pumping pressure resulting from high viscosity SCC's.

Another part of this dissertation deals with lateral formwork pressure exerted by SCC which is required to have a clear understanding of all the factors affecting the pressure and how to minimize it to have an economical design of the formwork without forgetting the safety of workers.

1.3 Objectives

Due to the need for understanding the connection between the rheology of SCC and the resulting formwork pressure from one side and the pressure drop in pipeline while pumping SCC from another side. The objective of this research can be summarized as follows:

1. To understand fluid mechanics concepts governing at rest and flow behavior of the viscoplastic SCC's.

2. Prepare an experimental setup for testing formwork pressure in full scale element.
3. Develop a finite element model (FEM) to predict formwork pressure.
4. Prepare an experimental setup for testing the pressure drop while pumping SCC.
5. Develop a model for the prediction of the pressure drop while pumping SCC.

CHAPTER 2

BASICS OF CONCRETE RHEOLOGY

2.1 Introduction

In the past century the main breakthroughs in the concrete industry were the development of superplasticizers and SCC. And since the initial stages of development of SCC in the late 80's by Ozawa et al. (1989), concrete researchers have diverted their research towards SCC in order to understand their behavior. This chapter will briefly highlight some rheology basic concepts, standard SCC tests in which the rheological parameters can be measured and then utilized in further tests and studies such as formwork pressure exerted by SCC and pumping of SCC in pipe in horizontal and vertical pipe line.

2.2 Rheology

Rheology, as a relatively new term used in concrete studies, it has been one of the most significant and important terms in describing flow behavior of SCC in the fresh state. Before becoming a total hardened element, concrete can be considered as a fluid material especially if we are talking about SCC. On the other, this cannot be totally true due to the fact that concrete is not a simple fluid, since it's main ingredient "Cement" reacts with water and hydrates which will cause the concrete to flocculate and build up a crystalline structure with time which in turn will convert this fluid material into a thicker fluid that is more viscous. Depending on the dose of the chemical admixture, concrete can stay in the

fluid state for a limited period of time in which the rheological parameters can be evaluated. Barnes et al. (1989) defines rheology as "the science of flow and deformation of matter" and therefor; relationship between flow, deformation and time is studied in this science.

To have a better and wider understanding of rheology of SCC, it is required to understand basic definitions and fundamental properties of materials. If a force *F* with a known value is applied to the top part of an element, a stress equals the force divide by area over which it was applied is produced, and the resulting stress can be found:

$$\sigma = \frac{F}{A} \qquad \text{Eq. 2. 1}$$

This stress will cause the material to deform; the shear strain is written as below (Figure 2.1).

$$\gamma = \frac{\Delta u}{\Delta z} \approx \alpha \qquad \text{Eq. 2. 2}$$

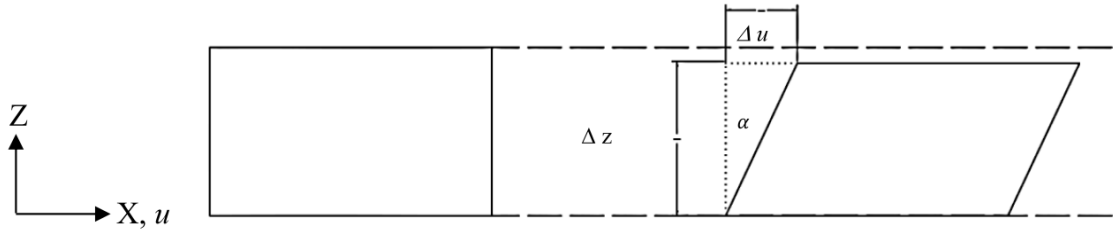

Figure 2.1: Shear Caused by Shear Stress

In order to understand the shear stress and flow relationship, fluid will be illustrated as layers with a gap in between containing the liquid. A velocity gradient will be produced while shearing a fluid material (Figure 2.2), the resulting shear stress will cause deformation in the *x* direction (*du*) during a specific period of time (*dt*).

Shear rate $\dot{\gamma}$ which can be defined as the rate of change of velocity at which one layer of fluid passes over an adjacent layer (Newman & Choo 2003), this can be expressed as follows:

$$\dot{\gamma} = \frac{d\gamma}{dt} \qquad \text{Eq. 2. 3}$$

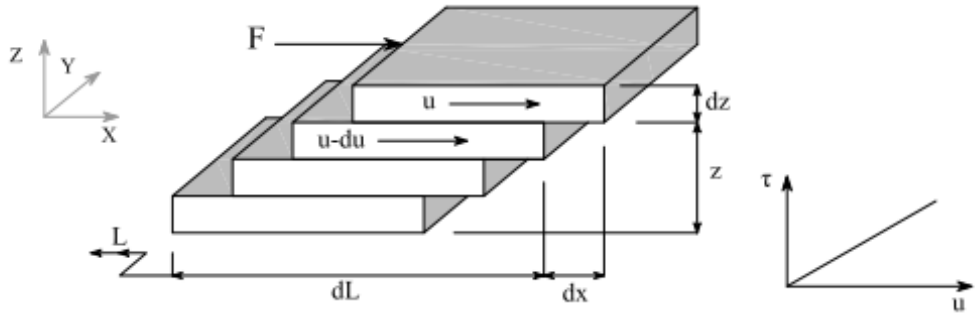

Figure 2.2: Velocity Gradient of a Sheared Fluid (Khatib 2013)

Measurement of a fluid's internal resistance to flow is called viscosity (μ) and can be easily written as the shear stress divided by shear rate:

$$\mu = \frac{\tau}{\dot{\gamma}} \qquad \text{Eq. 2. 4}$$

2.2.1 Elastic Behavior

Also called Hookian behavior which was establish by Rober Hooke in 1678 in which he stated that "the power of any spring is in the same proportion with the tension thereof "(Hooke 1678), and this can be explained as for a relative small deformation of an element, the deformation or displacement is directly proportional to applied load and that the element should go back to the original shape and dimensions once load is totally removed. The above definition is for springs but the same principle can be applied on any perfectly elastic material (Feys 2009), on the other hand, this behavior is basically for solids and it

has no dependency on time (Khatib 2013). Hooke's law is generally expressed in the following two forms:

$$\sigma = E\epsilon \quad \text{Eq. 2. 5}$$

$$\tau = G\gamma \quad \text{Eq. 2. 6}$$

where

σ = axial stress (Pa) *τ = shear stress (Pa)*
E = Young's modulus (Pa) *G = shear modulus (Pa)*
ε = strain *γ = angle of deformation*

2.2.2 Plastic Behavior

The material's ability to be shaped is usually know as plasticity, and more technical term, plasticity is the description of deformation of material undergoing irreversible changes in its original shape due to the applied load. The maximum capacity of any material to withstand external load without permanent deformation is referred to as the yield strength. Once this strength (or stress) is reached, material deformations are irreversible (Khatib 2013).

2.2.3 Viscous Behavior

As we defined viscosity as a measurement of a fluid's resistance to flow, it is basically a property that concerns fluids rather than solids. Figure 2.3 distinguishes the perfectly elastic material from the perfectly viscous material as reported by Feys (2009).

When a constant stress is applied on an elastic element, resulting angle of deformation would be also constant; on the contrary, if the same constant stress is applied on a viscous material, the angle of deformation will not be the same.

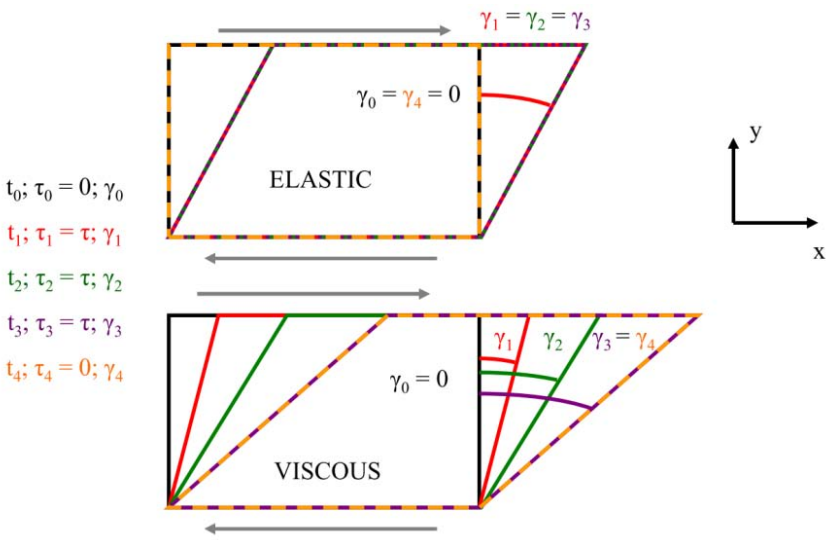

Figure 2.3: Difference between Elastic and Viscous Behavior (Feys 2009)

Consider the shear stress versus the strain rate (shear rate) relationship in Figure 2.4, based on the change of the shear rate, fluids are divided into two main groups; Newtonian materials and non-Newtonian materials. Newtonian fluids shows a constant shear stress and shear strain relationship, it exhibits a linear relationship and passing through the origin point. Any fluid that does not satisfy these conditions is considered non-Newtonian fluid.

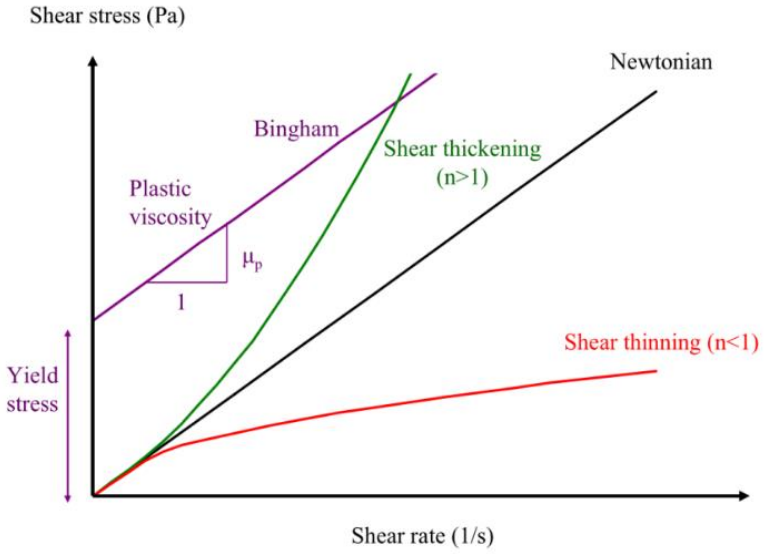

Figure 2.4: Different Flow Behavior of Fluids (Feys 2009)

2.2.4 Newtonian Fluid

A Newtonian fluid is a fluid having a linear shear stress shear rate relationship and passing through the origin point. The most famous fluid that exhibits Newtonian behavior is water. The Newtonian fluid equation can be expressed as follows:

$$\tau = \mu\dot{\gamma} \qquad \text{Eq. 2. 7}$$

where

τ: shear stress (Pa)
μ: viscosity (Pa s)
$\dot{\gamma}$: shear rate

2.2.5 Non-Newtonian Fluid

If any of the stated properties of Newtonian fluid are not satisfied, the fluid will be considered as non-Newtonian. For example, when the flow curve is linear and not passing through the origin point, it is considered as non-Newtonian. Similarly, if the flow curve is passing through the origin but it is non-linear, it is also considered non-Newtonian. Further details of Newtonian fluids will be explained in the following paragraphs.

Bingham Fluid

The main property the distinguish Bingham material from non-Newtonian material is the presence of yield stress. Yield stress can be defined as the critical stress after which the material starts to flow. Non-Newtonian material flows once this minimum force is reached; on the contrary, Newtonian material flows at any shear stress just like water. The equation that relates shear stress with shear rate for a Bingham material is written below:

$$\tau = \tau_0 + \mu_P \dot{\gamma} \qquad \text{Eq. 2. 8}$$

where

τ: shear stress (Pa)
τ_0: yield stress (Pa)
μ_P: plastic viscosity (Pa s)
$\dot{\gamma}$: shear rate

Shear Thickening and Shear Thinning Fluids

If the relationship between shear stress and shear rate is no longer linear the behavior of fluid will be considered as non-Newtonian behavior. If the flow curve passes through the origin and it is non-linear, there will two possibilities for this kind of behavior; when viscosity decreases with the increasing shear rate, the behavior is called shear thinning (or pseudoplastic), on the contrary, if the viscosity decreases with increasing shear rate, the behavior is called shear thickening (or dilatant). Graphical explanation for these two types is shown in Figure 2.5. These behaviors can be expressed as below:

$$\tau = m\dot{\gamma^n} \qquad \text{Eq. 2. 9}$$

where

τ: shear stress (Pa)
m: consistency factor (Pa s^n)
n: consistency index, n<1,shear thinning, n>1 shear thickening

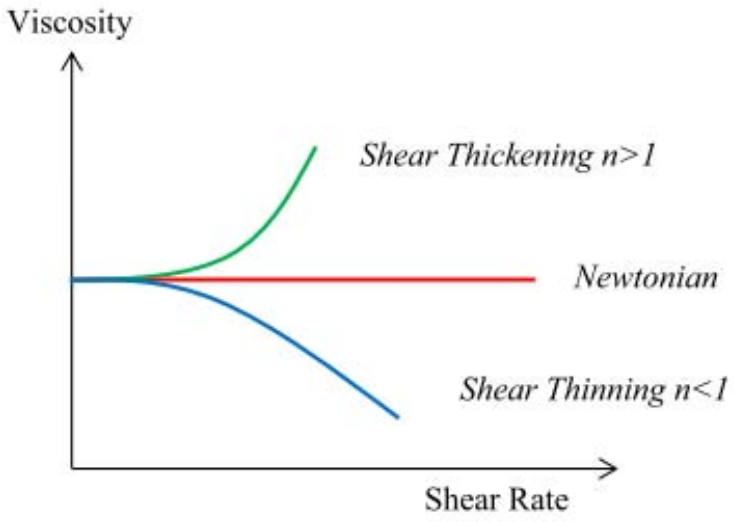

Figure 2.5: Viscosity Shear Rate Relationship for Newtonian and non-Newtonian Fluids

2.2.6 Measures of Viscosity

There are basically three types of measures for viscosity available in literature. Figure 2.6 shows how these types are differ from one to another; the tangential viscosity is defined as the slope of the line drawn at a specific shear rate. Similarly, apparent viscosity is defined as the secant slope of the line connecting the specific shear rate with origin point. Plastic viscosity is basically used for fluids obeying Bingham flow model, and can be defined as the flow line slope.

It should be highlighted that the plastic viscosity equals the tangential viscosity for any shear rate beyond zero. The three above viscosities will be exactly the same in case of a Newtonian fluid.

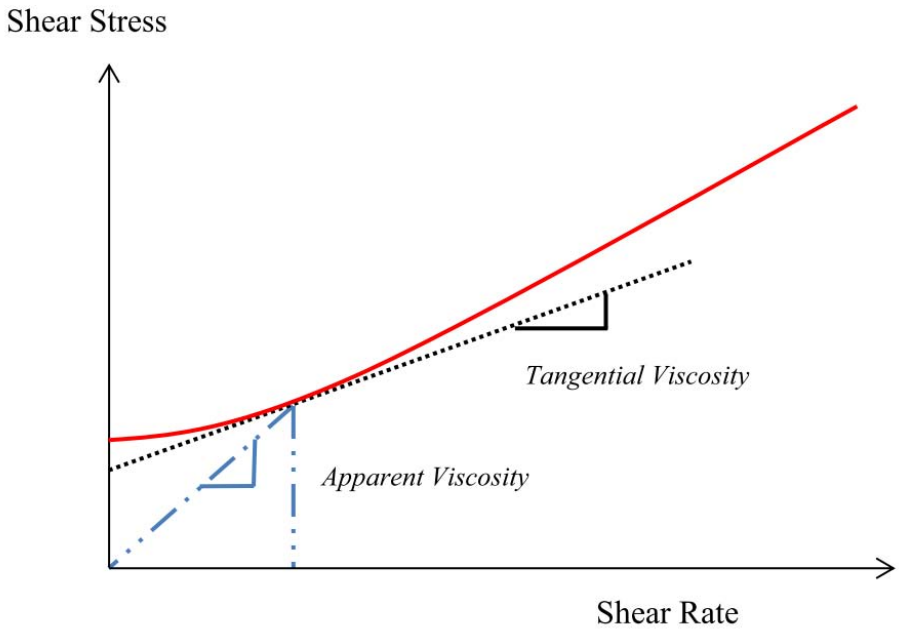

Figure 2.6: Different Types of Viscosities (Feys 2009)

2.2.7 Thixotropy

A material whose internal crystalline structure breaks down when sheared is called thixotropic material, Figure 2.7 illustrate this idea. Thixotropic fluids show time-dependent shear thinning behavior (Mewis 1979). It should be distinguished between thixotropy and its opposite, i.e. rheopexy. The viscosity of a rheopetic material increases as it is sheared (See Figure 2.8).

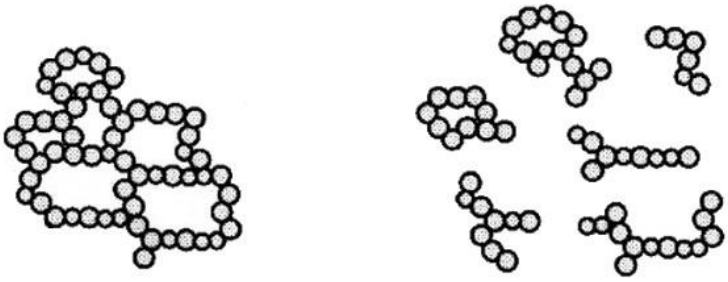

Figure 2.7: Particle Interaction in a Thixotropic Material

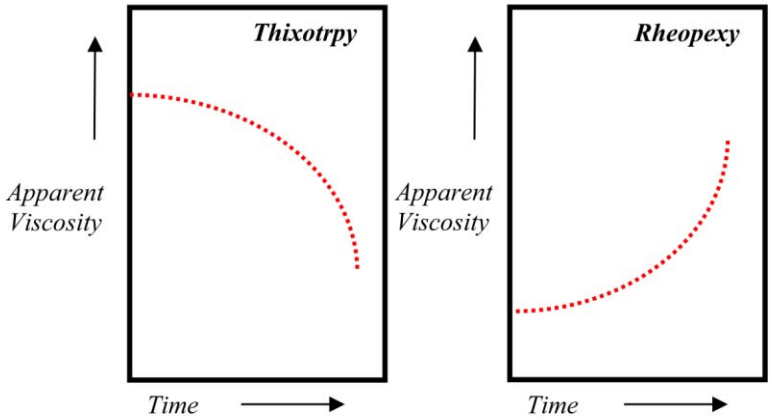

Figure 2.8: Difference between Thixotropic and Rheopectic Materials (Central Chemical Consulting 2014)

2.3 Concrete Rheology

2.3.1 Rheological Models

If all-time dependent properties of concrete are eliminated, almost all rheological models which describe the concrete behavior are considered in the steady state (Roussel 2010)

The commonly used models for describing the concrete flow behavior were summarized by Khatib 2013 in Table 2.1 except for the Newtonian material; all models have a common factor of having at least two parameters to describe the material behavior.

Table 2.1: Rheological Model for Cement-Based Materials (Khatib 2013)

Model	**Equation**
Newtonian	$\tau = \mu\dot{\gamma}$
Bingham	$\tau = \tau_0 + \mu_P\dot{\gamma}$
Herschel Bulkley	$\tau = \tau_0 + K\dot{\gamma}^n$
Casson Model	$\sqrt{\tau} = \sqrt{\tau_0} + \sqrt{\mu_P}\sqrt{\dot{\gamma}}$
Modified Bingham Model	$\tau = \tau_0 + \mu_P\dot{\gamma} + c\dot{\gamma}^2$
Sisko Model	$\eta = \mu_\infty + K\dot{\gamma}^{n-1}$

where

τ: *shear stress (Pa)*
μ: *viscosity (Pa s)*
$\dot{\gamma}$: *shear rate*
τ_0: *yield stress (Pa)*
μ_P: *plastic viscosity (Pa s)*
K: consistency factor in Herschel-Bulkley model (Pa s^n*)*
n: flow index in Herschel-Bulkley model
c: regression constant in the modified Bingham model (Pa s^2*)*
η*:apparent viscosity (Pa s)*
μ_∞*: viscosity at infinite shear rate (Pa s)*

2.3.2 Rheology of SCC

As it has been described earlier, rheology may be defined as the scientific description of flow. In most of the available models that describes the flow of materials, the two main rheological parameters are the yield stress and plastic viscosity as stated in Table 2.1. Generally speaking, most of concrete researchers agreed on using Bingham flow model in order to describe the flow of conventionally vibrated concretes (CVC) as well as SCC. In Bingham model, yield stress is the minimum force required to initiate the flow. For CVC, that force is called vibration. On the other hand, plastic viscosity is defined as the resistance of concrete to flow. SCC exhibits lower yield stress if compared to CVC which in turn facilitate the spread of concrete and makes it flowable.

Figure 2.9 shows a comparison between flow curves for different SCC mixes with CVC as summarized by Malik (2011). CVC has a relatively high yield stress compared to SCC; hence energy required for compaction is higher as it comes in the form of mechanical vibration. On the contrary, SCC mixes have lower yield stress and get compacted under its own weight without the presence of any vibration, but the rheological parameters may be different depending on the viscosity level. High plastic viscosity SCC will be very sticky

(hard to move), not easy to finish and very difficult to pump, whereas SCC with the low plastic viscosity will be very easy to pump but it will be prone to segregation. Thus, re-proportioning the ingredients can result in obtaining an optimal flowable mix that can have low viscosity and yield stress which would be enough to resist segregation with low stickiness level in order to achieve the required performance.

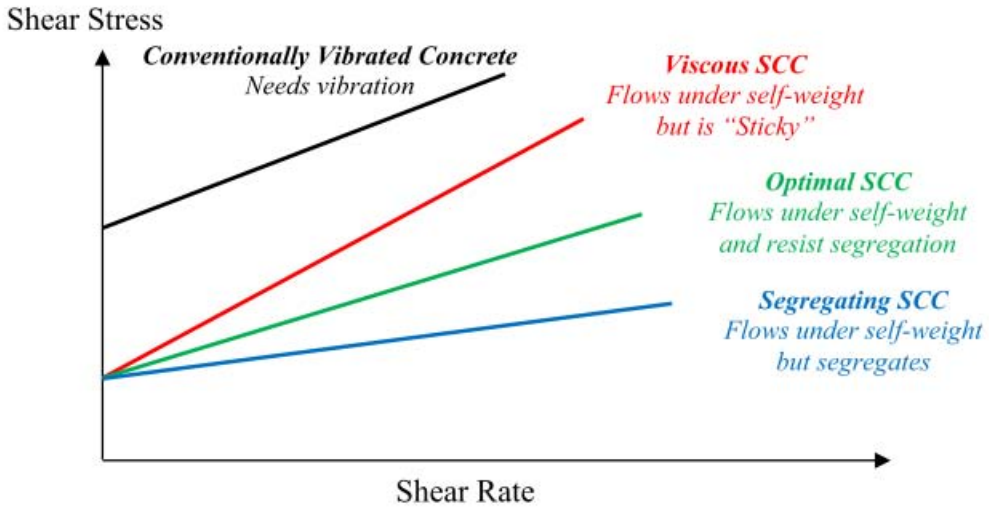

Figure 2.9: Different Flow Curves for Concrete

Behavior of fresh SCC can be totally understood only by understanding its rheology. Fresh properties of concrete including pumping, slump, placement, and compaction depend on its rheology. Understanding the rheology of concrete will help in predicting the behavior of fresh concrete, selection of materials and modeling of concrete flow.

2.3.3 Tests for Self-Compatibility

Some Existing tests for fresh SCC were discussed by Bartos (2000), according to him, SCC must have three main properties in order to be considered SCC; passing ability, filling ability and resistance to segregation.

The Slump Flow and T-50 Test

A cone similar to the one used in conventional concrete is also used here (See Figure 2.10). SCC is placed in the concrete slump cone but without any rodding, the cone is then left and concrete is allowed to spread. The diameter of the spread is measured and recorded. On the other hand, the time required to reach a diameter of 50 cm is measured and recorded as T-50. Generally speaking, SCC should have a spread value between 550 mm and 750 mm to be considered as SCC. This test gives an indication about filling ability of SCC.

Figure 2.10: Spread (Flow) Test

The V-Funnel Test

The V-funnel equipment is shown in Figure 2.11, a gate is fitted on the lower part for the concrete to escape from the funnel. SCC is poured into the funnel with no vibration, a container is then placed exactly below the gate. After 10±2 seconds from filling, the gate is opened and the time required to see the contained from above is recorded. This test gives an indication about the viscosity and filling ability of SCC.

Figure 2.11: V-Funnel Test Setup

The L-Box Test

Figure 2.12 shows the L-Box test setup. The concrete is filled in the vertical part while the trap-door is still in place, after opening the trap-door, the time required for the concrete to flow a distance of 200 mm denoted as T-20 and 400 mm denoted as T- 40 into the horizontal section is recorded, also the height of the concrete at both ends of the equipment (h_1 & h_2) is measured. The L-Box test gives an idea about the passing and filling ability of SCC.

Figure 2.12: L-Box Test Apparatus

The J-Ring Test

The same slump cone used in CVC is also used here, the cone is placed upside down inside what is called J-Ring as shown in Figure 2.13. Concrete is filled and the cone is left upwards. Similar to slump flow test, diameter and the time T-50 are measured and recorded, on the other hand the height of concrete inside and outside the J-Ring are measured and the difference is recorded, this should be between 0 and 100 mm.

Figure 2.13: The J-Ring Setup

Malik (2011) summarized the acceptance criteria for SCC in Table 2.2.

Table 2.2: Criteria for Acceptance for SCC (Malik 2013)

	Test Method	Unit	Minimum	Maximum
1	Slump Flow	mm	650	800
2	T-50	sec	2	5
3	V-Funnel	sec	6	12
4	L-Box	(h_2/h_1)	0.8	1
5	J-Ring	mm	0	100

2.3.4 Determination of Rheological Parameters

Rheological parameters are found using the ICAR rheometer shown in Figure 2.14. this equipment is composed of a steel container in which the fresh concrete is held, a driver head that equipped with an electric motor and torque meter; a four-blade vane that is held by the chuck on the driver; a red steel frame used to attach the driver/vane assembly to the top of the container; and a laptop computer unit to control the equipment and do all flow calculations. The inner surface of steel container contains a number of vertical plastic rods around the perimeter to prevent the slippage of concrete during operation. Based on the software of the ICAR Rheometer, two tests can be performed to assess the rheology of SCC; flow curve and stress growth test (ICAR 2008).

Figure 2.14: ICAR Rheometer

Stress Growth Test

In this test, the vane is rotated at a constant speed of 3.76 rad/sec. The torque build up during the test is measured as a function of time, and the torque required to initiate the flow of SCC (maximum torque) is used in calculating static yield stress.

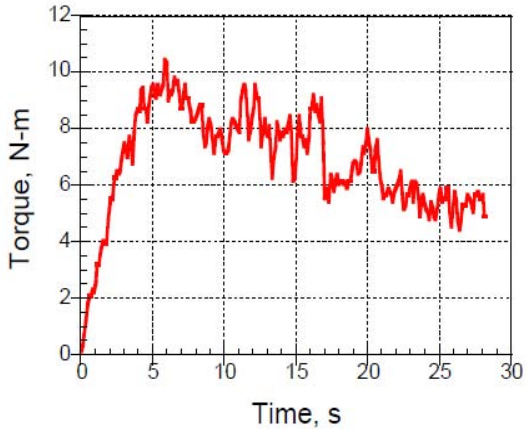

Figure 2.15: Typical Graph obtained in the Stress Growth Test

A typical stress growth test results is shown in Figure 2.15. The maximum torque along with test setup geometry are used to calculate the static yield stress. Stress calculation at the points other than the maximum is done using the Reiner-Riwlin equations. Two sets of equations were provided by ICAR Rheometer manual depending on whether all the material in the container is flowing or not.

Based on ICAR Rheometer manual, the effective radius that separates the flowing region from the non-flowing region is calculated as blow (ICAR 2008).

$$R_{2,eff} = \sqrt{\frac{T}{2\pi h \tau_0}} \qquad \text{Eq. 2. 10}$$

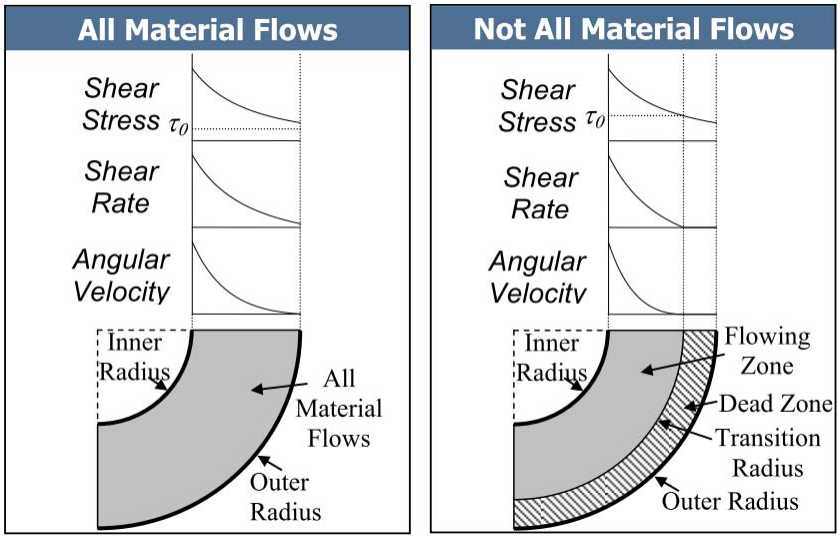

Figure 2.16: Representation of the Two Cases of Flow (ICAR 2008)

As shown in Figure 2.16 (right) the shear stress in the dead zone is blow the yield stress, and hence the material will not flow and the effective radius will be less than the container radius. If the material is flowing completely, the effective radius will be more than the container radius. In this case, at the beginning of the stress growth test, material will be partly flowing inside the container and after some time will completely flow.

Reiner-Riwlin equation when all material flows (ICAR 2008)

$$\dot{\gamma} = \frac{T}{4\pi h\mu}\left(\frac{1}{R_1^2} - \frac{1}{R_2^2}\right) - \frac{\tau_0}{\mu}\ln\left(\frac{R_2}{R_1}\right) \qquad \text{Eq. 2. 11}$$

Reiner-Riwlin equation when not all material flows (ICAR 2008)

$$\dot{\gamma} = \frac{T}{4\pi h\mu}\left(\frac{1}{R_1^2} - \frac{2\pi h\tau_0}{T}\right) - \frac{\tau_0}{2\mu}\ln\left(\frac{T}{2\pi h\tau_0 R_1^2}\right) \qquad \text{Eq. 2. 12}$$

Flow Curve Test

This test is utilized for the determination of the plastic viscosity and the dynamic yield stress. It starts with what is called breakdown period. In this breakdown period, the steel

vane is rotated at maximum speed of 3.76 rad/sec. This part of the test is intended to breakdown any thixotropic structure that might built up and to ensure having a harmonic shearing history before starting measurements for Bingham parameters. The speed of the vane is then reduced in many steps (in this case seven), and during each step the speed is held constant and the average speed and torque is measured and recorded. A typical plot of the torque versus vane speed shown in Figure 2.17.

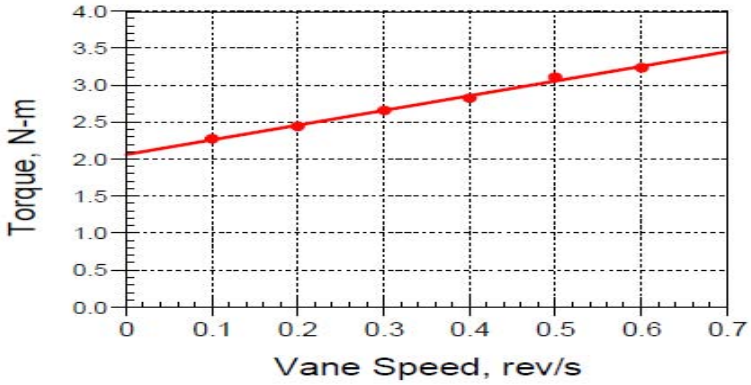

Figure 2.17: Flow Curve Test

CHAPTER 3

LITERATURE REVIEW

3.1 Introduction

Considerable research has been done earlier to simulate the flow behavior of SCC. According to Roussel (2007), in the flow of SCC, SCC can be treated as a single fluid, hence considering discrete modeling approach will not be required.

Modeling the flow of fresh concrete as single fluid was done to simulate the flow behaviore during actual concrete testing. On the other hand, computational flow modeling for full-scale elements was also done in some resent researches. Free surface displacement and yield stress behavior are considered the main difficulties in single fluid simulation. Navier-Stoke's equation is used most of the time to obtain flow behavior by applying the apparent viscosity.

Simulation of flow behavior of SCC can be categorized in three main areas; testing of fresh concrete simulation, this may include simulation of slump cone test, V-Funnel and the L-Box test. The second category is related to casting in full scale element and the resulting formwork pressure. The third category is basically the modeling of the pumping process of SCC in pipeline.

3.2 Simulation of Testing of SCC

Roussel (2004) has developed a 3D model to perform simulations for the slump test (Figure 3.1). The model was made using Flow 3D® package in which an elasto-viscoplastic model was selected in order to describe the flow behavior of fresh concrete with a yield stress ranging between 25 and 5500 pa, an incompressible and elastic solid was assumed up to the yield stress and a Bingham fluid beyond that point with no sliding at the base. Good matching was found with the experimental data.

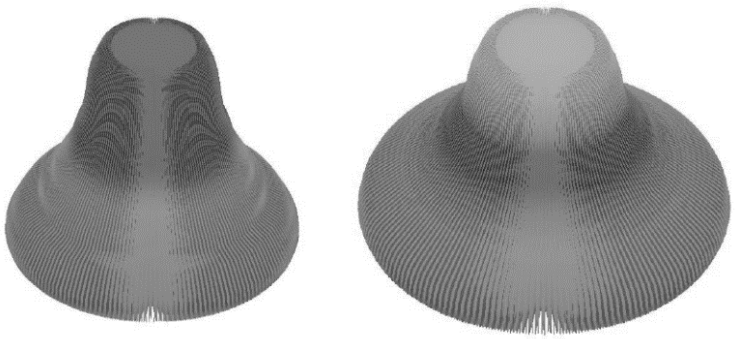

(a) (b)

Figure 3.1: Results for Slump Cone Test with Different Yield Stresses (Roussel 2004).

Kulasegaram et al. (2011) as reported by Mukhtar (2011), have used a Lagrangian particle-based method along with smooth particle hydrodynamics (SPH), to simulate the slump cone test for SCC, with and without steel fibers. Figure 3.2 and Figure 3.3 show the simulation of slump cone test for normal SCC and SCC with fibers.

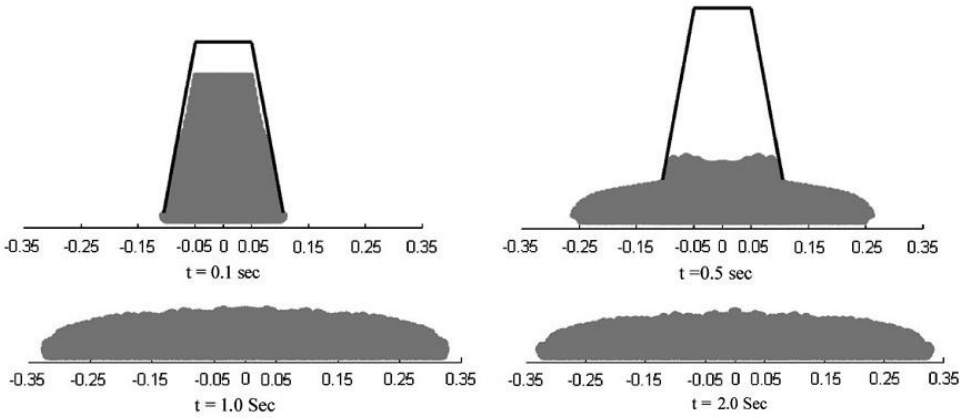

Figure 3.2: Modeling of Slump Cone Test for Normal SCC (Kulasegram et al. 2011)

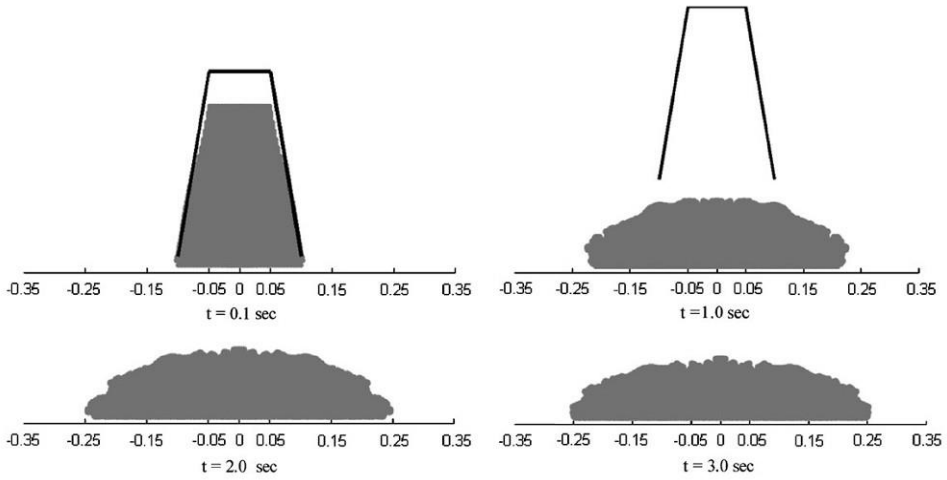

Figure 3.3: Modeling of Slump Cone Test for SCC Containing Fibers (Kulasegram et al. 2011)

Dufour and Pijaudier-Cabot (2005) as reported by Mukhtar (2011), presented a numerical model to simulate the flow of concrete based on homogeneous viscous fluid approach by using a finite element method along with Lagrangian integration points (FEMLIP). Bingham flow behavior was selected to describe the rheology of three concretes; one ordinary, high performance and SCC with different rheologies (See Figure 3.4).

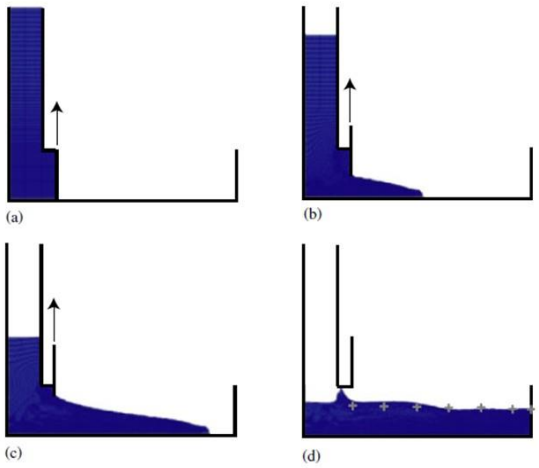

Figure 3.4: Simulation Results Obtained by Dufour and Pijaudier-Cabot (2005)

Two studies were conduct recently in KFUPM to model testing of SCC and validation of that by conducting experimental tests in the field. Malik (2011) has studied the segregation and rheology of SCC using different mineral admixtures; different percentages of fly ash, microsilica and lime stone powder were selected for testing, a number of tests on SCC including the spread test, V-Funnel test and L-Box test were conducted. Rheological parameters including yield stress and viscosity were found, and a relationship to find thixotropy from the rheological measurements was developed.

Table 3.1and Table 3.2 show the experimental results of the SCC mixtures used by Malik (2011), results of these tests have built a huge data base that can be utilized to validate any suggested model for these tests. Figure 3.5 shows shear stress variation with time at a constant shear rate as by the ICAR rheometer, the peak value represents the static yield stress while the straight line represents the dynamic yield stress. Figure 3.6 represents the variation of relative viscosity with time for different resting periods (1,5 and 15 minutes). It is concluded that by increasing the resting time, the relative viscosity will be initially higher due to flocculation of concrete, but with time, viscosities will come to similar levels.

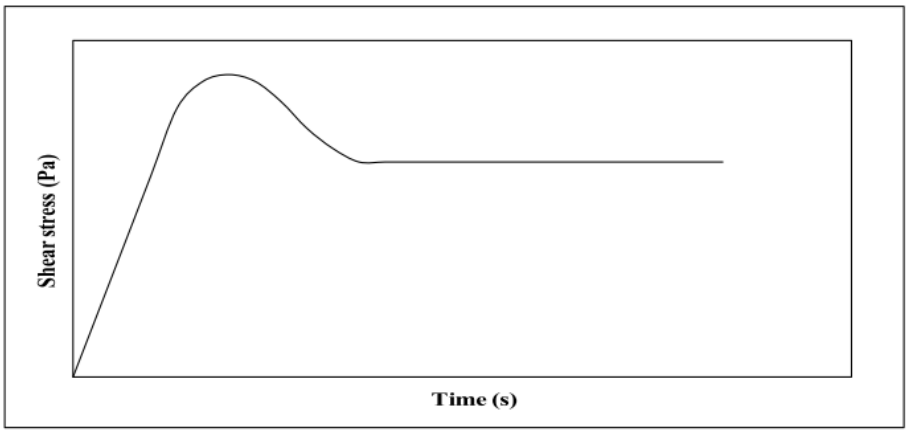

Figure 3.5: Shear Stress variation with Time (Malik 2011)

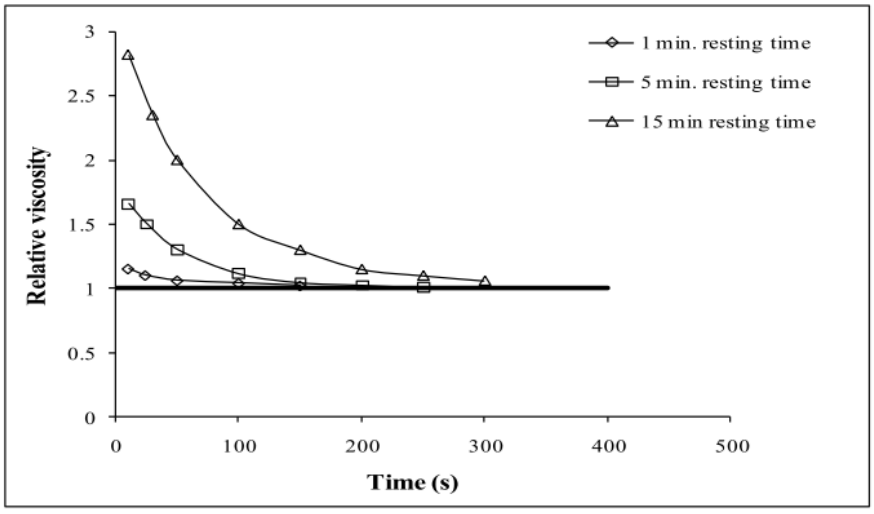

Figure 3.6: Relationship between Relative Viscosity and Time (Malik 2011)

Table 3.1: Fresh Properties of SCC as Reported by Malik (2011)

Mix	Slump flow (mm)	T-50 (s)	V-funnel(s)	L-Box Ratio	J-Ring (mm)
REF	720	4.5	12	0.97	630
SF 2.5%	690	6	11.4	1	630
SF 5%	680	4.5	11	1	650
SF 7.5%	700	5.4	12	0.96	660
LSP 5%	720	4	14	1.13	610
LSP 10%	755	3.5	17	1.15	580
LSP 15%	720	5	10	0.93	620
FA 5%	725	4.25	13	1.15	630
FA 7.5%	720	5.4	12	0.86	650
FA 10%	730	5.5	11.2	1.5	620

Table 3.2 : Experimental Results for Bingham Parameters of some SCC Mixtures as Reported by Malik (2011)

Mix	τ_0 (Pa)	μ (Pa-s)
REF	56.3	48.4
SF 2.5%	65.1	52.5
SF 5%	65.5	54.9
SF 7.5%	58.4	71.2
LSP 5%	39.3	59.2
LSP 10%	45.5	53.1
LSP 15%	36	63
FA 5%	34	48.9
FA 7.5%	47.4	62.9
FA 10%	32.2	58.6

At the same period, Mukhtar (2011) has modeled the flow of SCC for the three mentioned tests. The models were made in ANSYS Fluent environment where a computational fluid dynamics (CFD) approach is utilized. Bingham flow model was used in describing the flow behavior of SCC. The program used volume of fluid concept for running the model; in this case, two fluids are included in the model, SCC and air. Once the model is set to run, SCC will move by gravity and will be replaced by air while keeping the total volume of SCC and air without any change. Main parameters to be entered are the yield stress and viscosity.

Figure 3.7, Figure 3.8 and Figure 3.9 show the models proposed by Mukhtar (2011), good agreement between model and the results presented by Malik (2011).

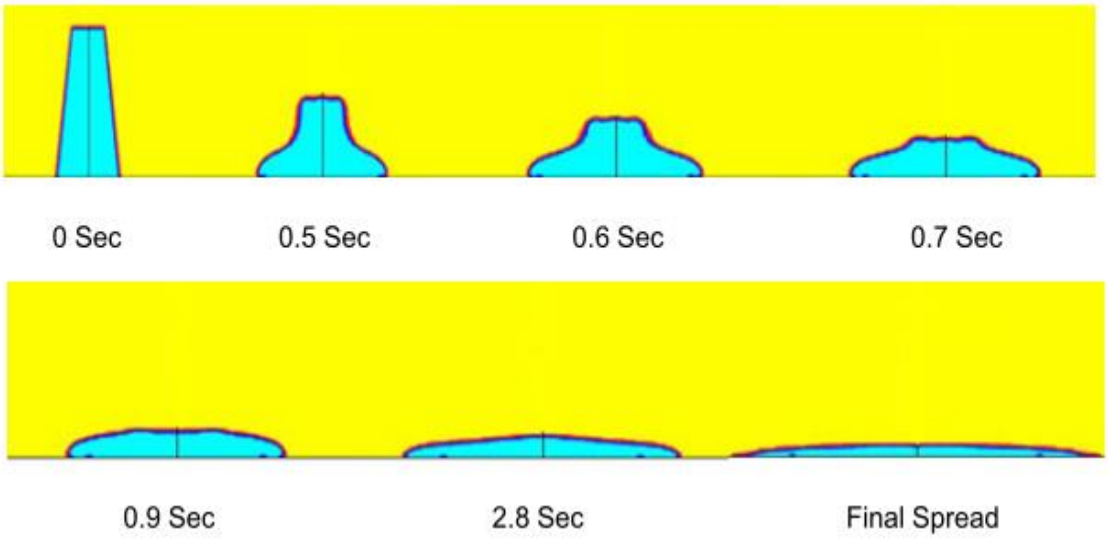

Figure 3.7: Simulation of Slump Cone Test of SCC (Mukhtar 2011)

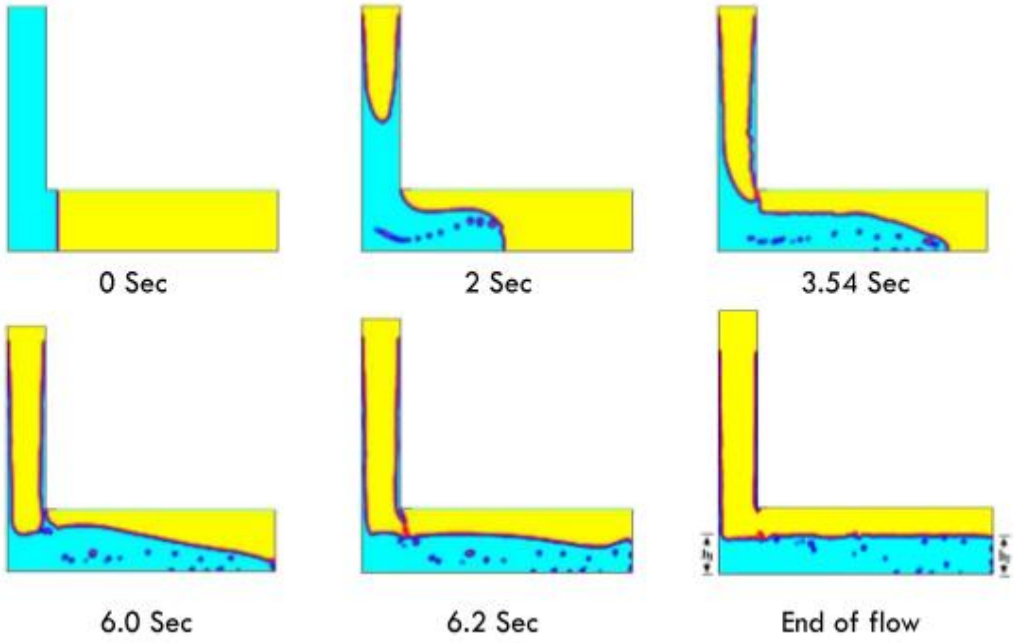

Figure 3.8: Simulation of L-Box Test of SCC (Mukhtar 2011)

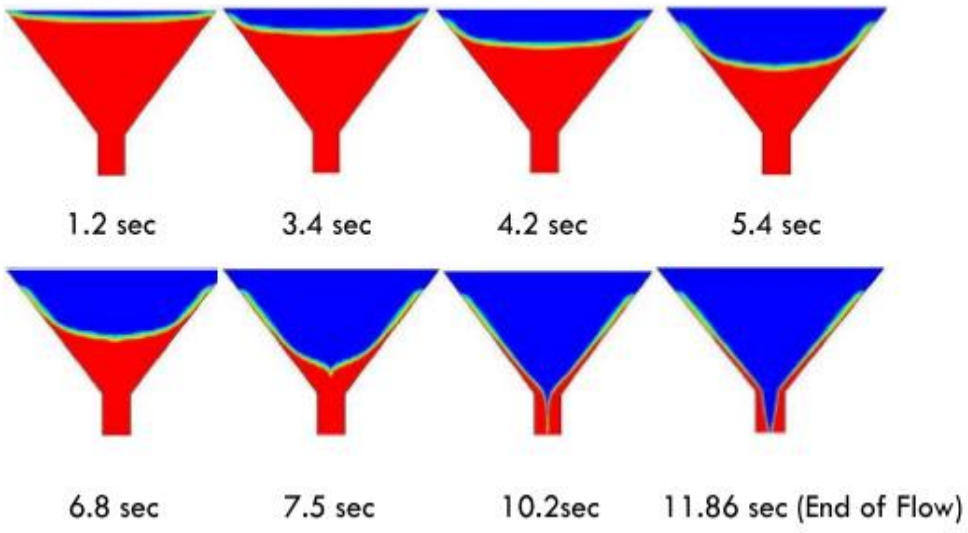

Figure 3.9: Simulation of V-Funnel Test of SCC (Mukhtar 2011)

The model developed by Mukhtar (2011) was utilized to have a wider understanding of the flow behavior of SCC by varying the rheological parameters of the mixtures, details in Appendix A.

3.3 Simulation of Formwork Pressure Exerted By SCC

One of the disadvantages of the highly flowable SCC is mainly due to large increase of the pressure on the formwork. Knowing the value of the pressure that is exerted on formwork by fresh concrete will ensure having a safe and economical design of formwork. In the beginning it was assumed that SCC will generate hydrostatic pressure since we are talking about fluid concrete, later it was discovered that this is not totally true due to the quick setting time of such types of concrete which in turn will make concrete stand by itself without the need of any support in a short period of time and will eliminate the hydrostatic pressure shortly after casting.

Mukhtar (2011) has reported that altering the concrete casting process and mix design, can reduce the formwork pressure and it can be less than the hydrostatic one. For example, Kim et al. (2011) have stated that incorporating mineral admixtures and chemical admixtures can reduce the formwork pressure, as the presence of such materials will change the thixotropic behavior of SCC.

The effect of the casting operation has been discussed by Ovalez and Roussel (2006), they reported that during concrete placement process, concrete behaves as a fluid but, if the casting process was too slow or the concrete is at rest, concrete will start building an internal structure which enables it to be able to carry the load from the above concrete without any increase in the formwork pressure.

An experimental program for simulating SCC formwork pressure reported by Gregori et al. (2008). A device was developed to evaluate mixture composition effect and the rate of casting by pressurizing a known volume of material inside a cylinder and measure the lateral pressure evolution (Figure 3.10). They simulated columns with different heights with value for the rate of casting. It was proven that formwork pressure can be less that the hydrostatic one. A sample of their results is shown in Figure 3.11.

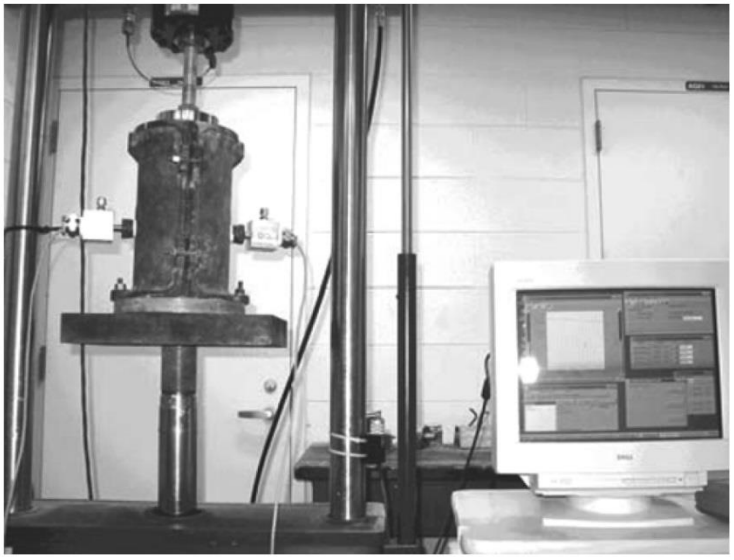

Figure 3.10: Testing setup Used by Gregori et al. (2008)

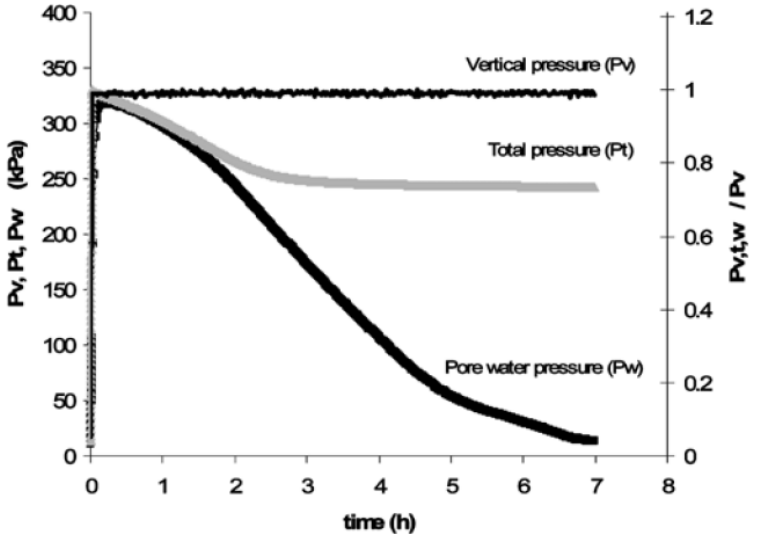

Figure 3.11: Gregori et al. (2008) Simulation Results

3.3.1 Factors Affecting Formwork Pressure

Khayat et al. (2007) have reviewed and summarized the parameters affecting the pressure exerted by fresh SCC on the formwork. Following paragraphs summaries these factors.

Raw Materials

- ***Cementitious Materials***

The type and content of cement and any other supplementary cementitious materials such as microsilica, limestone powder, fly ash and ground granulated blast furnace slag (GGBFS) have influence on the development of pressure exerted by normal concrete as well as SCC (Khayat et al. 2007).

Mixtures with higher cement content tend to develop higher lateral pressure. Roby (1935) investigated a number of concrete mixtures (lean, normal and rich), with different cement, sand, and coarse aggregate mass ratios. He concluded that cement content has a great impact on the lateral pressure, mixtures were made with ordinary Portland cement with a slump values between 50 to 150 mm. The recorded pressure for rich mixes was 40% higer than normal mixes, on the other hand, normal mixes showed 15% higher pressure compared to lean mixes. See Figure 3.12.

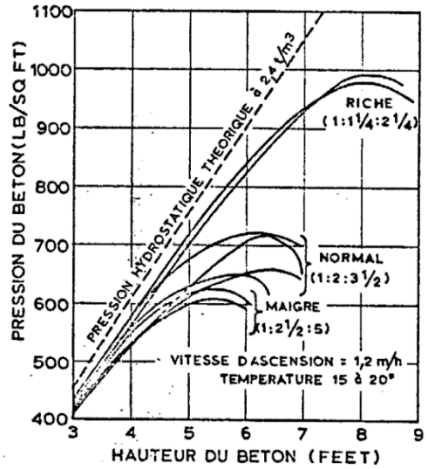

Figure 3.12: Cement Content Effect on Formwork Pressure (Roby 1935)

Supplementary Cementitious material showed an effect on the concrete lateral pressure. Gardner (1984) studied the replacement of cement by fly ash in conventional concrete, the fly ash he used was between 0 and 50%, and he found that it increases the lateral pressure.

Recently, SCC was investigated for formwork pressure. Assaad and Khayat (2005A, 2005B) studied lateral formwork caused by SCC with different supplementary cementitious material. Total cementitious materials content was varied between 400 and 550 kg/m3. Water-cement ratio was 0.40 for all mixes. Superplasticizer dosages were set to maintain a slump value of 650 ±15 mm. They concluded that a higher content of cementitious materials will lead to higher lateral pressure due to less aggregate content. Figure 3.13 shows what has been explained earlier.

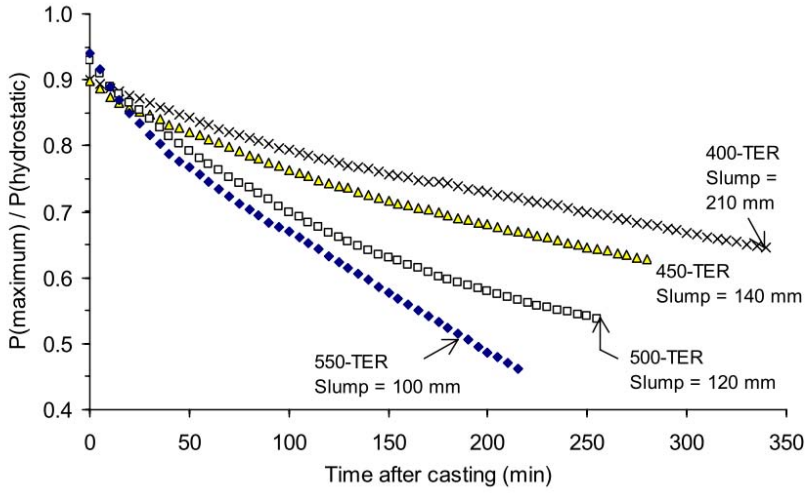

Figure 3.13: Pressure Decay for Different SCC Mixtures as reported by Assaad and Khayat (2005A)

- ***Coarse Aggregates***

Generally speaking, higher percentage of aggregate in any concrete mix will result in lower lateral pressure due to higher interlocking between aggregates and lower cement content. Assad and Khayat (2005C) reported that for high flowability mixes with a flow spread ranging between 635 and 665 mm. It was found that the increase in quantity of coarse

aggregate will decrease the formwork pressure and accelerate the pressure decay after casting. This was basically due to the increase of internal structural friction between aggregates (interlocking) which was reflected in lower pressure. Figure 3.14 represents the pressure decay with time after casting. Seven mixes were compared with sand to total aggregate ratio from 1.0 to 0.3; the pressure was measured at the bottom of a 2.8 m height wall with a casting rate of 10 m/hr. It clearly noticed that higher aggregate percentage will result in lower lateral pressure; the rate of drop was also noticed to be higher.

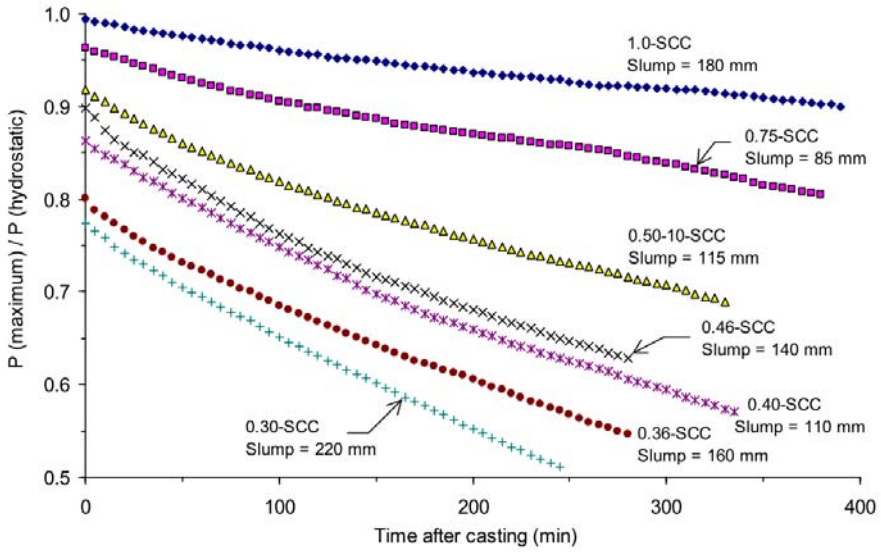

Figure 3.14: Pressure Decay for Different SCC Mixtures (Assaad and Khayat 2005C)

- ***Water-Cement Ratio***

Higher water content mix will result in higher lateral pressure due to higher fluidity of the mix. Khayat and Assad (2006) studied the effect of w-c ratio on the lateral pressure. As shown in Figure 3.15, three mixtures were selected for comparison with a w-c ratio of 0.36, 0.40 and 0.46, the initial lateral pressure was found to be maximum for the 0.46 mixture. This was a result of the increased paste and water content and the reduction of coarse aggregate content. Due to the higher percentage of PC-based HRWRA used in the 0.36

mixture, the rate of drop of lateral pressure was found to be lower than the other mixture, and this was a result of the retarding effect that present in such types of chemical admixtures.

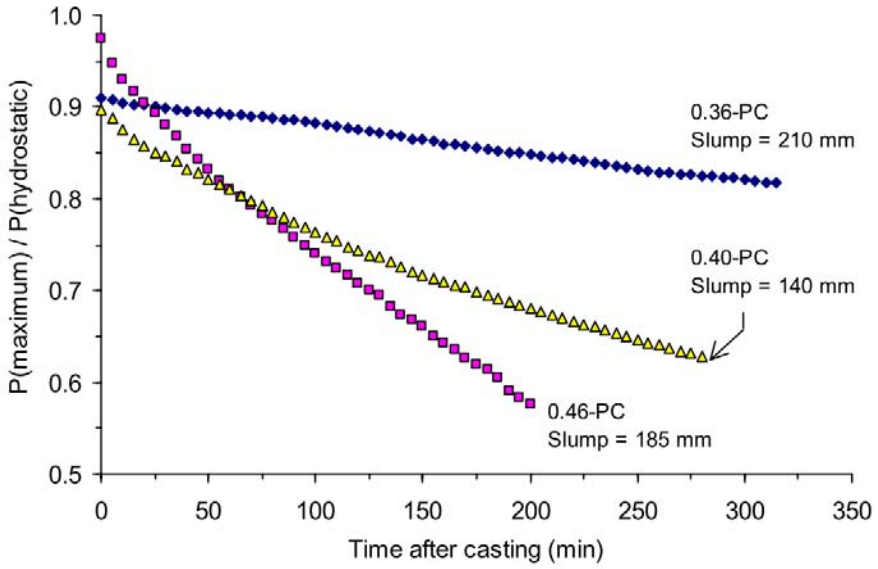

Figure 3.15: Pressure Decay for Different SCC Mixtures made with different water contents (Khayat and Assaad 2006)

- ***Chemical Admixtures***

Type of chemical admixture added to concrete will affect the rate of drop of lateral pressure after casting. Khayat and Assad (2006) evaluated three type of HRWRA, these types are made from different base material, namely; polycarboxylate (PC), Sulphonated Naphthalene (PNS) and Sulphonated Melamine (PMS). Figure 3.16 illustrate the variation of relative lateral pressure for the three different types of HRWRA mixtures having the same w-c ratio of 0.36 with elapsed time after casting. Initial lateral pressure was found to be the same for all mixtures, while the rate of lateral pressure drop was found to be maximum for PMS followed by PNS and the minimum for PC.

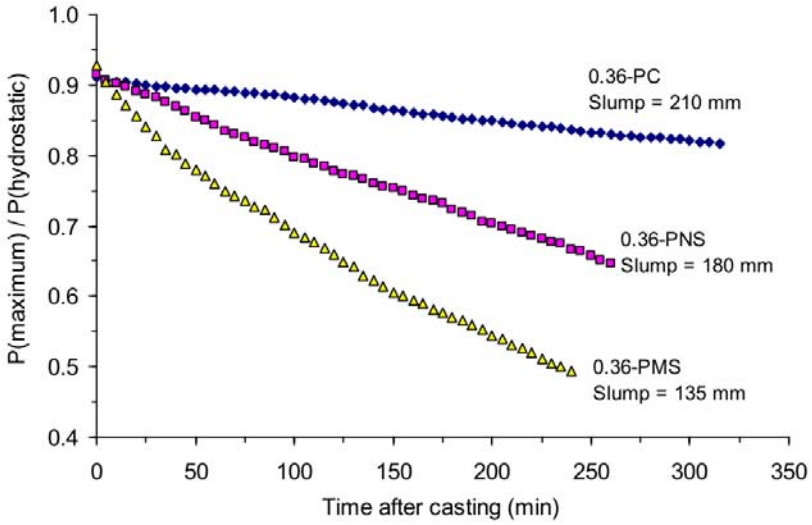

Figure 3.16: Pressure Decay for Different SCC Mixtures made with different types of Superplasticizers (Khayat and Assaad 2006)

Consistency Level

Consistency level has a direct effect on formwork pressure exerted by fresh concrete, as the slump increases the fluidity increases which in turn increase the pressure due to the reduced shear between the particles. Rodin (1952) evaluated the effect casting rate and the consistency level on the maximum lateral pressure, it was noted that concrete with higher slump develop higher lateral pressure (see Figure 3.17). The effect of internal vibration was found to increase the lateral as compared to the hand placed concrete.

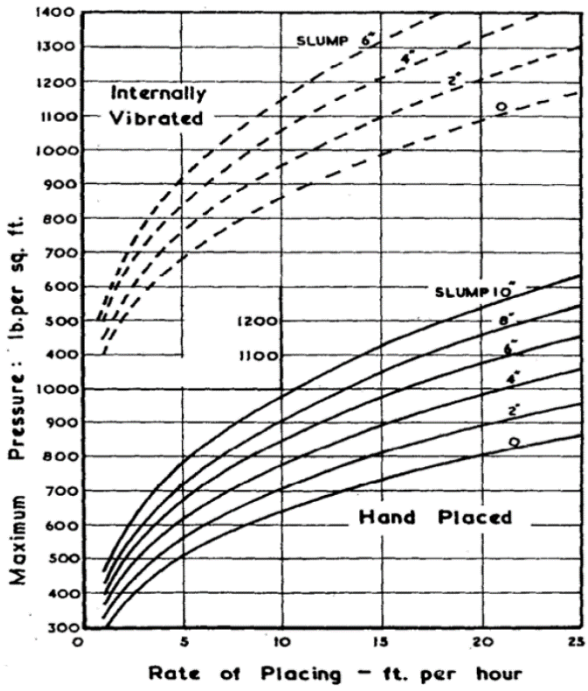

Figure 3.17: Maximum Pressure as a funtion of Casting Rate and Workability as reported by Rodin (1952)

Placement Conditions

- ***Rate of Casting***

Rate of casting has a direct effect on the lateral pressure exerted by concrete in the fresh state especially on the initial values with almost no effect on the pressure drop after casting. Rodin (1952) reported that for the same consistency level, higher casting rate will lead to higher maximum pressure (Figure 3.17). Roby (1935) concluded from his study that increase the rate of casting from 1 to 10 ft/h increases the lateral pressure (Figure 3.18).

The rate of casting effect has been studied by Assaad and Khayat (2006), a pressure column was used with a total height of 2.8 m and a diameter of 200 m. Three casting rates were used; 25, 10 and 5 m/hr, and the maximum relative pressure was obviously obtained by the 25 m/hr rate. Farther more, dropping the rate from 25 to 5 m/hr was reported to reduce the

pressure by 15% (Figure 3.19). It was also reported that if a resting period was introduced during casting, a considerable drop in pressure can be obtained.

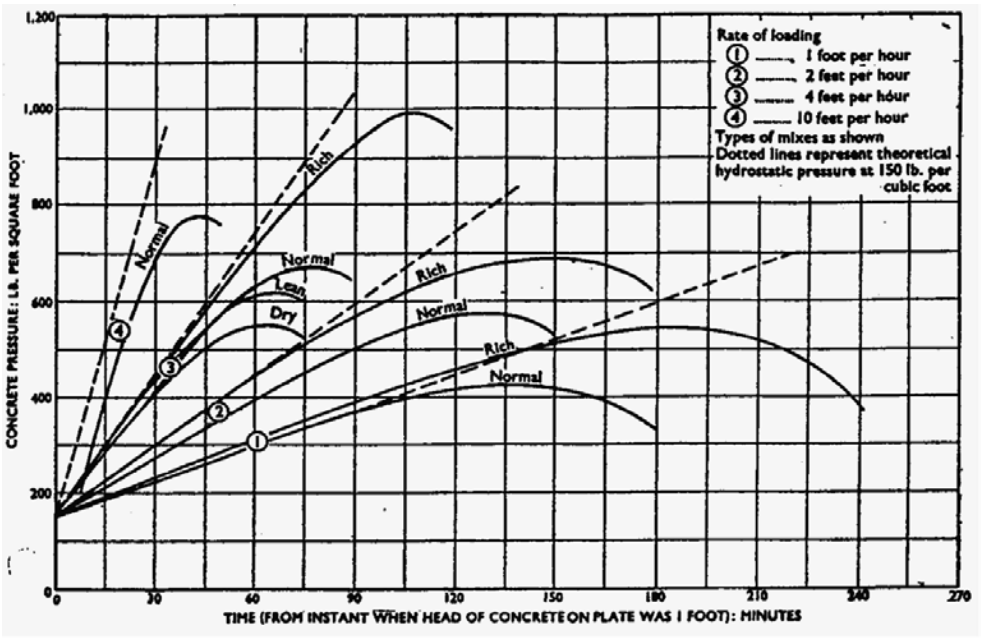

Figure 3.18: Casting Rate Effect on Formwork Pressure as reported by Roby (1935)

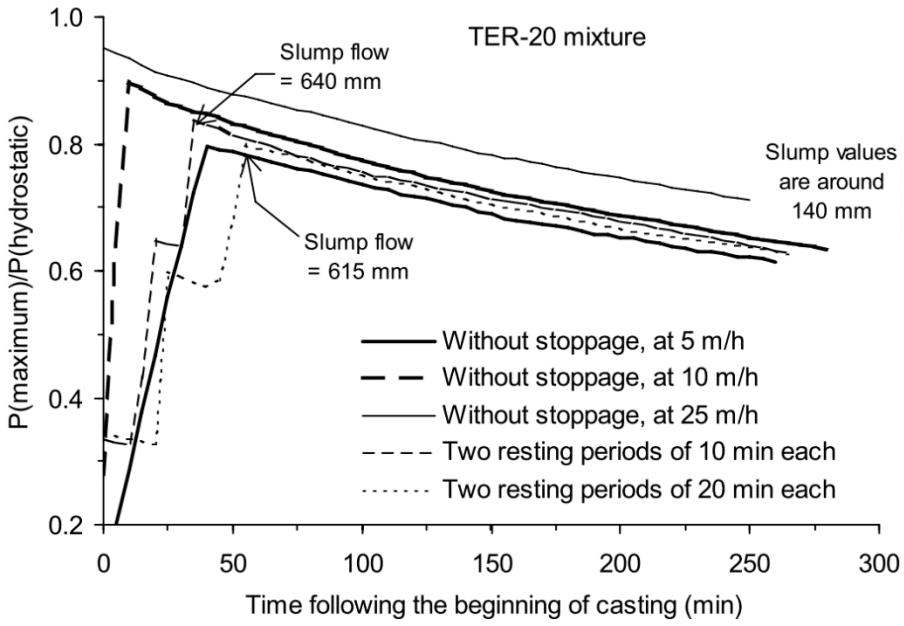

Figure 3.19: Casting Rate Effect on Formwork Pressure (Assaad and Khayat 2006)

- ***Placement Method***

The placement method affects the magnitude of the lateral pressure. Brameshuber and Uebachs (2003) investigated the lateral pressure on a full scale wall with a total height of 3.3 m, width of 3.51 m and thickness of 0.24 m (Figure 3.20). Five walls were cast, two with SCC being poured from top at a rate of 2 and 10 m/h, two with SCC being pumped from bottom at a rate of 2 and 10 m/h and one with CVC being poured from top at a rate of 7.5 m/hr. Results of this investigation are presented in Figure 3.21, SCC pumped from bottom developed a high relative pressure that is close to hydrostatic and almost twice the one resulted from pouring SCC from top. CVC poured from top showed a relative pressure close to hydrostatic pressure. Lower the casting rate while pumping concrete from bottom required higher pumping pressure.

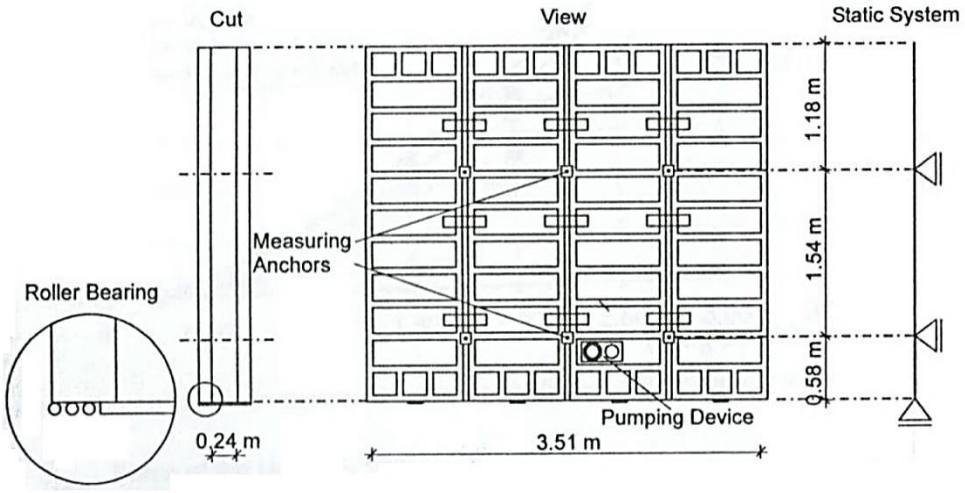

Figure 3.20: Test Setup as proposed by Brameshuber and Uebachs (2003)

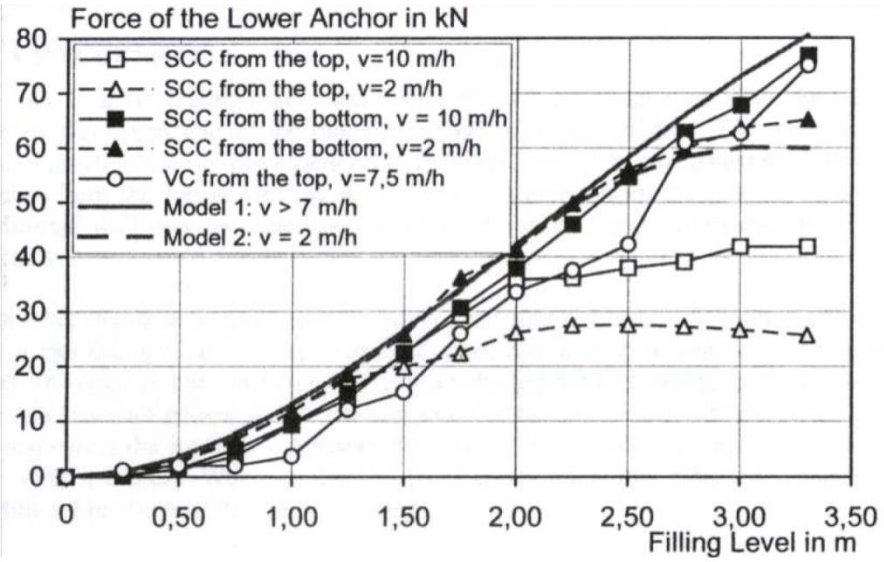

Figure 3.21: Relationship of the Force of the Lower Anchor vs. Rate of Casting as reported by Brameshuber and Uebachs (2003)

- ***Ambient Temperature and Concrete Temperature***

Roby (1935) reported that the developed pressure will be less in hot weather as compared to the one developed during moderate temperature, he reported that a concrete mixture poured at 38 ^{o}C developed 60%-75% less than the same mixture poured at 16^{o}C. Figure 3.22, represents the results for relative pressure for different concrete temperatures obtained by (Assaad and Khayat 2006), three temperatures were used for this comparison (30, 20 and 10 ^{o}C), it was reported that concrete with different temperature developed the same initial lateral pressure but the pressure decay is highly effected by the temperature, for example concrete with a temperature of 30^{o}C (TER-30) had the highest rate among the three mixtures.

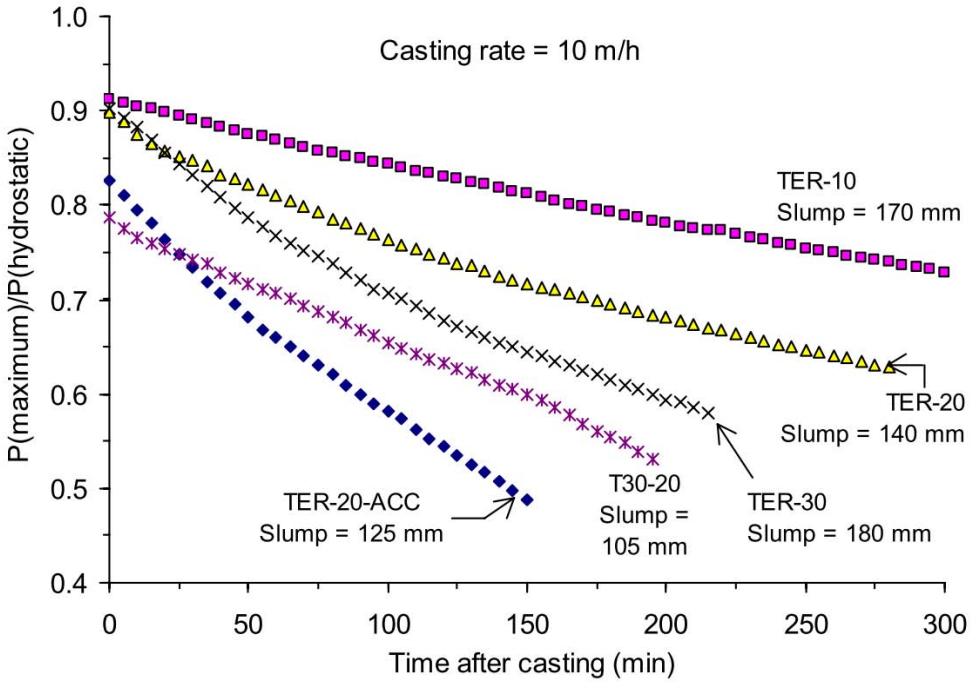

Figure 3.22: Variations in Relative Pressures as a Function of Temerature (Assaad and Khayat 2006)

Formwork Characteristics

- ***Formwork Dimensions***

Rodin (1952) reported that smaller cross sections will develop lower pressure. Recently, Khayat et al. (2005A) evaluated formwork dimensions effect by using two columns of 920 mm and 200 mm diameter, it was found that the initial relative pressure was very close for both columns (99% and 96%) for 920 and 200 mm column respectively (Figure 3.23), however, the pressure drop was found to be higher in case of 920 mm column.

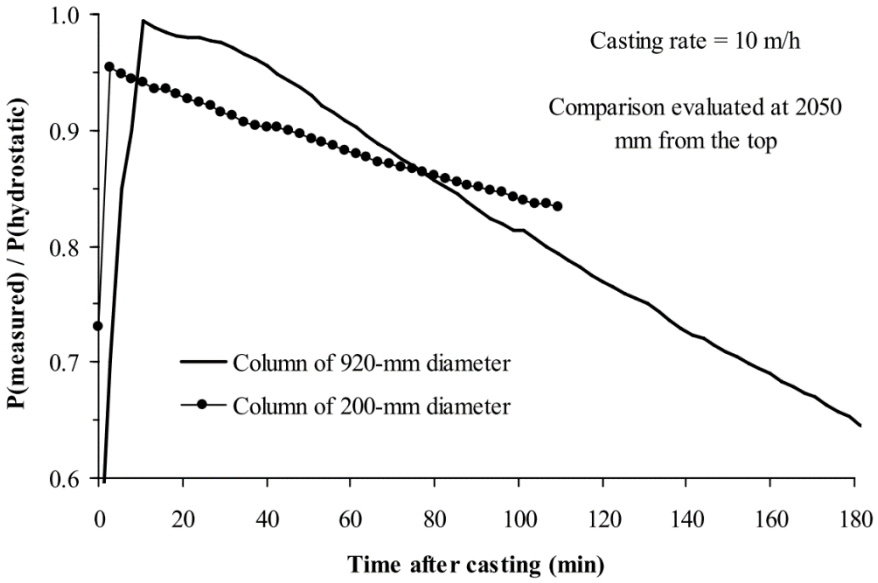

Figure 3.23: Section Width Effect on Formwork Pressure (Khayat et al., 2005A)

- ***Presence of Steel Reinforcement***

The presence of rebars can reduce the lateral pressure since it can prevent further movement of concrete within the formwork, on the other hand, this positive effect can be cancelled in case of increased vibrating (Rodin 1952).

- ***Formwork Surface Material***

Arslan et al. (2005) investigated the effect of the formwork surface material type on the resulting lateral pressure. Seven walls were made for this study with a thickness of 0.15 m, 1 m in length and 2 m in height (Figure 3.24).

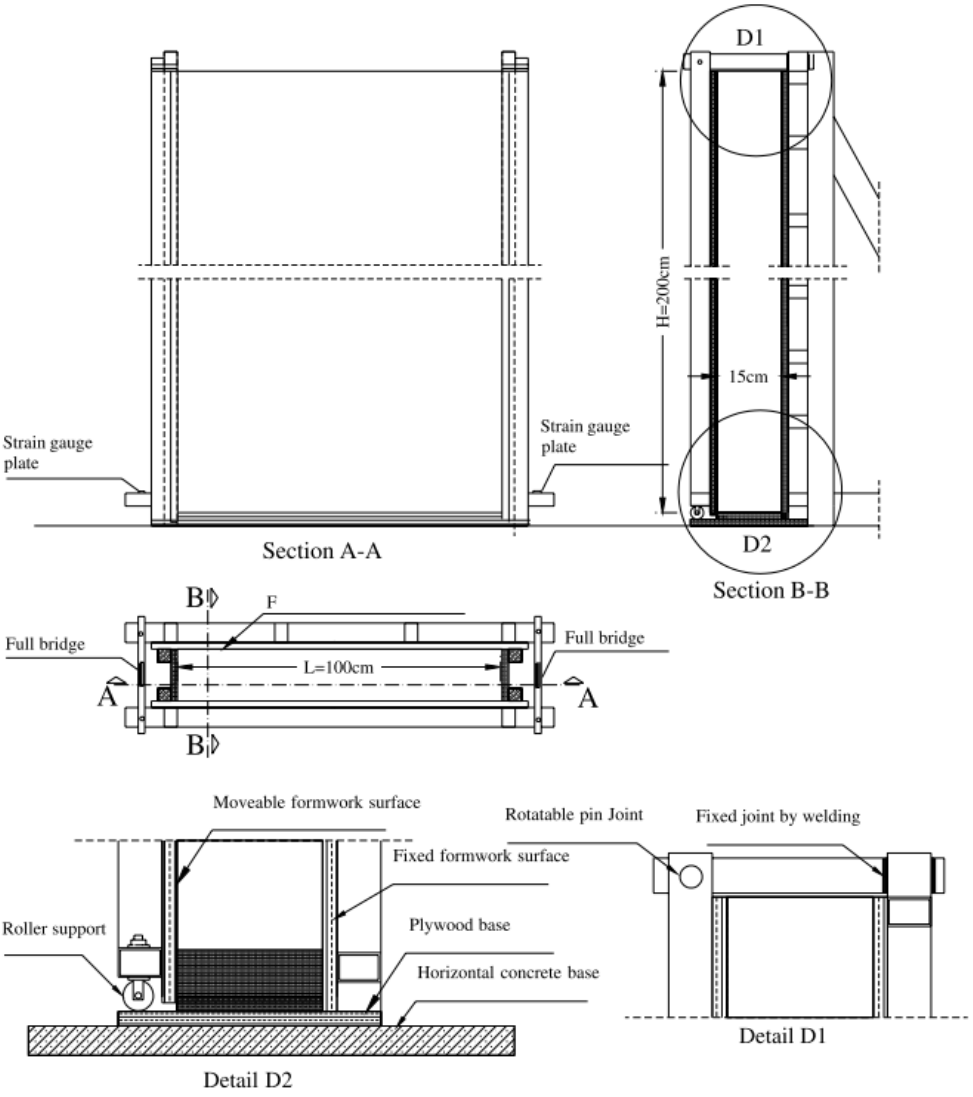

Figure 3.24: Formwork Details of Arslan et al. (2005)

Four materials were selected for testing (Table 3.3), form release agent was applied on all surfaces, except for steel, and one of each pair of material was watered before testing. The limiting value of pressure by three different standards was calculated and listed in Table 3.3. Reported tests results showed that watered surface developed higher lateral pressure; lateral pressure on steel was reported to be the highest and almost equal to the limiting value provided by ACI 347.

Table 3.3: Lateral Pressure on Formwork Surface (kPa) (Arslan et al. 2005)

Formwork code and surface process	Lateral Pressure (KPa)		
	Mean	Minimum	Maximum
F1 Populus Nigra (watered)	22.85	21.77	23.74
F2 Populus Nigra	20.93	19.94	21.88
F3 Pinus Silvestris (watered)	23.68	21.39	25.11
F4 Pinus Silvestris	19.91	18.01	21.15
F5 Plywood (watered)	24.55	22.47	25.96
F6 Plywood	21.48	19.22	22.81
F7 Steel	26.19	24.70	26.97
Limiting value of ACI 347			26.92
Limiting value of CIRIA			30.98
Limiting value of DIN-18218			30.98

- ***Formwork Drainage***

Arslan (2002) studied the effect of the presence of the draining system on formwork lateral pressure. He concluded that by applying drainage to the formwork surface and covering the surface with a special lining material the pressure exerted by concrete can be decreased by 40%.

3.3.2 Empirical Models to Predict Formwork Pressure

Many researchers have developed and proposed models to predict the formwork pressure exerted by both normal conventional concrete and self-compacting concrete, Khayat et al. (2007) summarized these models. ACI models will be explained in the following paragraphs.

ACI Committee 622 (1952) currently designated as ACI347 “Formwork for Concrete” proposed that the diagram for lateral pressure exerted by concrete is trapezoidal in shape, this diagram is presumed to be triangular from the upper free end up to certain depth after which the pressure is considered constant. The variables considered in this model are listed below followed by the proposed equations; placemen rate and method, coarse aggregate

concentration, aggregate nominal size, consistency level, form work size and shape, compaction method, pore-water pressure, concrete temperature, concrete head, cement type and content and finally, the smoothness and permeability of formwork material.

For wall element

R < 2.14 m/h

$$P_{max} = 7.19 + \frac{785R}{17.78 + T} < 95.8 \; or \; 23.5H \quad \text{Eq. 3. 1}$$

2.14 < R < 3 m/h

$$P_{max} = 36 + \frac{244R}{T + 17.78} \quad \text{Eq. 3. 2}$$

$$P_{max} = 7.19 + \frac{1156}{T + 17.78} + \frac{244R}{T + 17.78} < 95.8 \; or \; 23.5H \quad \text{Eq. 3. 3}$$

R > 3 m/h

$$P_{max} = 23.5H < 95.8 \quad \text{Eq. 3. 4}$$

For column element

$$P_{max} = 7.19 + \frac{785R}{17.78 + T} < 143.7 \; or \; 23.5H \quad \text{Eq. 3. 5}$$

For walls and column

$$P_{max} = \gamma_c H \quad \text{Eq. 3. 6}$$

where:

P_{max}: maximum lateral pressure (kPa)
R: rate of casting (m/h)
T: Concrete temperature (^oC)
H: Head of concrete (m)

Note: These formulas are used only for normal internal vibration, immersion of vibrator ≤ 1.2 m in fresh concrete, Type GU cement, no pozzolans or admixtures, γ_c = 2,400 kg/m 3 , slump ≤ 100 mm at time of casting, and any required re-vibration is allowed only in plastic stage;

Later in 2002 Hurd realized that these equations are too conservative to be used now, as it is becoming too expensive. Hurd (2002) proposed to apply coefficients to ACI equations in order to account for unit weight, supplementary cementitious materials and the presence of chemical admixtures:

For wall and columns

R<2.14 m/h

$$P_{max} = C_W C_C \left[7.19 + \frac{785R}{17.78 + T}\right] \quad \text{Eq. 3. 7}$$

$$30C_W(kPa) \leq P_{max} \leq 150C_W C_C(kPa) \; , \; P_{max} \leq \gamma_c H$$

where:

γ_c: Unit weight of concrete (kg/m^3)
H: Head of concrete (m)
P_{max}: maximum lateral pressure (kPa)
R: rate of casting (m/h)
T: Concrete temperature (^oC)
C_W: Unit weight coefficient calculated as below:

$$C_W = 0.5\left[1 + \frac{\gamma_c}{23.2}\right] \; but \geq 0.8 \qquad for\ \gamma_c < 2240\ kg/m^3$$

$$C_W = 1 \qquad for\ 2240\ kg/m^3 < \gamma_c < 2400\ kg/m^3$$

$$C_W = \frac{\gamma_c}{23.2} \qquad for\ \gamma_c > 2400\ kg/m^3$$

C_C: chemistry coefficient calculated as follows:

C_C = 1.0 for cement Type GU or HE without retarder

C_C = 1.2 for blended cement without retarder (blended means: Type GU cement with < 70% slag or < 40 % fly ash replacements).

C_C = 1.4 for blended cement with retarder (retarder refers to set retarder, water-reducing agent, or superplasticizer).

3.3.3 Theoretical Models to Predict Formwork Pressure

Gallego et al. (2010) have developed a finite element model (FEM) to assess the formwork pressure due to normal concrete. The results obtained from this model was promising and the model was validated using some experimental values from Arslan et al. (2005). Some fresh concrete mechanical properties were incorporated in this model, this includes, angle of internal friction, dilatancy, cohesion, Poisson coefficient, modulus of elasticity, and the concrete-to-wall friction coefficient.

A 3-D numerical was developed later by Gallego et al. (2011), they used ANSYS finite element program in their simulation. The model was intended to simulate fresh concrete behavior and the formwork walls in order to find the lateral pressures for a complex-shaped formworks. It has been highlighted that an influence due to the inclination of the formwork on the lateral pressures does exist.

Comparison of formwork pressures are shown in Figure 3.25 as reported by Gallego et al. (2011), this was done for the formwork wall shown in Figure 3.26. Their results show that

the maximum lateral pressures are lower than the ones suggested by the some international standards.

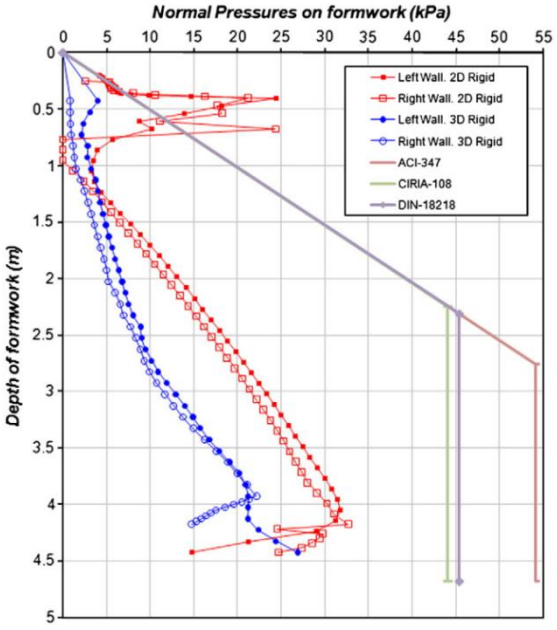

Figure 3.25: Normal Pressure at Different Points Along the Depth for Different Models and Equations (Gallego et al. 2011)

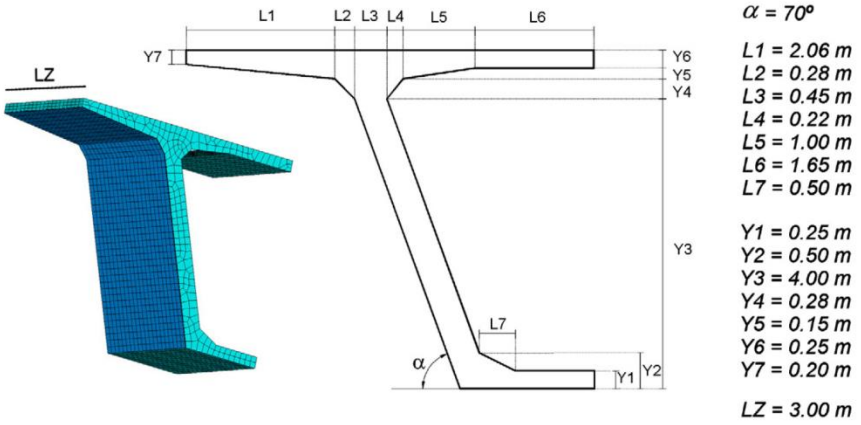

Figure 3.26: Formwork Geometry used by Gallego et al. (2011)

Ovarlez and Roussel (2006) have presented a physical model for the prediction lateral stress exerted by self-compacting concrete during and after casting. It was justified based on a theoretical point of view. SCC was considered to be characterized by a yield stress

τ_0 (increasing with the resting time). For simplicity, they considered the yield criterion as Tresca criterion (with τ_0 as the maximum shearing stress). Thus, SCC is being treated as an elastic material below this stress level.

Starting with the basics of elastic theory, linear relation between stress tensor components σ_{ij} and strain tensor components ε_{ij} were given below

$$E\varepsilon_{ij} = (1 + \upsilon_p)\sigma_{ij} - \upsilon_p \delta_{ij}\sigma_{kk} \qquad \text{Eq. 3. 8}$$

Where, *E* is the modulus of elasticity, and υ_p the Poisson's ratio. Imposing the Tresca boundary conditions everywhere at the walls,

$$\tau_{xz}(L/2\,, y, z) = \tau_{yz}(x, e/2, z) = \tau_0 \qquad \text{Eq. 3. 9}$$

And infinitely rigid walls, the displacement boundary conditions give

$$u_x(\pm L/2\,, y, z) = u_y(x, \pm e/2, z) = 0 \qquad \text{Eq. 3. 10}$$

Using the stress-strain relation Eq. 3. 5 and internal equilibrium relation, $\sigma_{ij,i} = -\rho g_j$ they arrived at the expressions below.

$$\sigma_{zz}(z) = (-\rho g + 2\tau_0(1/L + 1/e))z \qquad \text{Eq. 3. 11}$$

$$\sigma_{xx}(z) = \sigma_{yy}(z) = K(-\rho g + 2\tau_0(1/L + 1/e))z \qquad \text{Eq. 3. 12}$$

$$\tau_{xz}(x, y, z) = -2\tau_0\, x/L \;\; and \;\; \tau_{yz}(x, y, z) = -2\tau_0\, y/e \qquad \text{Eq. 3. 13}$$

Where ρ is the mass density, and *K* is the Janssen parameter (the ratio of horizontal to vertical stresses which is less than 1). Finally, they reported that the maximum pressure during casting for the rectangular and circular section as follows

For a rectangle having a width e

$$\sigma_{xx} = \sigma_{yy} = K\left[\rho g H - \frac{(H - e)^2 A_{thix}}{eR}\right] \qquad \text{Eq. 3. 14}$$

For a circle having a radius r

$$\sigma_{xx} = \sigma_{yy} = K\left[\rho g H - \frac{(H-r)^2 A_{thix}}{rR}\right] \qquad \text{Eq. 3. 15}$$

Where A_{thix} is the flocculation coefficient, ρ is the mass density and K is the Janssen parameter.They have validated their model using experimental data obtained from Billberg (2003) and Khayat et al. (2005) (see Figure 3.27). The casting rate effect on the formwork lateral pressure can be clearly seen in Figure 3.27.

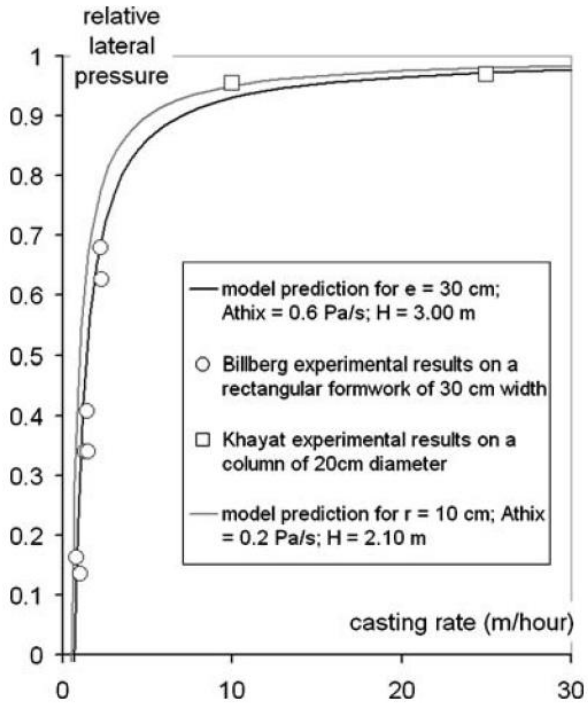

Figure 3.27: Results Obtained by Ovalez and Roussel (2006).

3.4 Background in Pumping

One of the techniques that have helped and still heling the construction industry is concrete pumping. In simple words, pumping is the way to put the concrete where it needs to be placed in a formwork using a machine to transfer the liquid concrete. Concrete pumping is an applied casting method that enables fast and efficient concrete placement (Feys 2010). ACI (2000) defines pumped concrete as concrete that is transported through rigid or

flexible pipeline by means of a pump, and Jolin et al. (2006) defined the pumpability as the ability of confined concrete to flow under pressure while maintaining its initial properties.

The concept of concrete pumping exited since 80 years, considerable improvements and technologies were introduced since that time and particularly in the pumps (Kaplan 2005). Concrete now can be pumped using a 70 m long boom pump. On the other hand, a much longer distances were recorded when a stationary pump is in use, for example, in Burj Khalifa (Dubai/UAE) the records confirms that the concrete was successfully pumped to a height of 606 m. The boom pump is normally used in small jobs that can last for short period of time, while the stationary pump is normally placed where a large volume of concrete is going to be placed as in skyscrapers.

Kaplan (2005) has summarized the advantages of concrete pumps in construction as follows:

- Rapidity of placement (a pump can convey between10 and 150 m3/h of concrete depending on its size, power plant, and type of concrete);
- Concreting can be performed where access is difficult(for example, in tunnels);
- The rate of placement is constant so concrete crews can be used more efficiently.

The concrete pump consists of a hopper which receives the concrete from the mixer and then delivers it to the pump itself which will push the concrete into the pipeline to the pouring point. There are two main types of concrete pumps to transport the concrete from one point to another; piston (direct acting) concrete pumps and rotary or squeeze type pumps.

3.4.1 Piston (Direct Acting) Concrete Pumps

The majority of the concrete pumps available in the market are of this type. The operation of such pump is simple. The concrete is fed into the hopper by gravity and partly by suction. This suction is created by the rotary motion of the horizontal piston, at this time, both of the semi-rotary valves open and close alternately (if one is closed the other is open and Vis versa).

Figure 3.28 shows a simple piston pump, two types of strokes exist in this system; the first one is called the suction stroke. During this stoke, the inlet valve opens and concrete is allowed to go into the pumping cylinder, at this stage the outlet valve remains closed. The second stroke is called the delivery stroke. During this stroke, the inlet valve closes and the outlet valve gets opened, due to that, the concrete is forced into the delivery pipeline. With a series of these impulses, the concrete will keep moving in the pipe and the pipe will remain full. Similarly, a more advanced type of this pump is shown in Figure 3.29. The two pistons pump works by filling one cylinder while emptying the other one and this is done through valve shifting opening towards the feeder (inlet) and shutting towards the pipe (outlet). This will push the concrete towards the delivery pipeline. Single piston pumps can transport concrete up to a maximum distance of 1000 m horizontally or 120 m vertically (Neville 1995).

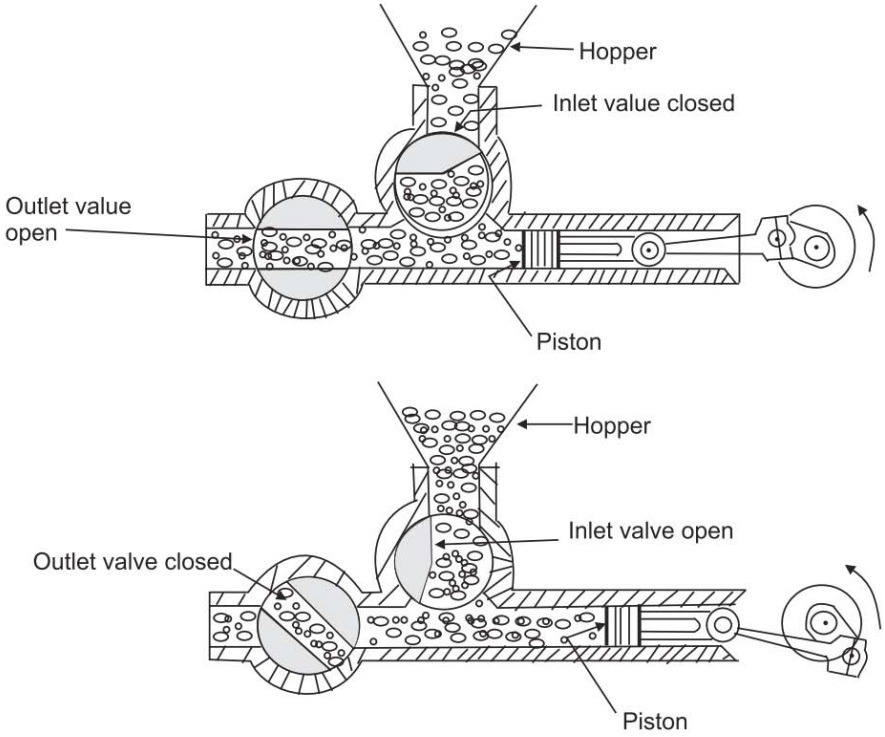

Figure 3.28: Single Cylinder Piston Pump (Neville 1995)

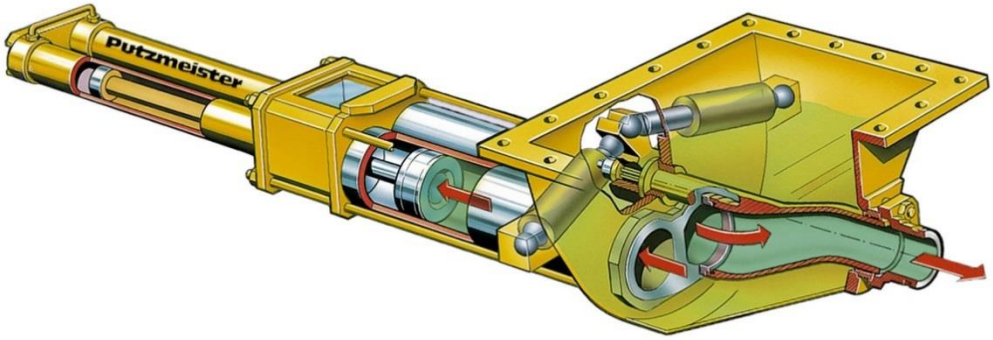

Figure 3.29: Double Cylinder Piston Pump (PMW Central Services 2011)

3.4.2 Squeeze Pump

Squeeze pump (portable peristaltic pump) is shown in Figure 3.30. The concrete is fed into the hopper, and by the use of a rotating blades, the concrete is pushed into a flexible pipe connected to the pumping chamber. This chamber is under vacuum, and this vacuum will

keep the section of the pipe circular, except when being squeezed by the rotating rollers, this will ensure a continuous concrete flow. The rotating rollers mounted on planetary drives are responsible for squeezing the flexible hose which will push the concrete into the delivery pipe. Squeeze pumps can transport concrete up to a maximum distance of 90 m horizontally or 30 m vertically (Neville 1995).

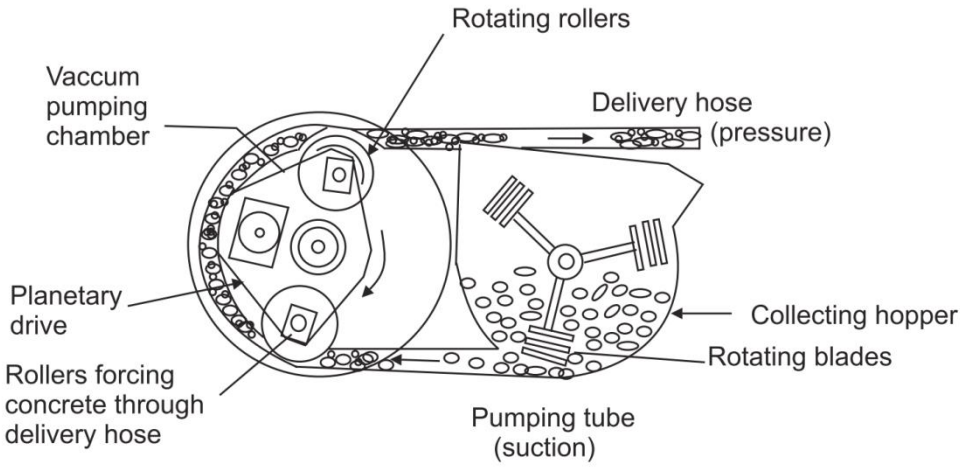

Figure 3.30: Squeeze Pump (Neville 1995)

3.5 Pumping Guidelines

Spiratos et al. (2003) defined two basic properties of pumpability; sufficient paste content so that there is enough grout for a slip layer, and a suitable grout consistency and structure between aggregate grains to hinder forced or pressurized bleeding due to pump pressure.

To produce a pumpable concrete, a set of criteria should be satisfied; it should be viscous enough to satay homogenous throughout the pipe, but at the same it should not be to viscous so it does not deform when facing a change in direction such as elbows.

Since the beginning of the last century, the slump test is the most popular on site concrete workability test. Several pumping guidelines were given by pumps manufacturers and

researchers, an early recommendation by Stephenson (1968) was that a slump less than 50 mm gives an unpumpable concrete, slump between 50 and 100 mm ensures pumpability and finally a slump more than 100 mm gives an unpredictable pumpability. Some empirical relationships exist in the form of diagrams to relate the slump to the other pumping parameters.

In Figure 3.31, Sakuta (1989) developed an empirical diagram to relate the effect of fresh concrete slump on the pressure drop per linear meter as a function of the flow rate for 100 mm and 125 mm pipe diameters.

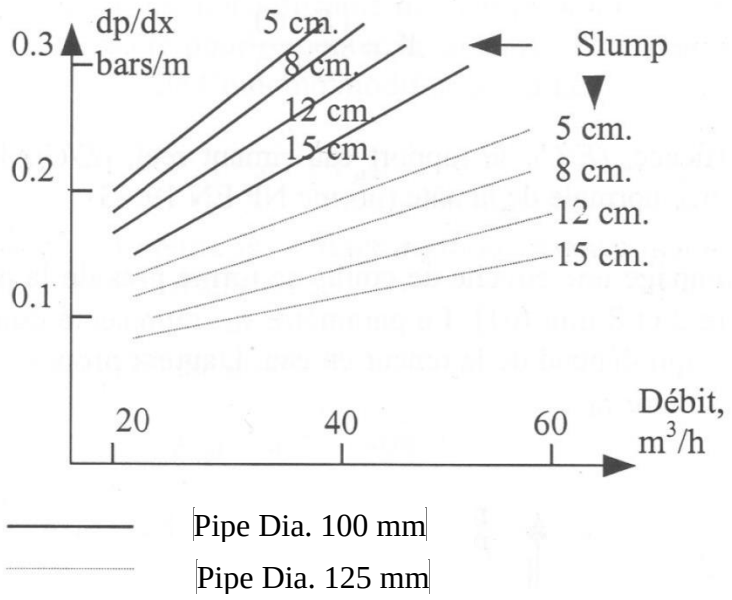

Figure 3.31: Diagram to Relate Slump and Pressure Drop (Sakuta 1989).

Another diagram developed by ACI (1995) is shown in Figure 3.32. In the beginning, the placing capacity selected, and then based on the pipe line diameter, pipeline length, and concrete slump the required pumping pressure is found. After the pressure value is found, an addition pressure should be added according to the details shown on the diagram.

A third diagram developed by PMW Central Services (2011) is shown in Figure 3.33. This diagram is made to determine the require pump power based on the require flow rate, slump, pipeline length and diameter.

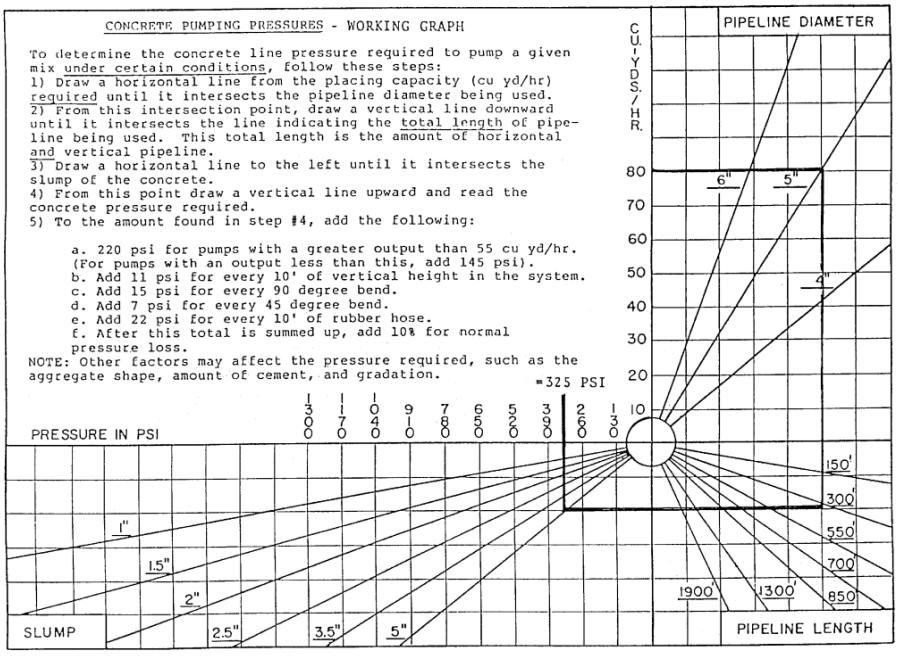

Figure 3.32: Diagram to Determine the Required Pumping Pressure for a Data (ACI 1995)

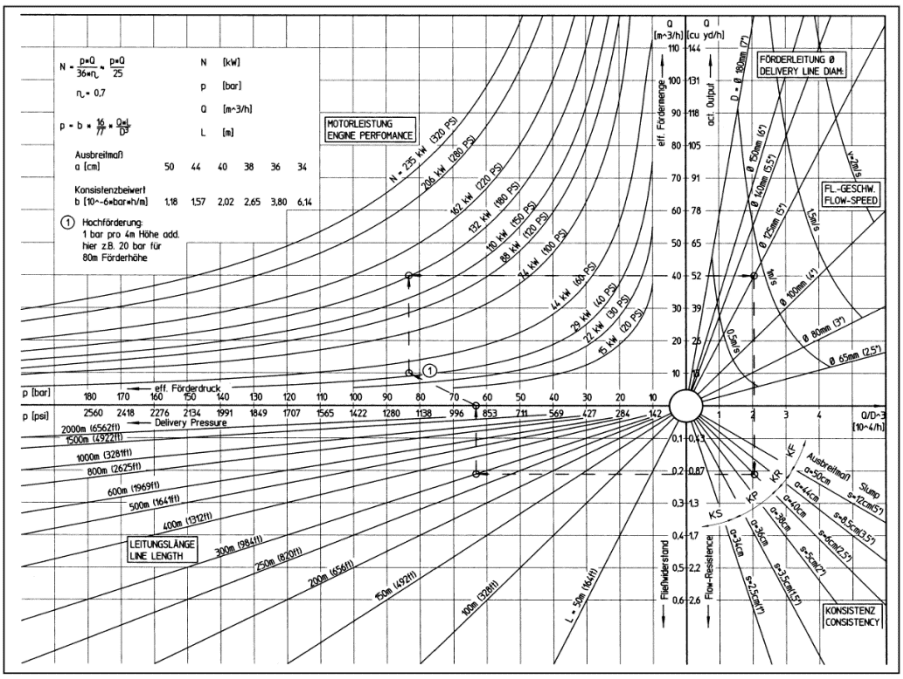

Figure 3.33: Diagram to Determine the Required Pump Power (PMW Central Services 2011)

3.6 Pumping Problems at Site

In order to understand what happens to the concrete when it is pumped through pipeline, it necessary to cover all the fundamentals of concrete pumping. Pumpable concrete moving in the pipeline flows in the form of a plug separated from the pipe walls by a thin lubricating layer consisting mainly of cement paste (Figure 3.34).

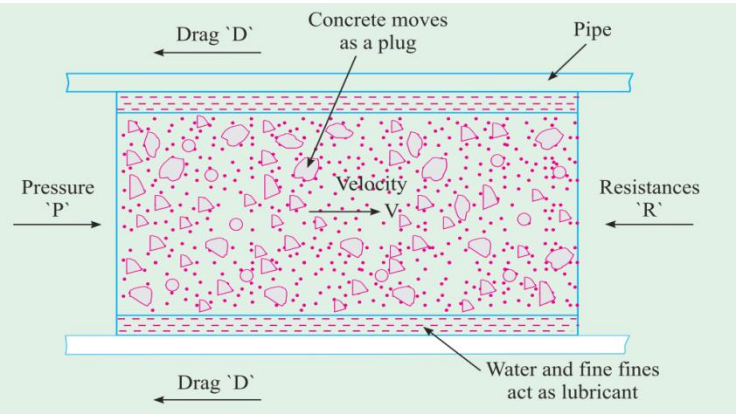

Figure 3.34: Concrete Flow Under Pressure (Shetty 2005)

In order to have a continuous plug movement, the pressure generated by the flow resistance should be lower than the pump pressure rating. Therefore, the concrete should not be too stiff which will require a pressure higher than the pump rating or too soupy (has a high w/c) which will cause the water to go in front of the mix and cause blockage (Figure 3.35).

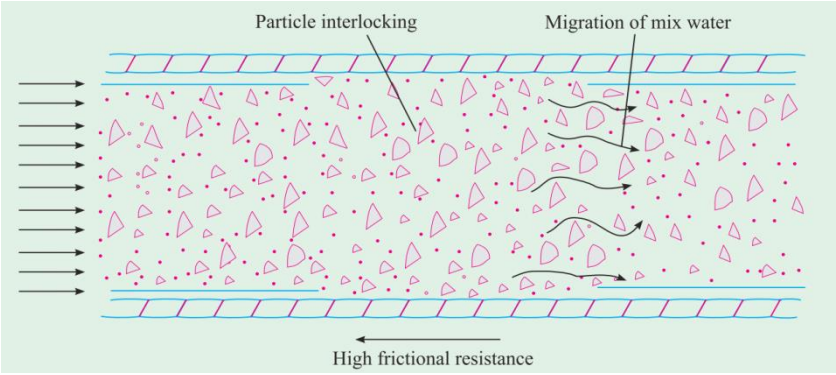

Figure 3.35: Water and Paste Getting Separated from the Mix (Shetty 2005)

Whether we are talking about normal slump concrete or SCC, the problems occurring at the job site are almost the same? If the human error is eliminated, two sources of problems in the pumping process can be addressed; pipeline setup and concrete mix design. Pipeline setup might be too complicated for the concrete to go through, for example, too many elbows, the long horizontal distance and the vertical distance can lower the velocity of the flow. This will require a higher pumping pressure to overcome these losses. On the other hand, the concrete mix design have a significant role in pumping process, for example, a very viscous mix will require a high pumping pressure and might block the pipeline.

The main problems in pumping process can be summarized as follows:

1. **Blockage:** It is defined as stop or delay in the flow of concrete which normally accompanied by elevated pumping pressure. Blockage can happen due to the escape of the water from mixture which prevents the transfer of the pressure to aggregate. On the other hand, the presence of high paste content will increase the friction resistance of the mix and the pressure exerted by the pump will not be sufficient to move the concrete.
2. **Segregation:** The separation of large particles from the paste can occur due to many reasons, such as high w/c, which cause the paste to go in front and leave the coarse aggregate behind. Similarly, poorly graded mix can have such problem.
3. **Loss of Air Content:** using pumping systems to transport concrete will result in loss of air as reported by Jolin et al. (2009). He reported two mechanisms by which the air is lost; suction and dissolution.

4. **Pressure Loss:** During pumping, the initial pressure given at the starting point will not remain the same due to pipeline arrangements such as, the length, the height and number of elbows. On the other hand, the viscosity of the mix itself can also lower the pressure.

The main difference between normal slump concrete and SCC in the fresh state is that SCC has a very low yield stress which allows it to spread without the need for any vibration.

Although normal slump concrete and SCC are not the same, but still it being pumped in the same way same guidelines being followed. In the following paragraphs the rheological behavior of SCC will discussed in order the flow behavior of SCC in pipelines.

3.7 Parameters Influencing Pumping Pressure

3.7.1 Viscosity and Yield Stress

It has been agreed by many researchers that concrete can be treated as a Bingham material with a plastic viscosity and yield stress. Yield stress is defined as the critical applied stress, beyond which the material will start to flow; Viscosity is a measure of the material's resistance to flow (beyond the yield stress). Using rheometers like the ICAR rheometer, plastic viscosity and yield stress can be easily measured.

Plastic viscosity and yield stress are not constant but changing with time due to the thixotropic nature of concrete (Feys 2010).

The simple form of Bingham model can be written as

$$\tau = \tau_0 + \mu_P . \dot{\gamma} \qquad \text{Eq. 3. 16}$$

Where τ is the shearing stress in (Pa), $\tau_0$is yield stress in (Pa) μ_p is the plastic viscosity in (Pa s) and $\dot{\gamma}$ is the shear rate in (s^{-1}). Figure 3.36 shows a graphical representation of Bingham model. The physical explanation of this model is that to put a Bingham fluid in motion, a minimum force is require to trigger the flow and exceed the yield stress (τ_0). Once the material started to flow, the force increment required to deform the concrete is proportional to the shear strain (shear rate $\dot{\gamma}$) increment applied and is attributed to the plastic viscosity term (Jolin et al. 2009)

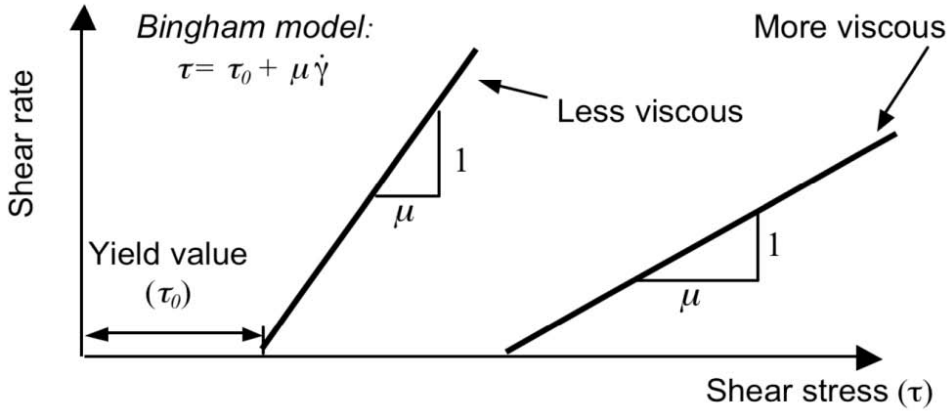

Figure 3.36: Graphical Representation of Bingham Model (Jolin et al. 2009)

Hansen (1988) conducted a large scale study of Bingham parameters versus pumpability. Bingham parameters were measured using a coaxial viscosimeter and pumpability was measured as the pressure in hydraulic oil of a concrete piston pump. The test was done on a highly flowable concrete mix of a slump of 190-240 mm. Their results confirmed that yield stress and plastic viscosity are related to hydraulic oil pressure. The increase in the yield stress caused the oil pressure to increase in order to maintain the same pumpability. On the other hand, increased slump (a more flowable mix) showed a relation of reduced oil pressure. The measurements of yield stress that were taken before and after pumping showed an increase due to pumping.

In conclusion of the study done by Hansen (1988), it was recommended that pumpable concrete should have the minimum possible yield stress and plastic viscosity without losing the stability. Also, he concluded that the largest effect of rheology on pumpability of concrete was expected for pipes with diameter, high pump flow and horizontal pipes having many bends.

3.7.2 Lubrication Layer

During the process of pumping, some components of the concrete mixture namely, the fine materials and some droplets of water travel from the middle of the pipe toward the walls creating a lubricating layer. The presence of this layer will prevent coarse aggregate from entering in solid to solid contact with the steel pipe wall (Khatib 2013).

Khatib (2013) stated that failure to build a lubrication layer will eliminate the lubrication effect at the pipe wall and will drastically increase the friction and the required pumping pressure.

Browne and Bamforth (1977) defined two situations to describe how the concrete interact with the wall of the pipe. In the first situation (as explained by Feys 2013), transfer of stresses is dominated by the friction between coarse aggregate, and hence, the required force to push the concrete is related to this friction and this is defined as unsaturated concrete. An example of this kind of concrete was given by (Feys 2013) in Figure 3.37 (b). In this case unsufficient amount of paste was available to lubricate the aggregates. And according to Browne and Bamforth (1977), the pressure decreases exponentially with pipe length as shown in Figure 3.38 (b).

On the other hand, when enough amount of paste is available, coarse aggregate will not be in direct contact and cement paste will be the lubricating material in which the shearing will occur (Feys 2013). Browne and Bamforth (1977) define this situation as saturated concrete, Feys (2013) represented this this type of concrete in Figure 3.37 (a). In this case the pressure decreases linearly with pipe length as shown in Figure 3.38 (a).

(a) Saturated (b) Unsaturated

Figure 3.37: Saturated and Unsaturated Concretes (Feys 2013)

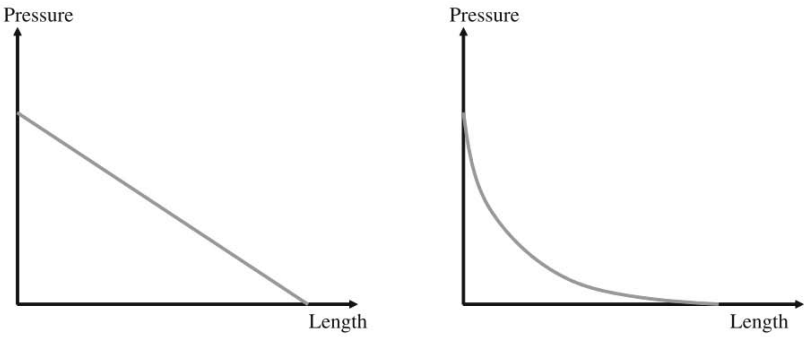

(a) Saturated (b) Unsaturated

Figure 3.38: Pressure Decrease with pipe Length in Saturated and Unsaturated Concretes (Feys 2013)

3.7.3 Pipeline Arrangement, Horizontal and Vertical Distances and the Presence of Bends

As a role of thump, the longer the horizontal distance that concrete travels, the higher the drop in the pumping pressure. In the same manner vertical distance will also cause a drop in the pumping pressure, but in this case it would be higher due to gravity which works in the opposite direction.

Bends on the other hand, will have a great effect on the pumping pressure. Many pumping standards and pumping manufacturers have given an approximate estimation of the pressure drop due to the presence of elbows in the pumping circuit as compared to a horizontal distance. Schwing (1983) as pumping manufacturer, stated that a 90^{o} bend will cause a drop in pressure that is equivalent to the drop caused by a 3 m horizontal distance. It should be also highlighted that the pipe material has an impact on the pressure drop. A rubber pipe will induce higher friction force compared to steel pipe which will cause a larger drop in pumping pressure.

3.8 Simulation of Concrete Pumping

Part of understanding the rheology of SCC is to understand the fundamentals of flow of SCC in pipes aiming to reduce the required pumping pressure and avoid the problems related to pumping such as segregation and blockage. In order to have a solid background in this subject, recent concrete pumping research are summarized and understood to ensure having proper research plan and clear goals.

Feys (2009) in his PhD thesis entitled “Interactions between Rheological Properties and Pumping of Self-Compacting Concrete” has investigated the major aspects related to concrete pumping. He made a full-scale pumping test for three different pipe arrangements with a total length of 25, 81 and 105 m with an inner diameter of 106 mm (Figure 3.39, Figure 3.40 and Figure 3.41) a number of bends were included in the design of the proposed circuits in order to account for losses caused by their presence.

The pipes were arranged in a closed circuit so that the concrete is used for more than one cycle. These circuits were utilized to determine the relationship between rheological properties and pumping pressure.

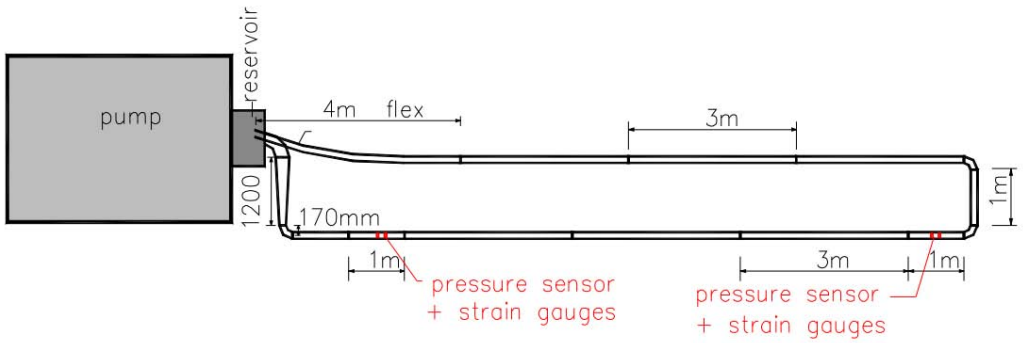

Figure 3.39: Design of the 25 m Long Circuit and Position of the Measurement Sections (Feys 2009)

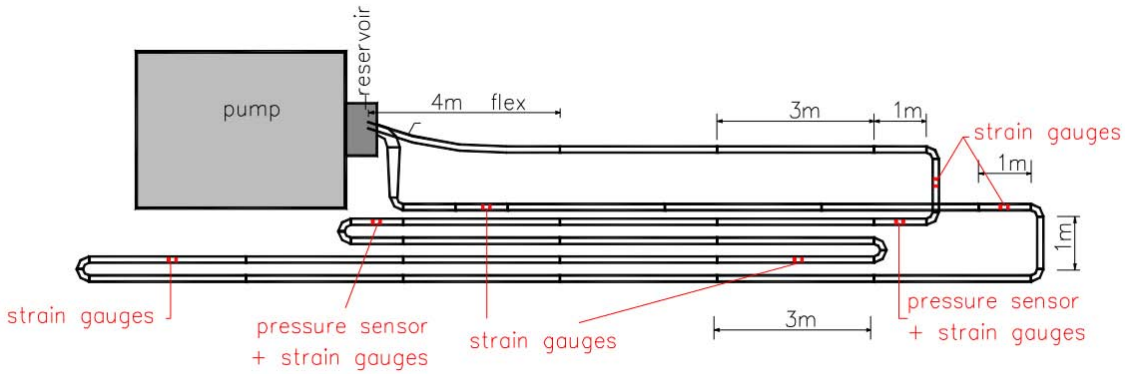

Figure 3.40: Design of the 81 m Long Circuit and Position of the Measurement Sections (Feys 2009)

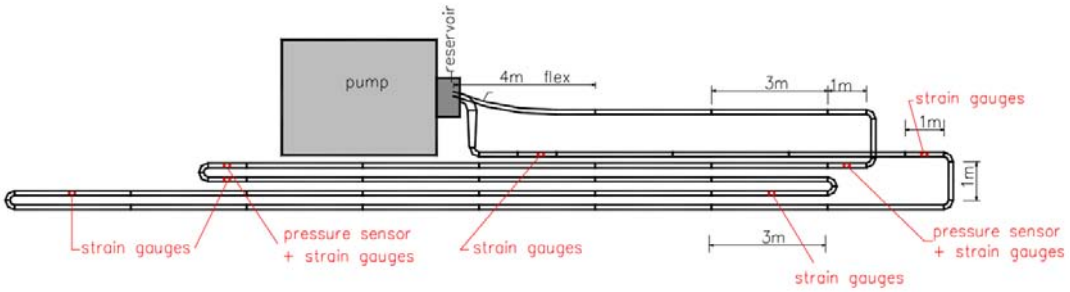

Figure 3.41: Design of the 105 m Long Circuit and Position of the Measurement Sections (Feys 2009)

The pump used in these tests was a truck-mounted type, capable of delivering a pressure of 95 bar or a discharge rate of 150 m^3/h. Internally, the pump has two pistons which alternately pull the concrete form the concrete reservoir and push it in to the pipe, this process includes a sudden short change in pressure (increase or decrease) called stroke which can clearly hear during pumping.

To measure the pressure loss at different points, pressure sensors and strain gauges were installed at these points, pressure sensors were the primary source of data while the strain gauges served as a backup system in case of failure of the sensors.

Figure 3.42 shows the upstream pressure evolution as a function of time, test begun with a high flow which was decreased gradually.

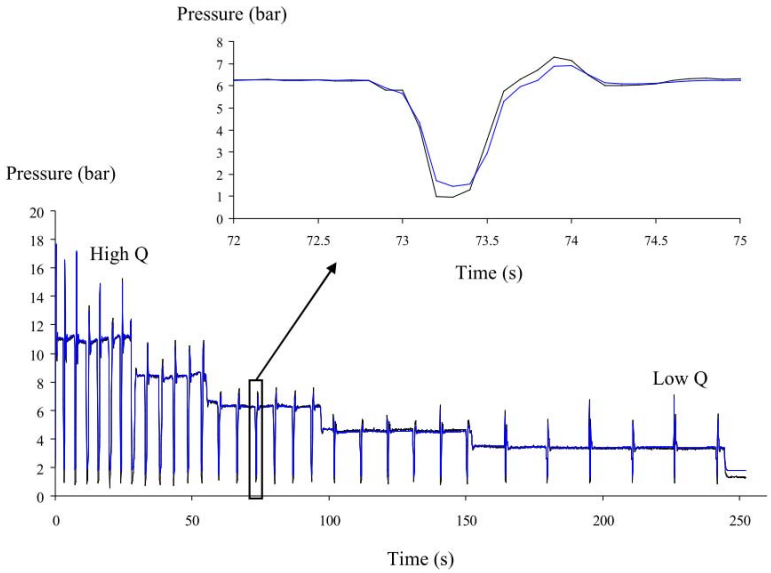

Figure 3.42: Upstream Pressure Evolution as a Function of Time (Feys 2009)

Nineteen concrete mixes were tested in this study of which 18 mixtures were SCC and one was a pumpable CVC. At the time of testing, all fresh SCC test were done including the rheological tests.

Pressure loss was related to the rheological parameters and other SCC test results. Figure 3.43and Figure 3.44 shows some of these results.

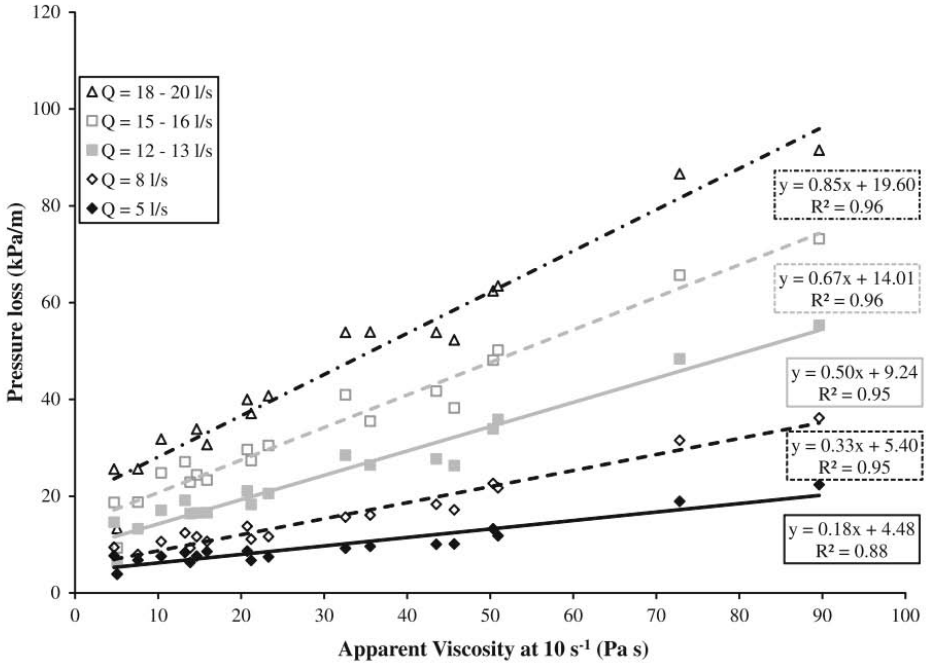

Figure 3.43: Pressure Loss per Linear meter vs. Apparent Viscosity (Feys 2009)

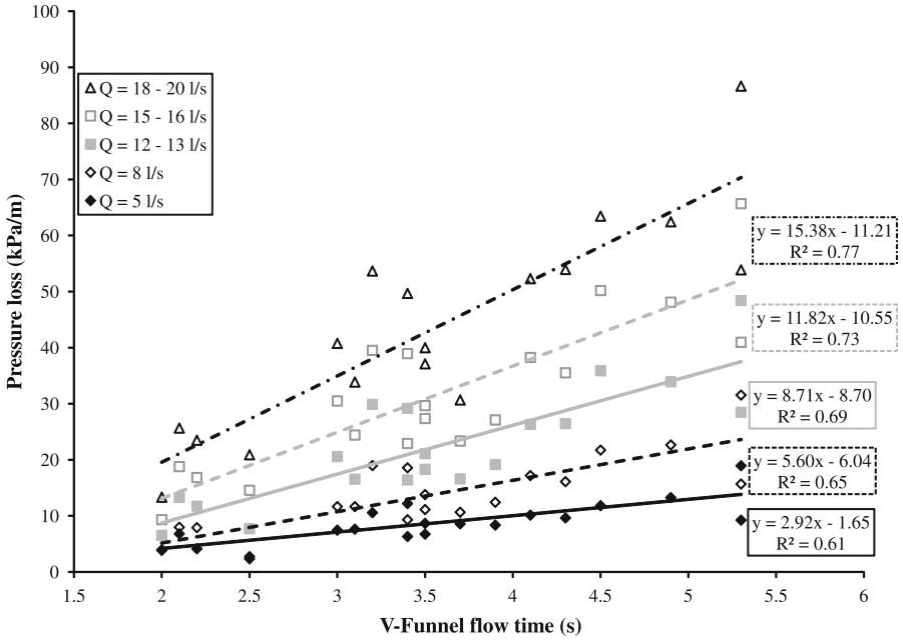

Figure 3.44: Pressure Loss per linear meter vs. V-Funnel flow Time of SCC (Feys 2009)

Khatib (2013) in his PhD thesis entitled "Analysis and Prediction of Pumping Characteristics of High-Strength Self-Consolidating Concrete" studied the fundamental

principles of pumping of high strength self-compacting concrete. He reviewed theoretical aspects of rheology and the fundamental properties of materials, the flow of SCC in pipelines and conducted a full-scale pumping test; the idea of lubrication layer was also covered in this study.

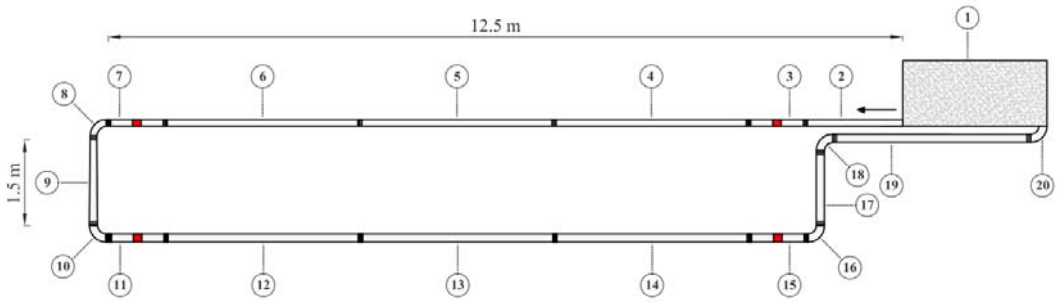

Figure 3.45: Pumping Circuit Used by Khatib (2013)

A 30 m closed circuit was prepared to pump 26 different concrete mixtures, the circuit had two parts; one with 102 mm diameter pipes and the remaining with 127 mm diameter pipes, elbows were present in this circuit to evaluate the effect of the bends (Figure 3.45). A truck-mounted pumped was used here, the pump is capable of delivering a maximum pressure of 60 bar or maximum flow rate of 90 m^3/h. Similar to Feys (2009) ,Khatib used both measuring systems; strain gauges and pressure sensors which broke at early stage of testing. Figure 3.46, Figure 3.47 and Figure 3.48 shows some of the results obtained by Khatib correlated to concrete fresh properties.

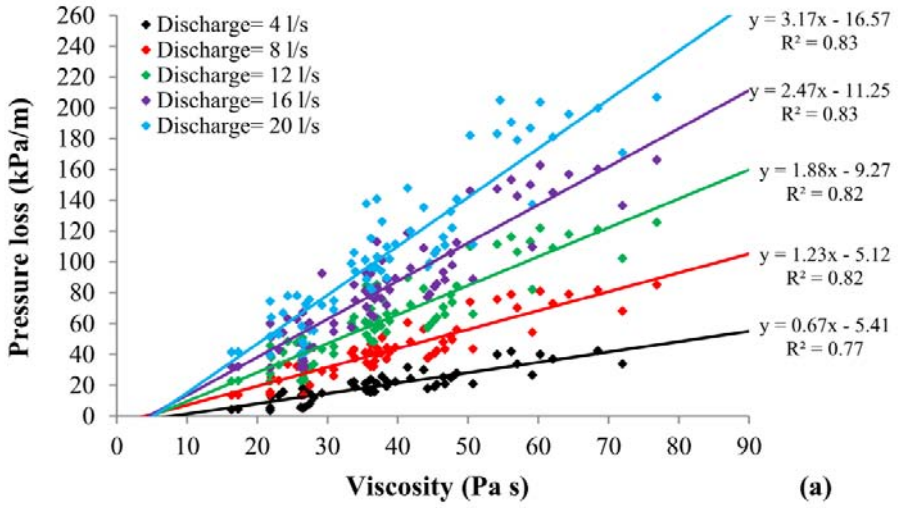

Figure 3.46: Viscosity Effect on Pressure Loss (Khatib 2013)

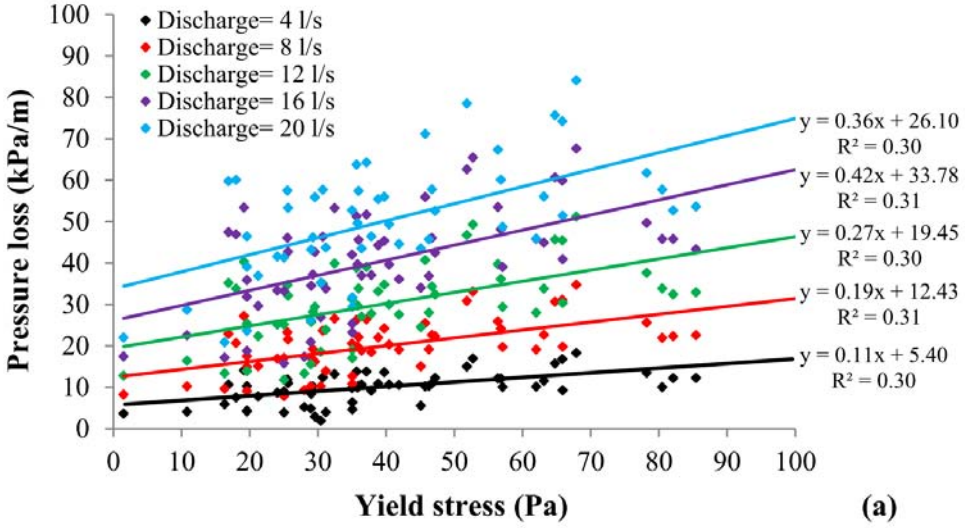

Figure 3.47: Yield Stress Effect on Pressure Loss (Khatib 2013)

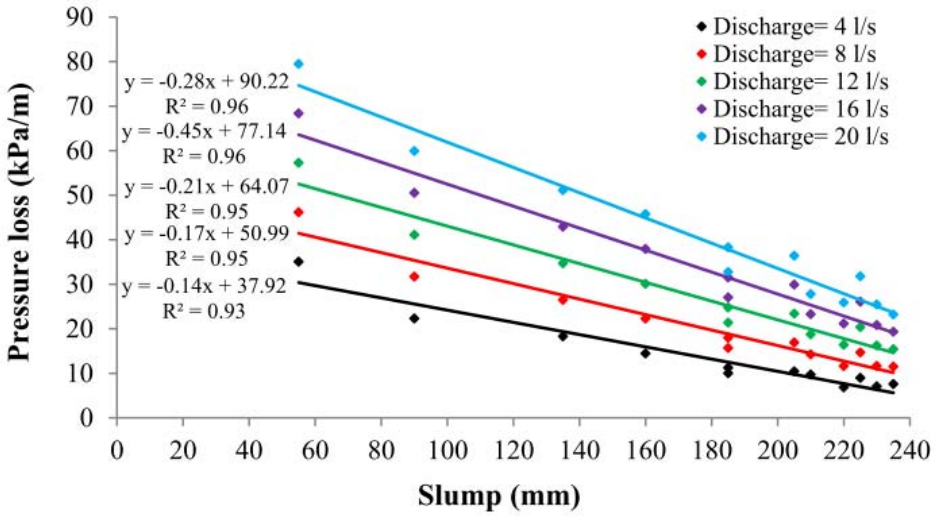

Figure 3.48: Slump Effect on Pressure Loss (Khatib 2013)

CHAPTER 4

MODELING AND EXPERIMENTAL PROGRAM FOR FORMWORK PRESSURE EXERTED BY SCC

4.1 Introduction

Modeling is a very efficient tool for the prediction of the response caused by applying the expected load; it can save the time required for actual testing and help engineers in performing an economical and safe design of structures. The following sections represent a proposed model for formwork pressure which will be later validated using data from actual test conducted in the field.

4.2 The Proposed Model

A new FEM-based model is proposed in this research for simulating the formwork pressure exerted by SCC. This proposed model considers SCC as an isotropic linear elastic homogeneous material having a density of ρ and confined in a rigid body.

The proposed model calculate unknown stresses using a 2-D plain strain FEM. The values boundary shear stress varies at different locations depending on the resting time, which is the time interval between casting the portion under consideration to the instance at which the pressure measurement is made.

4.2.1 Boundary Conditions

Figure 4.1 shows the geometry and the coordinate system for the formwork to be used for the development of the FEM. Boundary shear stress conditions was treated based on the equations provided by Roussel (2006) in which a model is proposed for the determination of thixotropy of concrete in the fresh state.

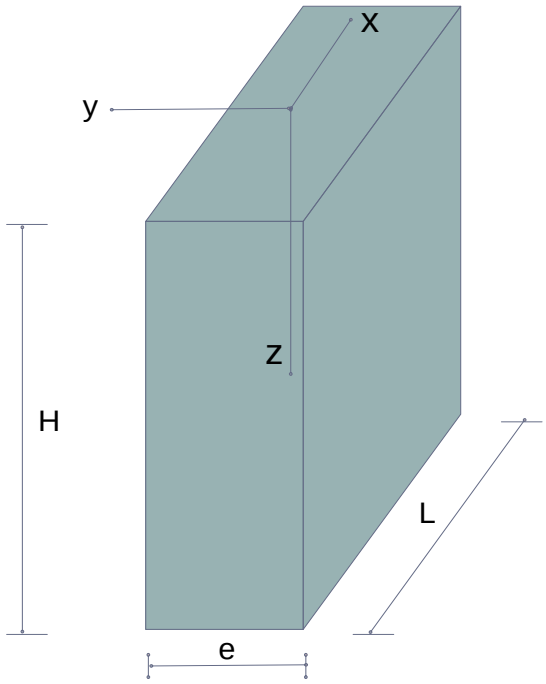

Figure 4.1: Proposed Geometry of the Formwork

The thixotropy model provided by Roussel (2006) uses Bingham material model to describe concrete flow in the steady state, it assumes that yield stress increases with time linearly (when the material is at rest). This resulted in

$$\tau = (1 + \lambda)\tau_0 + \mu\dot{\gamma} \qquad \text{Eq. 4. 1}$$

$$\frac{\partial \lambda}{\partial t} = \frac{1}{T} - \alpha \lambda \dot{\gamma} \qquad \text{Eq. 4. 2}$$

Where, λ describes the flocculation state of concrete, T and α are the thixotropy parameters. It should be highlighted that the characteristic time of flocculation (T) is assumed to be long as compared to the characteristic time of the deflocculation.

Hence,

$$\tau(t = 0) = (1 + \lambda_0)\tau_0 = \tau_0 + \tau_0 \left(\frac{t}{T}\right) = \tau_0 + A_{thix} t \qquad \text{Eq. 4. 3}$$

where $\lambda_0 = \lambda(\dot{\gamma} = 0)$

With

$$A_{thix} = \frac{\tau_0}{T} \qquad \text{Eq. 4. 4}$$

Where, τ_0 is the initial yield stress of SCC, $t = t_{rest}$ is the time of resting and A_{thix} is the flocculation parameter which is found experimentally.

The flocculation state is determined by the flow history. The term $\lambda_0 \tau_0$ refers to thixotropic yield stress (apparent) due to flocculation, and it equals zero immediately after mixing.

The value of λ_0 will change starting from zero to a positive value through the steps of casting and the yield stress will become larger than the initial yield stress. It was suggested by Ovarlez and Roussel (2006) that τ_0 can be assumed to be zero due to its insignificant value as compared to the one due to flocculation and resting ($A_{thix} t$). Therefore, we can write

$$\tau(t = 0) \cong A_{thix} t_{rest} \qquad \text{Eq. 4. 5}$$

The casting will start at a time $t_{rest} = 0$, a number of layers of materials will be deposited with the final (last) layer having the minimum rest time. Figure 4.2 shows a linear rectangular variation in $\tau(t)$ that is expected in this case.

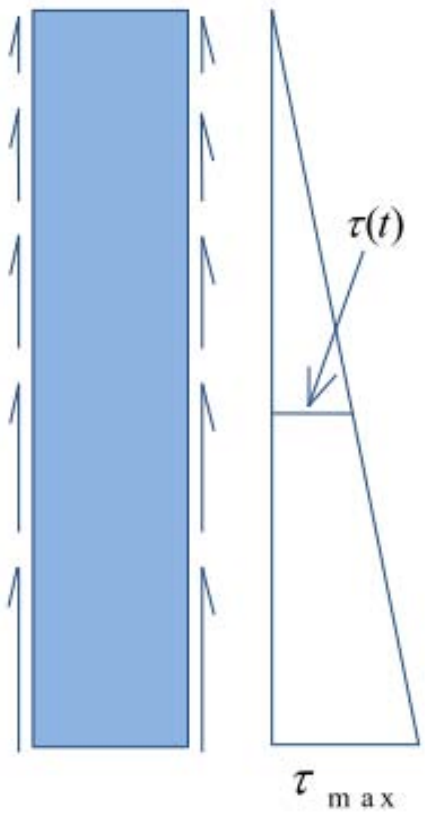

Figure 4.2: Linear Variation of Shear Stress

In the proposed model, the boundary shear stress $\tau(t)$, which is time dependent, is being treated as a discrete spring elements having a stiffness *k* as illustrated in Figure 4.3.

Since *k* is used to simulate the distribution of shear stress along the vertical edges, there should be a way to link *k* to a time dependent variable considering the rheological properties of SCC in the fresh state. Hence, $k(t)$ will be used instead of only *k*.

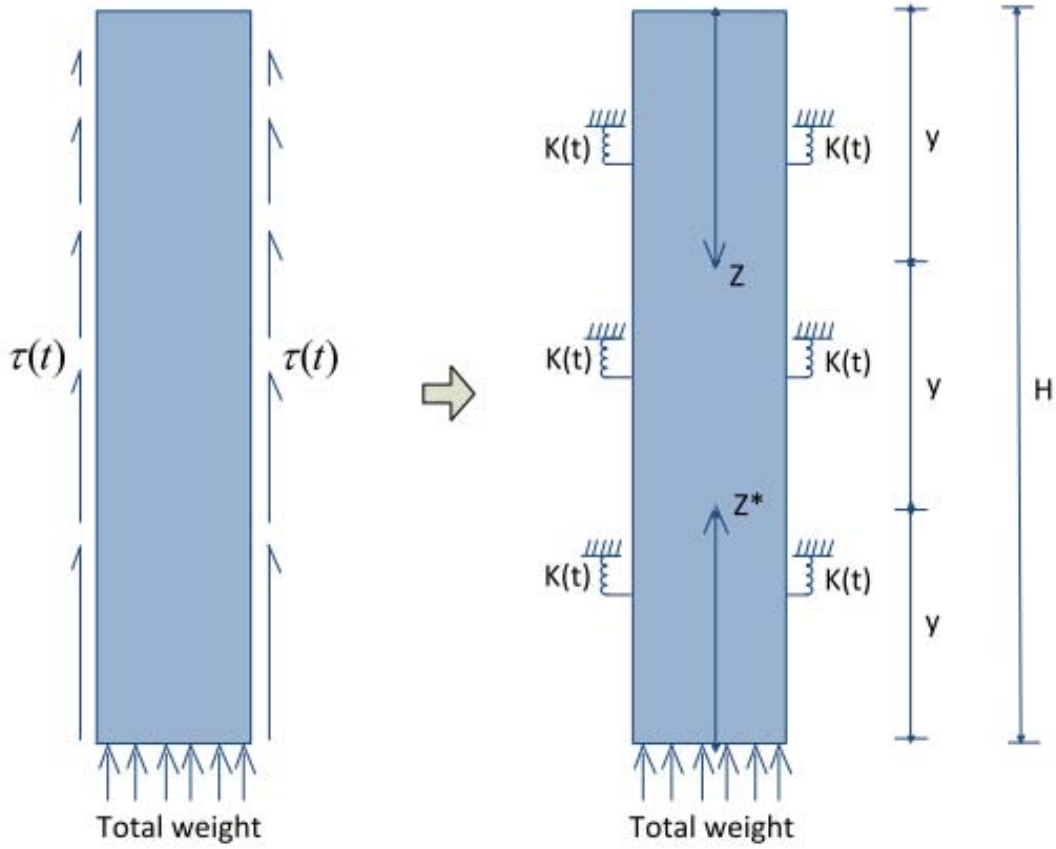

Figure 4.3: Modeling of Shear Stress on the Wall

Stiffness is the force per unit length. Thus, each spring will have a tributary length *y* which will be multiplied by $\tau(t)$ to give the force in each spring. The local vertical deformation is denoted by u_y, hence, the time dependent stiffness can be written

$$k(t) = \frac{\tau(t) \times y}{u_y} \qquad \text{Eq. 4. 6}$$

Substituting Eq. 4. 5 into $\tau(t)$, Eq. 4. 6 yields

$$k(t) = \frac{A_{thix} \times t_{rest} \times y}{u_y} \qquad \text{Eq. 4. 7}$$

The rate of casting R will affect the time dependent shear stress $\tau(t)$, and consequently the stiffness $k(t)$, and will affect the lateral stress evolution since it a function of the resting time,

$$R = \frac{H}{t} \qquad \text{Eq. 4. 8}$$

Before the formwork is totally filled up, SCC will rise to a known depth z*, at which the time can be written as

$$t^* = \frac{z^*}{R}, \quad 0 < z^* < H \; and \; z + z^* = h \qquad \text{Eq. 4. 9}$$

And hence, t_{rest} can be written as

$$t_{rest} = (t - t^*) = (t - \frac{z^*}{R}) \qquad \text{Eq. 4. 10}$$

Therefore, Eq. 4. 5 becomes

$$\tau(t) = A_{thix}(t - \frac{z^*}{R}) \qquad \text{Eq. 4. 11}$$

Eq. 4. 10 indicates that the bottom layer of SCC will be having the maximum resting time as compared to the ones above.

Finally, by substituting Eq. 4. 10 into Eq. 4. 7, the spring stiffness $k(t)$ can be written as below

$$k(t) = \frac{A_{thix} \times (t - \frac{z^*}{R}) \times y}{u_y}, \quad 0 \le t \le \frac{H}{R} \qquad \text{Eq. 4. 12}$$

and

$$k(t) = \frac{A_{thix} \times (t + \frac{H - z^*}{R}) \times y}{u_y}, \quad t > \frac{H}{R} \qquad \text{Eq. 4. 13}$$

Where, Eq. 4. 12 is applicable from the beginning of casting while and Eq. 4. 13 is applicable once the casting is complete.

4.2.2 Solving the Problem Using ANSYS Package

ANSYS (ANSYS 2007), the finite element program was used here to solve this problem. The 2-D formwork was analyzed using different experimental data obtained from actual wall casting in addition to some experimental data from literature. Wall geometry has been already explained in Figure 4.1. Note that the wall is relatively long in one direction, which will allow the simplification to a 2-D problem.

Fresh concrete was modeled using eight-noded plane element. Revolute joint element was used here to simulate fresh concrete wall interaction. The revolute joint element which is similar to the spring-damper element, is a uniaxial tension-compression element having two degrees of freedom at each end: translations in the x and y directions. For modeling purposes, the element was placed on a number of locations on the exterior wall of the formwork. The translational stiffness of these element are calculated based on Eq. 4. 12 or Eq. 4. 13 (depending on the time of measurement) and the lateral pressure evolution is found. The calculation of the stiffness should be done at each time step due to the time dependency of this parameter.

Figure 4.4 represents a flow chart outlining the steps needed to solve the problem. Initially, materials properties are defined and entered. Four material properties should be defined; modulus of elasticity E, density ρ, Poisson's ratio ν and A_{thix}. A modulus of elasticity of 7 GPa is used here, and the actual density of the concrete is also entered. Since SCC is considered as an incompressible fluid, a value of 0.498 is initially used for Poisson's

ratio ν. It should be noted that the value of ν will remain the same while the concrete is in the fluid state which is normally less than 120 minutes and following which, the value of ν will get smaller with time which has been incorporated in this model.

Figure 4.5 shows a typical formwork model created by ANSYS, a mesh of 10 by 100 was created, boundary conditions used were; fixed (all degrees of freedom) at the end of each spring element, rollers to restrain the movement in the horizontal direction and allow for vertically movement for the vertical sides and finally, rollers to restrain the vertical movement and allow for horizontal movement for the bottom base.

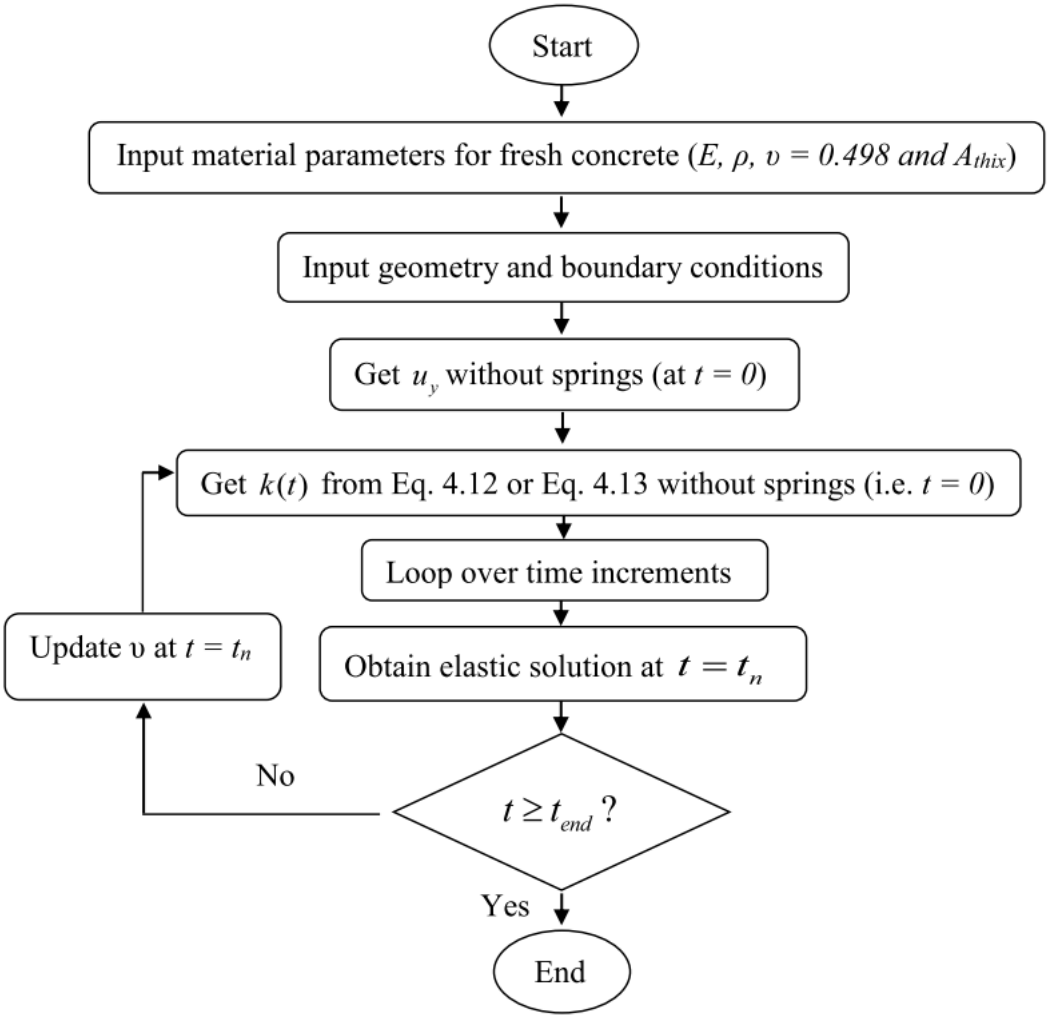

Figure 4.4: Flowchart Outlining Steps Needed to Solve the Problem

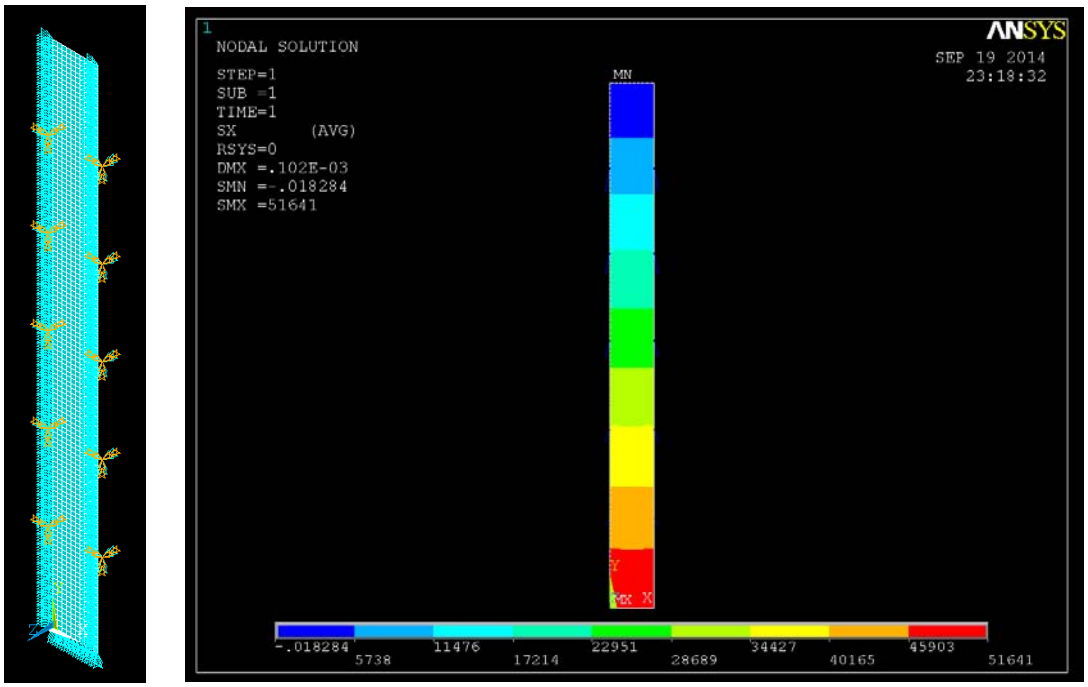

Figure 4.5: A Snapshot from ANSYS showing the discretization and boundary condition (Left) and Contour Plot for The Lateral Pressure

4.3 Experimental Program for Formwork Pressure

An experimental program was planned to validate the model's ability and accuracy in predicting the lateral pressure exerted by SCC.A steel formwork was fabricated in a local workshop to be used to in casting different mix designs of SCC (Figure 4.6 and Figure 4.7). The mold dimensions were; 3.10 m in height, 3.00 m in width and 0.20 m in thickness. The mold was designed to carry a fully hydrostatic load exerted by SCC and to avoid any unexpected failure of the mold, 4 bolts were used in the middle part of the formwork to serve as a bracing system.

Four different concrete mix designs were used in this work composed of different mineral admixtures. Table 4.1 contains a summary of all mix designs and the date of casting.

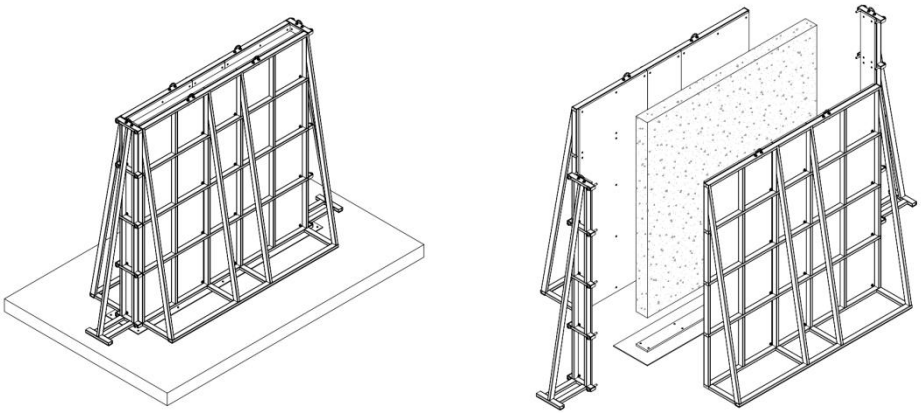

Figure 4.6: A 3-D Drawing of the Designed Formwork

Figure 4.7: Actual Formwork without Bracing (left) and with Bracing (right)

Table 4.1: Concrete Mix Designs

	Control Mix (SCC – C)	30% Fly Ash (SCC – FA)	7% Silica Fume (SCC - SF)	60% GGBFS (SCC - GGBFS)
Date of Casting	11/02/2014	25/02/2014	29/03/2014	27/04/2014
Cement (Kg)	500	350	465	200
Mineral Admixture	0	150	35	300
Water (L)	165	165	165	165
20 mm Agg. (Kg)	390	390	390	390
10 mm Agg. (Kg)	295	295	295	295
5 mm Agg. (Kg)	240	240	240	240
Dune Sand (Kg)	775	775	775	775
SP – Adva314 (L)	3	2	3.5	1.85

The pressure transducers were placed on one side of the formwork at various heights from the bottom base, 10 cm, 60 cm, 110 cm, 155 cm and 205 cm (Figure 4.8). These transducers were connected to data acquisition system (data logger) type TDS-300 made by Tokyo Sokki (Figure 4.9). The gauges were AB/HP pressure transducers made by Honeywell (Figure 4.10).

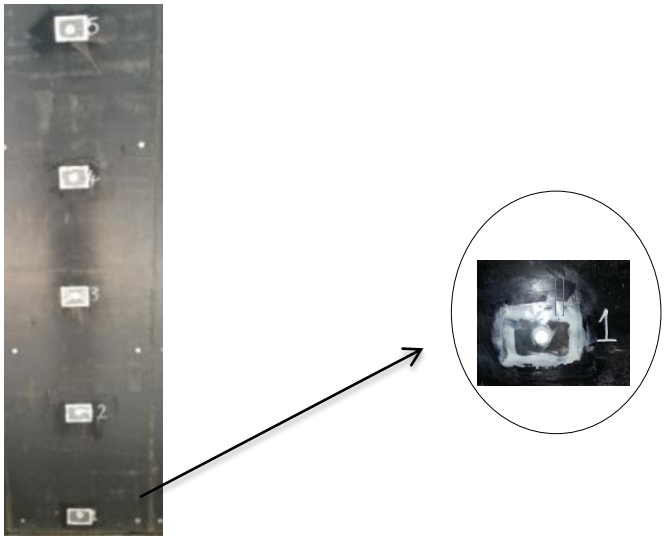

Figure 4.8: Pressure Transducers Arrangement on the Inner Surface of the Formwork

Figure 4.9: Data Acquisition Equipment

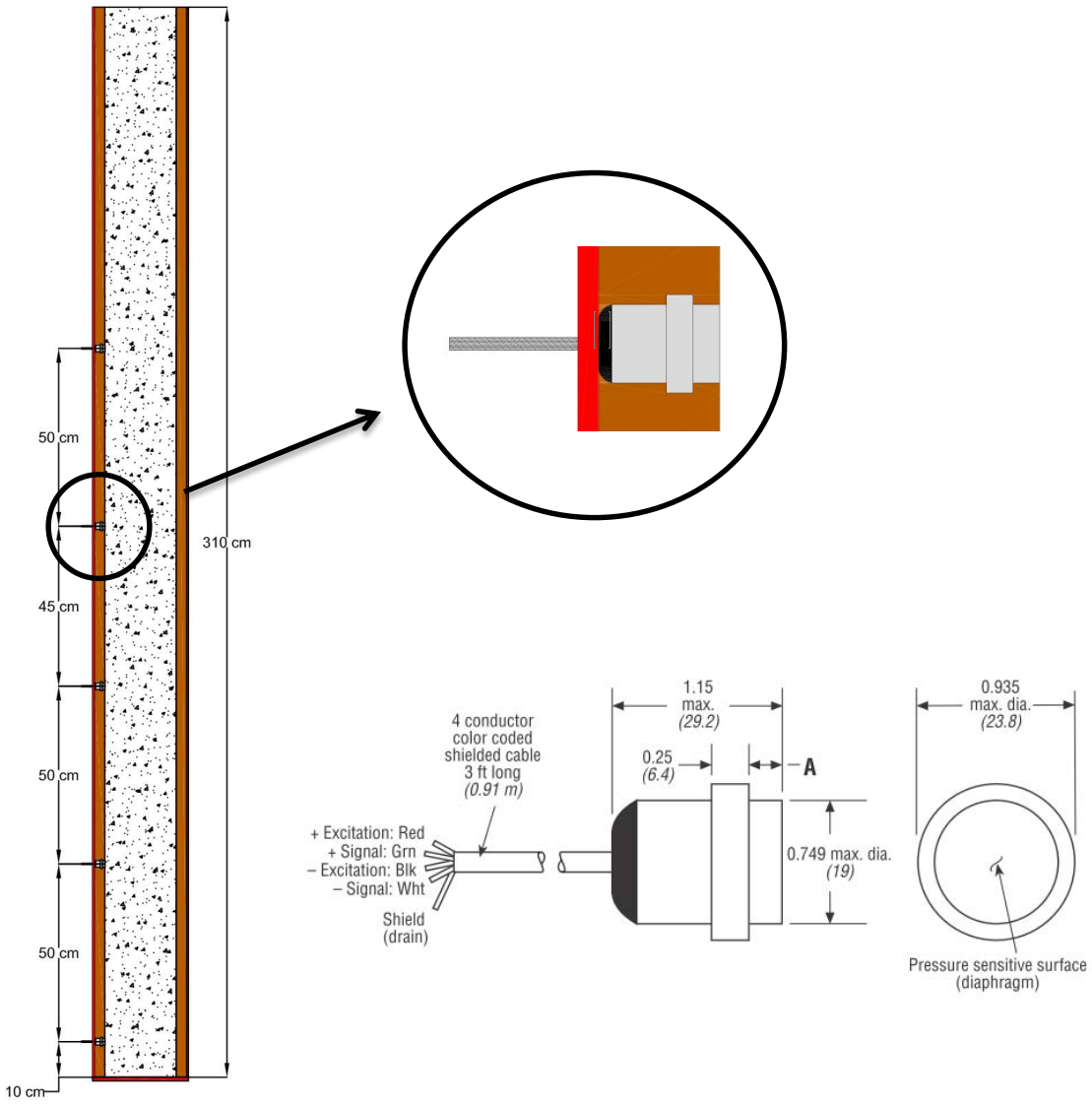

Figure 4.10: Side View of the Steel Formwork Showing the Pressure Transducers

Prior to connecting the pressure transducers (sensors), simple calibration was achieved to find the calibration coefficient to be used in the data acquisition equipment software. Figure 4.11 below shows all the equipment used in the calibration operation. Water with known height and density of 1000 g/l was used to fill a plastic rigid container and the lateral pressure caused by water is read in the data acquisition equipment. This value is compared to the hydrostatic pressure (ρgh) and necessary adjustment is calculated.

Figure 4.11: Setup to Determine Transducer Coefficient: Plastic Container (Left) and Data Acquisition Equipment (Right)

Figure 4.12 shows the poring of SCC. The ingredients of each of the above mixes were mixed in the concrete batch plant and then discharged into a rotary concrete mixer. After a thorough mixing, the concrete was then discharged into a concrete pump and finally pumped into the formwork. The pressure transducers measure the lateral pressure and it being automatically recorded.

Figure 4.13 shows the ICAR rheometer which has been utilized to measure the rheological parameters of the four SCC mixes. Concrete was poured in the steel container and two tests were done; flow curve and stress growth test. Figure 4.14 shows the ICAR Rheometer software window, the flow curve test on the right side was used to find Bingham parameters including viscosity and yield stress. This was done placing the concrete in the container and immediately run the test, the laptop will automatically measure and record the test results. On the other hand, stress growth test on left side was used to find the value of A_{thix}. The concrete was initially filled in the container and kept to rest for 1 minute and then, the first stress growth test was performed and the yield stress value was recorded, the same procedure was again repeated after 5 minutes of resting time, and finally after 15 minutes resting time. The values of the yield stress versus the resting time were plotted and the A_{thix} value is taken as the slope of that line (Figure 4.15).





Figure 4.12: Pouring a 3 m High SCC Wall

Figure 4.13: Measurement of Rheological Parameters

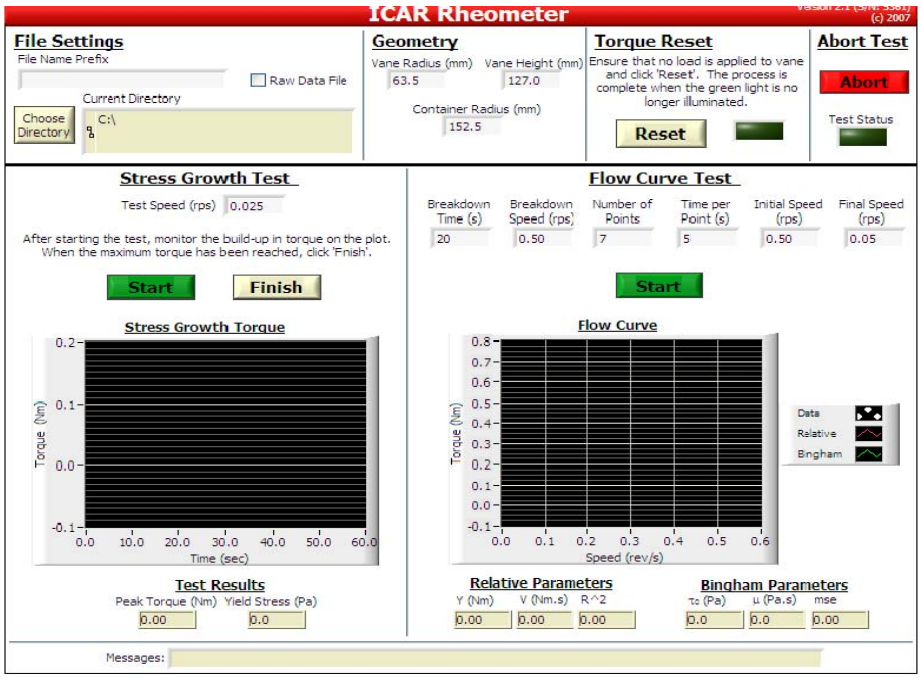

Figure 4.14: ICAR Rheometer Graphical Interface

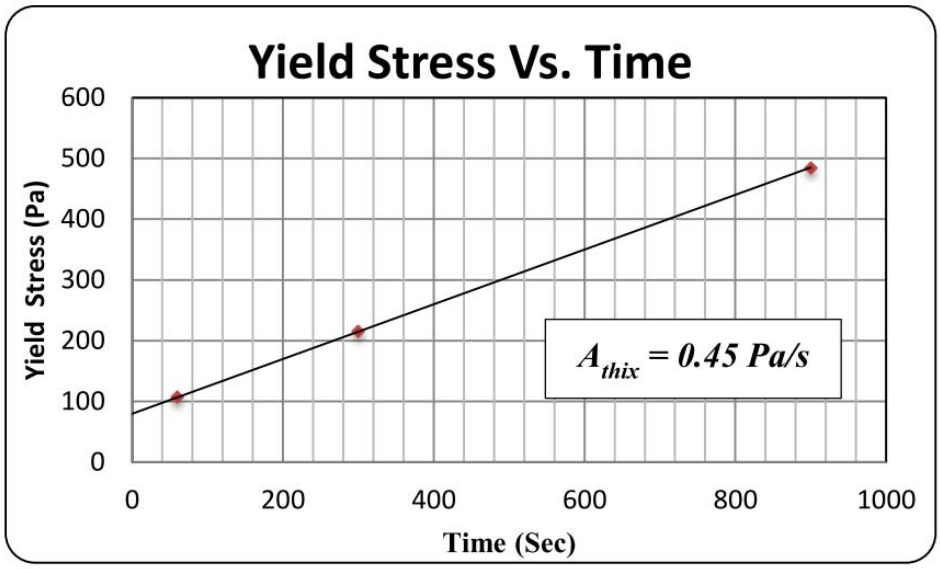

Figure 4.15: Finding A_{thix} Value using the Yield Stress vs. Resting Time Graph for SCC – C

Roussel (2006) suggested some values for A_{thix} based on the level of thixotropy of SCC, Table 4.2 represents these values.

Table 4.2: A_{thix} values for Different Thixotropy Levels (Roussel (2006)

A_{thix} (Pa/s)	SCC Type
$A_{thix} < 0.1$	Non-Thixotropic
$0.1 \leq A_{thix} \leq 0.5$	Thixotropic
$A_{thix} > 0.5$	Highly Thixotropic

CHAPTER 5

MODELING AND EXPERIMENTAL PROGRAM FOR PRESSURE DROP PIPELINE DURING PUMPING SCC

5.1 Introduction

The experimental part of this study was performed on full-scale pumping setup installed at Saudi Ready Concrete Company located in the city of Khobar. This setup was constructed for the purpose of investigating the pressure drop in pipe lines during pumping of SCC.

5.2 Design of the Pumping Setup

The 60 m length pumping setup shown in Figure 5.1 was designed to evaluate the pressure variation during pumping of different SCC mixtures. The setup was designed in this way in order to simulate difficult pumping situation. Exactly 18 elbows of 90^{o} angel were used in this setup to simulate pumping in longer distances, knowing that the pressure drop caused by one elbow is equivalent to certain horizontal distance. This setup was constructed by connecting many pipes along with 90^{o} elbows; Figure 5.1 represents a schematic representation of the proposed pipe arrangement. The whole pipe line was laid horizontally except at the discharge point, a 4 m vertical pipe was attached in order to discharge the concrete into a truck mixer directly. Initially, the steel pipes were placed on hollow blocks, but due to vibration that will be generated during pumping process, it was

placed directly on the ground and was hooked by means of steel bolts (Figure 5.2 and Figure 5.3).

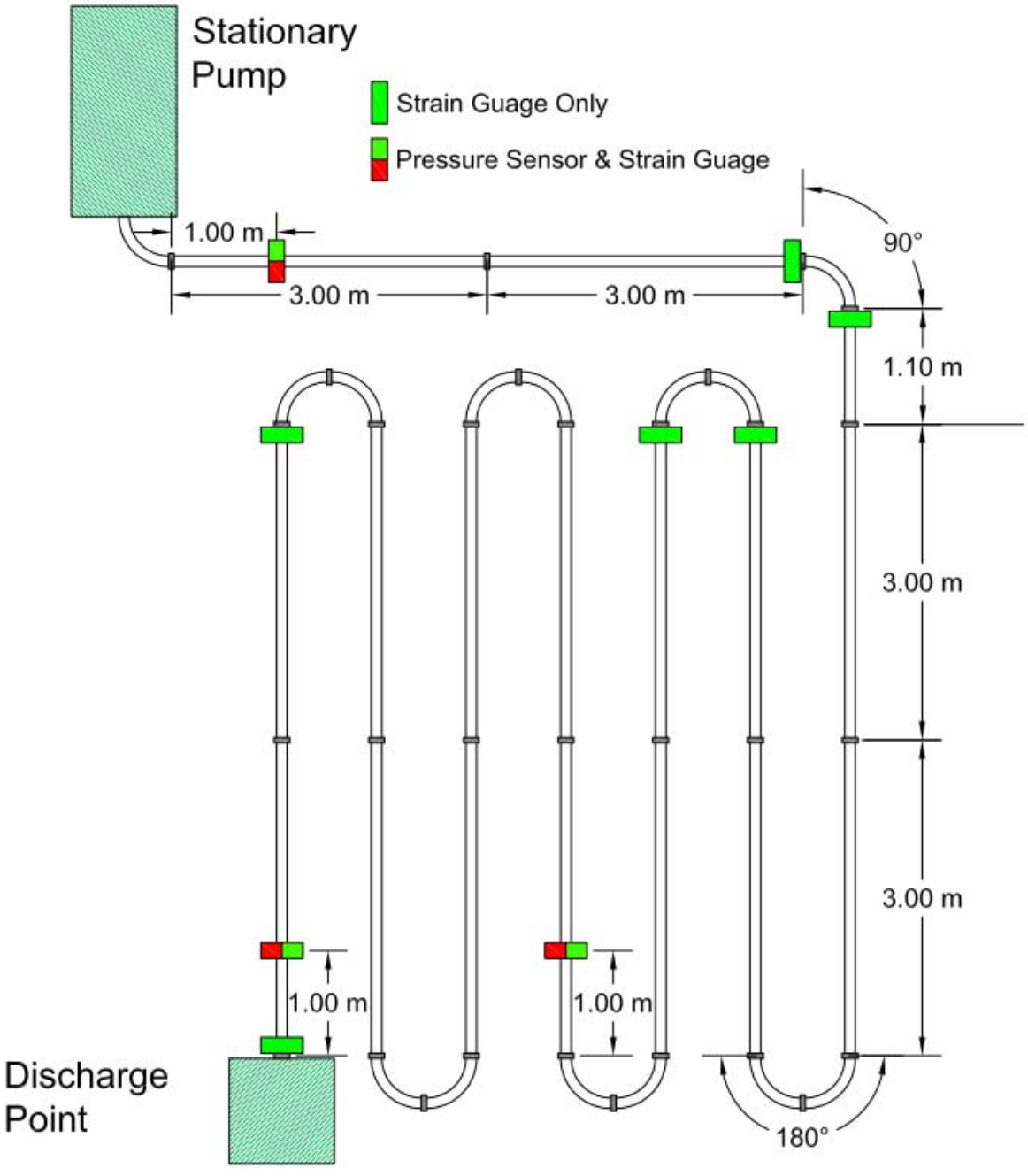

Figure 5.1: Schematic Representation of the Pumping Setup

Figure 5.2: Initial Arrangement of the Pumping Setup

Figure 5.3: Final Arrangement of the Pumping Setup

After completing all the require tests on the first setup, a second setup was constructed by eliminating many of the internal pipes and elbows in first setup (Figure 5.4). The total length of setup was about 22 m, pipes and elbows were of the same size of the previous

test. Details for the new arrangement and the vertical pipe are shown in Figure 5.5 and Figure 5.6.

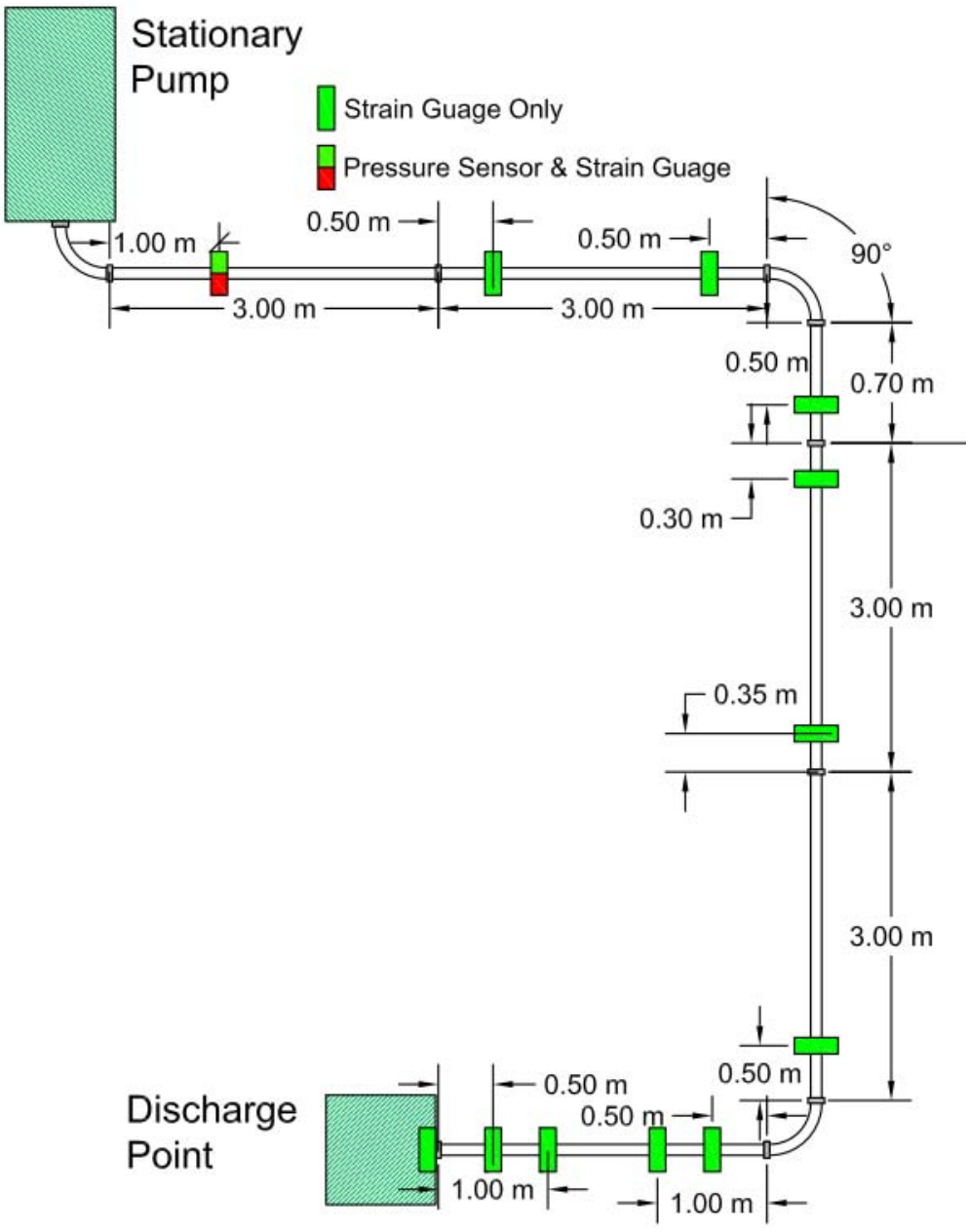

Figure 5.4: Schematic Representation of the Pumping Setup 2

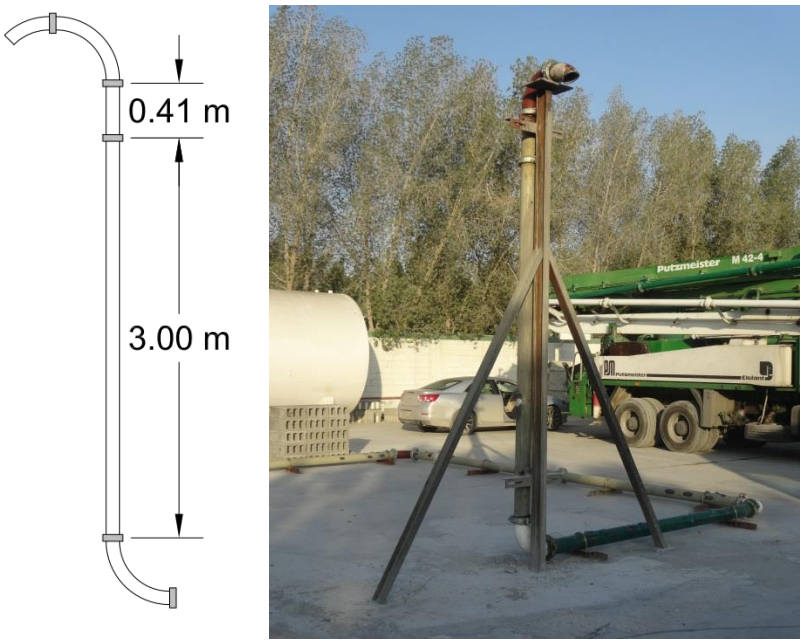

Figure 5.5: Pipe at the Discharge Point

Figure 5.6: Final Arrangement of the Pumping Setup 2

5.3 Experimental Setup

5.3.1 Stationary Pump

A Shewing SP4800 stationary pump has been used in this test. The pump has a capacity of umping up to 129 bars (rod side) and a maximum flow rate of 66 m^3/hr. The pump is powered by a diesel engine of 330 kW power and has a hopper of 0.6 m^3 capacity. SP4800 pump is equipped with two shifting cylinders with 180 mm diameter and total stroke length of 2 m (Figure 5.7).

Figure 5.7: Schwing Stationary Pump (www.schewing.com)

5.3.2 Steel Pipes and Elbows

A number of 3 m long steel pipes were used to construct the pumping setup; these pipes have a constant inner diameter of 125.5 mm and 7.1 mm thick walls. These pipes were connected by means of coupling and when there is a turn in direction, a steel elbow 28.1 cm radius was used and connected in the same way for the pipes.

5.3.3 Rheometer

ICAR Rheometer, a concrete rheometer which was developed at the International Center for Aggregate Research (ICAR) located at The University of Texas at Austin. Details about this equipment and how it is operated were discussed in section 4.3.

5.3.4 Flow Spread Setup

The equipment used in this test is similar to the ones used in the conventional slump test. Fresh was brought from the concrete mixer by trolley and then poured into the slump cone. Before lifting the cone, the level of the concrete was leveled and any concrete on the steel plate was removed. The slump cone was then removed and the spread diameter was measured and recorded (Figure 5.8).

Figure 5.8: Flow Spread Test (Slump Flow)

5.4 Measuring Systems

In order to measure the pressure drop while pumping SCC two measuring systems where utilized; pressure sensors (transducers) and strain gauges.

5.4.1 Pressure Sensors

Three pressure sensors where available to measure the pressure at three different locations along the pipe line. The sensors were made by Tokyo Sokki model PWF-50 MPa as shown in Figure 5.9 and Figure 5.10. These sensors can sense the pressure up to 50 MPa (500 bar) and have a threaded part to facilitate the installation process.

Figure 5.9: PWF-50 MPa Pressure Sensor

Figure 5.10: Pressure Sensor and Strain Gauge on the Steel Pipe

5.4.2 Strain Gauges

Due to unavailability of many pressure sensors, it was required to find another method to measure the pressure at different points along the pipe line. Strain gauges were utilized to measure the expansion of the steel pipe at specific points and by using the approximate relationship for the stress at the inner wall of thin-walled vessels for tubes in the hoop direction, pressure can be found as below:

$$\sigma = \frac{pr}{t} \quad \text{and} \quad \varepsilon = \frac{\sigma}{E} \quad \text{then} \qquad \text{Eq. 5. 1}$$

$$p = \frac{\varepsilon E t}{r} \qquad \text{Eq. 5. 2}$$

Where
p: Pressure
ε: Strain
E: Modulus of elasticity
t: Pipe thickness
r: Pipe inner radius

5.5 Concrete Mix Design

A total of three mixtures were used for each setup, they were made plain Portland cement, a blend of 70% cement and 30% fly ash and finally a blend of 93% cement and 7% silica fume (Table 5.1).

5.6 Procedure for Testing

In order to facilitate the testing process, the previously shown setup was installed at a ready mix plant allowing immediate testing after concrete batching. Concrete mix designs were fed into the batch plant system and a 5 m^3 truck load of concrete was made for each test. A total of six mixtures were tested, three for each pipe arrangement.

Table 5.1: Concrete Mix Designs

	Control Mix (SCC – C)	30% Fly Ash (SCC – FA)	7% Silica Fume (SCC - SF)
Date of Casting	11/02/2014	25/02/2014	29/03/2014
Cement (Kg)	500	350	465
Mineral Admixture	0	150	35
Water (L)	165	165	165
20 mm Agg. (Kg)	390	390	390
10 mm Agg. (Kg)	295	295	295
5 mm Agg. (Kg)	240	240	240
Dune Sand (Kg)	775	775	775
SP – Adva314 (L)	3	2	3.5

At the beginning of each test, the concrete was initially tested for the flow spread and the rheological parameters and immediately after that; the concrete is fed to the stationary pump and being pumped through the whole length of the pipe line.

All sensors and strain gauges were initialized (zeroed) before testing and started to give vale once the concrete started moving inside the steel pipes. Figure 5.11 and Figure 5.12 respectively, show the concrete entering the stationary pump and leaving at the discharge point.

Figure 5.11: Concrete Entering the Stationary Pump

Figure 5.12: Concrete at the Discharge Point

5.7 Modeling of Pumping Process

After completing all pumping experiments, models simulating the pumping process were prepared using ABAQUS/CFD; the models were made with the same dimensions of the actual pipe arrangement. In order to simplify the models, they were made in xy plane ignoring the height effect of the short vertical pipe as shown in Figure 5.13 and Figure 5.14. Three boundary conditions shall be specified for each setup; inlet, outlet and wall, at the inlet and outlet user can specify pressure or velocity, at the wall, user can specify the condition as no slip, shear or infiltration. Material was modeled as a Newtonian material with known viscosity and mass density. Since there no vertical element defined in model, gravity was neglected. For each mix, viscosity, mass density (taken as 2400 kg/m^3 for all mixtures) and boundary conditions were specified (inlet and outlet pressures are as measured on site to compared the pressure drop) and after submitting the job for analysis results for pressure along the pipe were given.

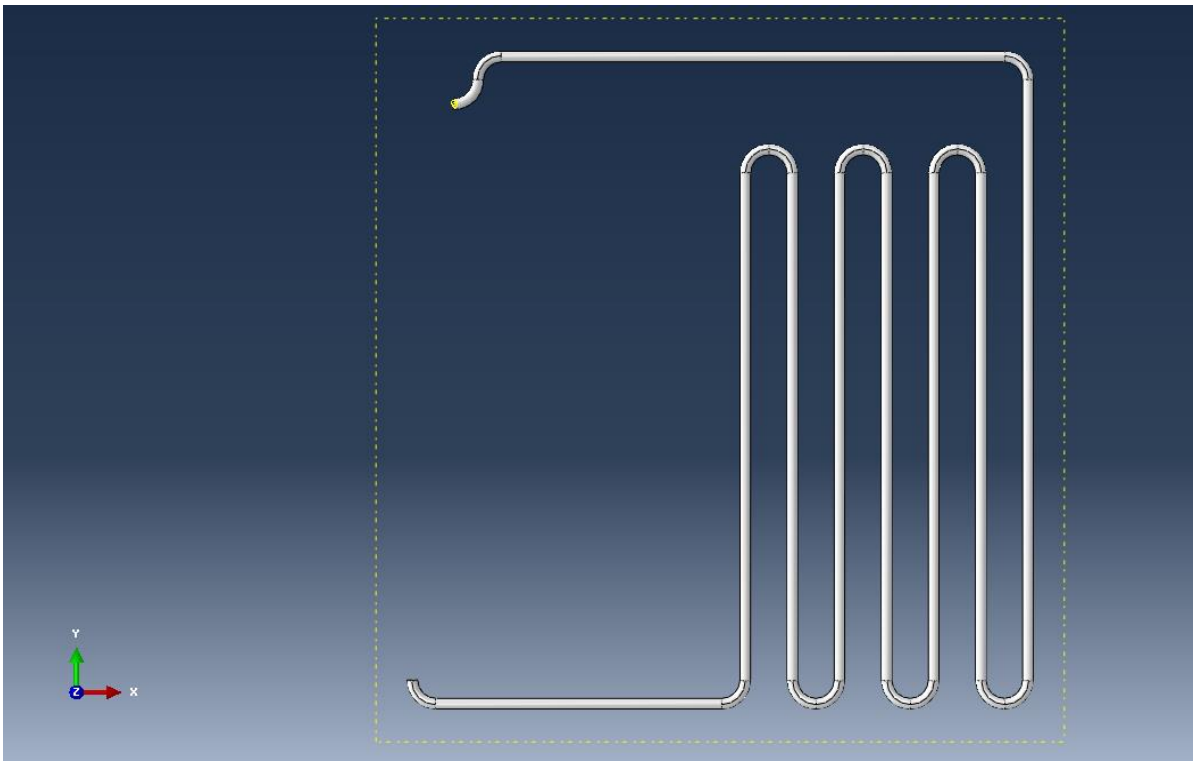

Figure 5.13: ABAQUS Model for Pumping Setup 1

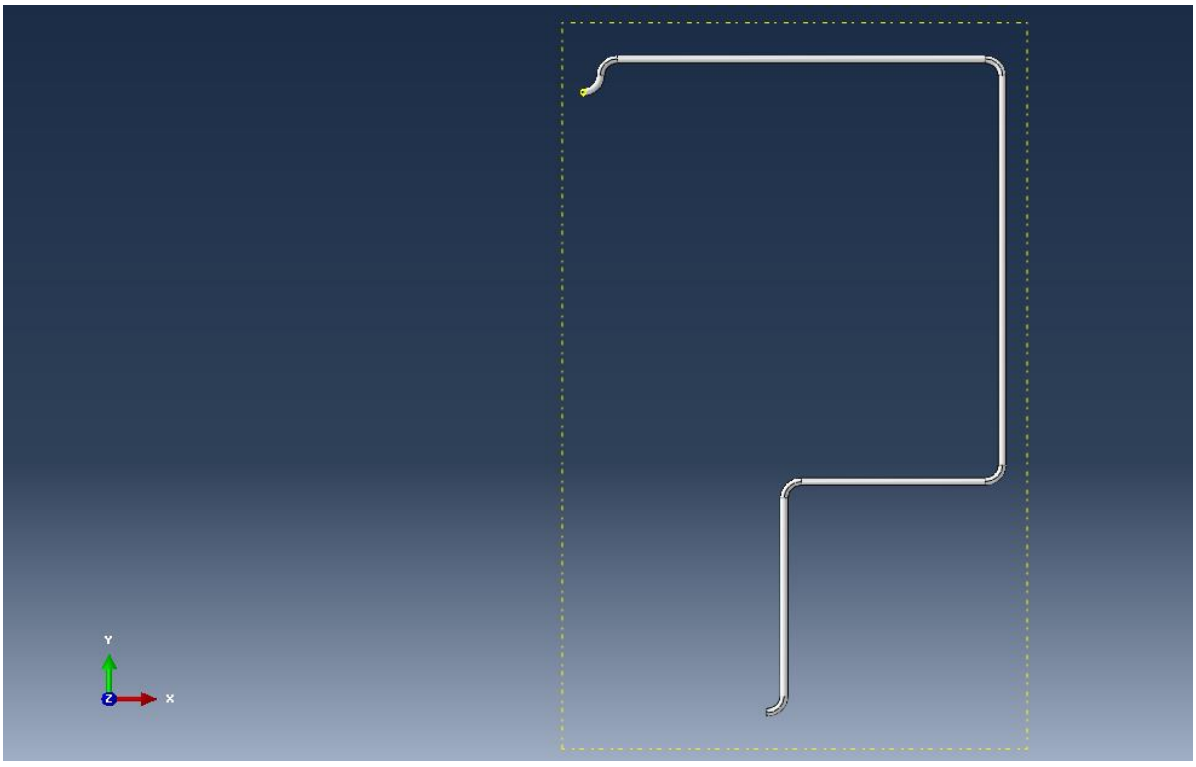

Figure 5.14: ABAQUS Model for Pumping Setup 2

CHAPTER 6

RESULTS AND DISCUSSION

6.1 Model Prediction for the Decay of Lateral Formwork Pressure with Time

To illustrate the response of the FEM developed in this research, the experimental results obtained were utilized. The lateral pressure determined by the model changes with each time increment, this time increment is represented by the stiffness *k*. The value of *k* increases by time due to the increase in the concrete height and stiffening of concrete (during casting) and due to stiffening of concrete (after casting). Five revolute joint elements were placed on each side of the model, each element has a value of *k*, which increases with time as concrete is stiffening. The comparison between the model and the experimental values was made for the pressure values after casting; hence, Eq. 4.13 was used to find *k*.

Due to some technical difficulties, each formwork was filled up to a certain limit that is different from the other formworks, resulting in different total heights for each formwork. Hence, it was required to make a special model for each formwork using its dimensions. Total height of each formwork (for each mix) will be presented in a later paragraph.

The material parameters were entered and the k values were calculated then as per the flowchart in Figure 4.4. Table 6.1 shows the *k* values for mix SCC – C.

Table 6.1: K values for Mix SCC – C

Time (min)	k_1	k_2	k_3	k_4	k_5
0	1.09E+06	4.79E+05	2.66E+05	1.50E+05	6.84E+04
80	2.72E+07	1.48E+07	1.09E+07	9.12E+06	8.27E+06
160	5.33E+07	2.92E+07	2.15E+07	1.81E+07	1.65E+07
240	7.94E+07	4.36E+07	3.22E+07	2.71E+07	2.47E+07
320	1.06E+08	5.79E+07	4.28E+07	3.60E+07	3.29E+07
400	1.32E+08	7.23E+07	5.34E+07	4.50E+07	4.11E+07
480	1.58E+08	8.66E+07	6.41E+07	5.40E+07	4.93E+07
560	1.84E+08	1.01E+08	7.47E+07	6.30E+07	5.75E+07
600	1.97E+08	1.08E+08	8.00E+07	6.75E+07	6.16E+07

It should be highlighted that Poisson's ratio was initially entered as 0.498 and was kept the same for all time increments and found that after an average period of 120 to 180 minutes, the pressure did not decrease and stabilized. After further investigation, a lower value of Poisson's ratio was used in the model for the time increments beyond the above period which led to good matching with experimental results. This make sense, due to the fact that the concrete will stay in the fluid state (with the use of superplasticizers and retarders) for about 120 to 180 minutes at which it can be considered as an incompressible fluid with a Poisson's ratio of 0.50 (in our case we used 0.498), and once the concrete stiffening process starts, this value will go down and can reach approximately to (0.1 to 0.2) after 28 days.

The experimental results obtained from casting the previously stated mixes were analyzed. The four mixes under discussion were poured on four different dates with different ambient temperature which led to significant difference in the behavior in terms of the pressure decay with respect to time. Table 6.2 shows the maximum and the minimum ambient temperatures recorded on the day of casting for each mix, A_{thix} values obtained from rheological measurements, casting rate, and the actual height of the cast formwork.

Table 6.2: Mix Properties

Mix ID	Max. Temp. (°C)	Min. Temp. (°C)	A_{thix} (Pa/s)	Casting Rate (m/hr)	Total Height (m)
SCC - C	21	5	0.4503	34.20	2.280
SCC - FA	28	17	0.4663	35.42	2.952
SCC - SF	33	16	0.4606	23.75	3.099
SCC - GGBFS	43	25	0.4225	20.88	2.958

6.2 Model Prediction versus Experimental Results

Figure 6.1 to Figure 6.16 represent a comparison between actual lateral pressure decay and the pressure decay obtained by the proposed model with ANSYS environment. Four graphs were made for each mix; each graph represents the pressure at the point at which pressure transducer was fixed. In general, all the experimental values showed good match with the proposed model which proves the accuracy of this model. Figure 6.1 to Figure 6.4 represent the values for the control mix (SCC – C). It can be clearly seen that due to the low temperature, the concrete stayed in the fluid state for about 200 minutes and started to flocculate afterwards. As a result, the pressure was stable and almost equal to the hydrostatic pressure for about 200 minutes and started to drop afterwards. Figure 6.5 to Figure 6.8 show the mix which was made with fly ash, for which the ambient temperature was higher by 7 degrees as compared to the previous mix, and hence the drop was immediate and faster.

Figure 6.9 to Figure 6.12 represent the graphs for the third mix made with 7% silica fume which normally causes the concrete to hydrate faster and to lose its slump faster. It can be clearly noticed that the drop in the pressure is most quick compared to the other mixes due to the presence of silica fume and the high ambient temperature which was 33 °C on that

day. Finally, for the GGBFS mix (Figure 6.13 to Figure 6.16) the rate of pressure decay was relatively small due to the fact that GGBFS has a low rate of hydration compared to OPC.

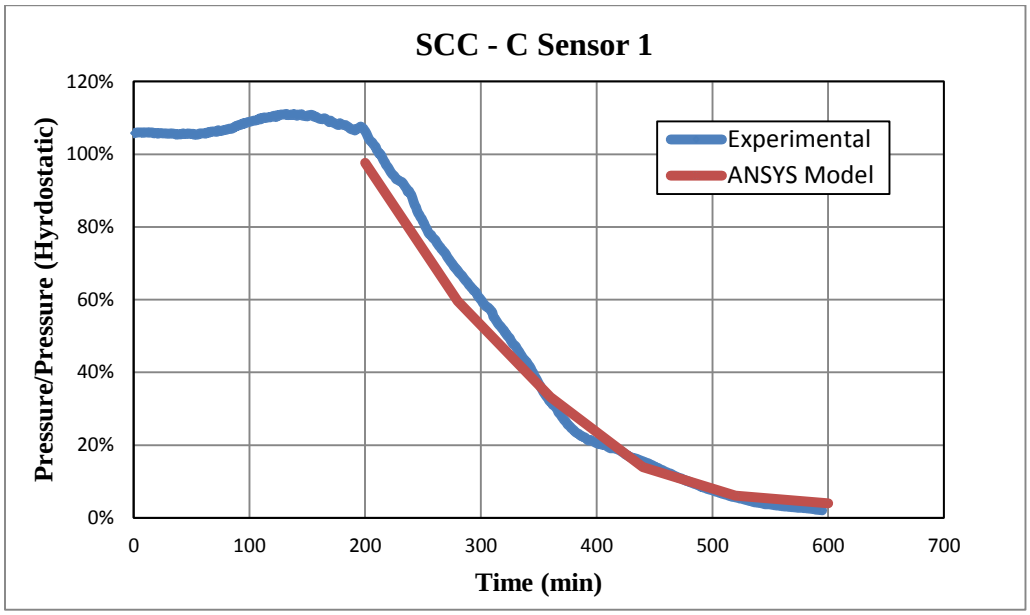

Figure 6.1: Experimental and Numerical Results for SCC – C for Sensor 1 at 10 cm from Bottom Base

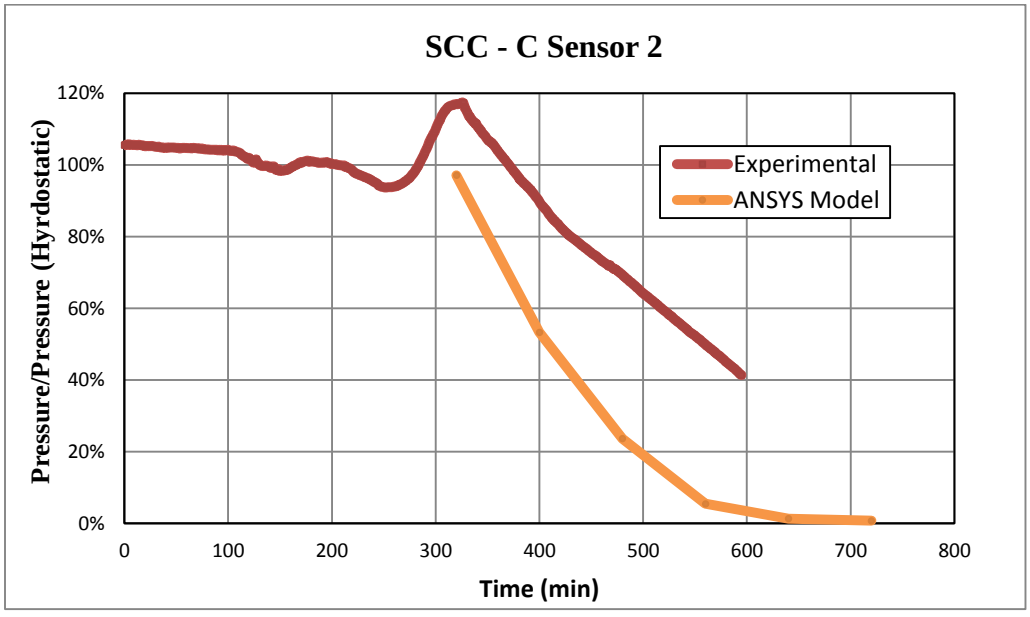

Figure 6.2: Experimental and Numerical Results for SCC – C for Sensor 2 at 60 cm from Bottom Base

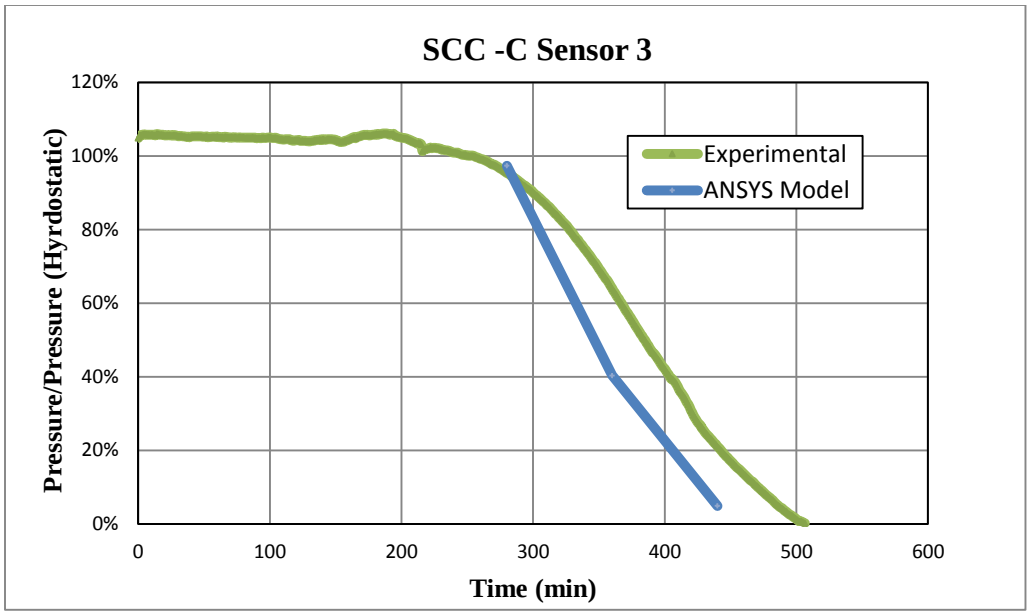

Figure 6.3: Experimental and Numerical Results for SCC – C for Sensor 3 at 110 cm from Bottom Base

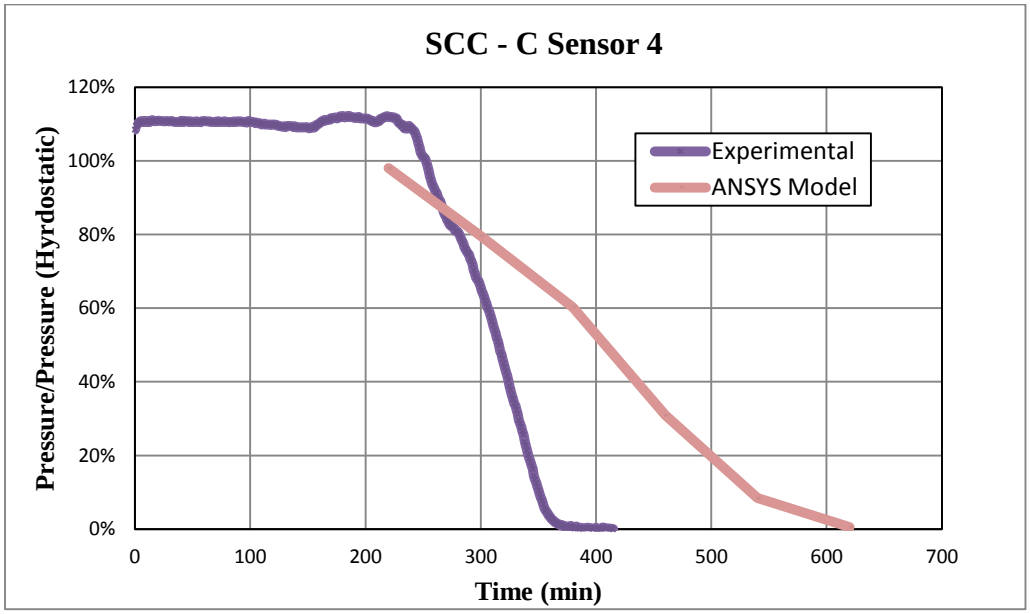

Figure 6.4: Experimental and Numerical Results for SCC – C for Sensor 4 at 155 cm from Bottom Base

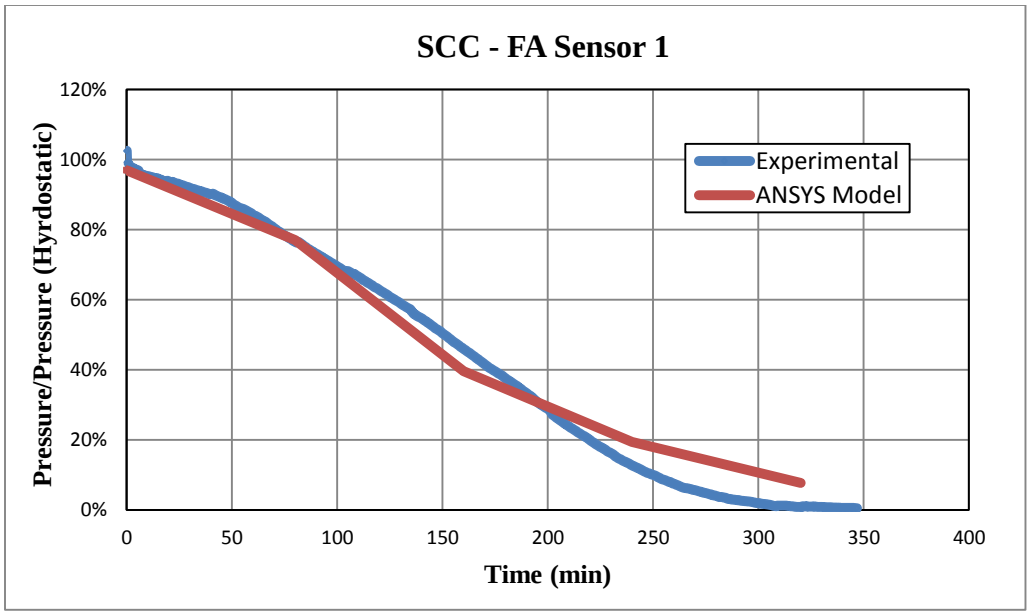

Figure 6.5: Experimental and Numerical Results for SCC – FA for Sensor 1 at 10 cm from Bottom Base

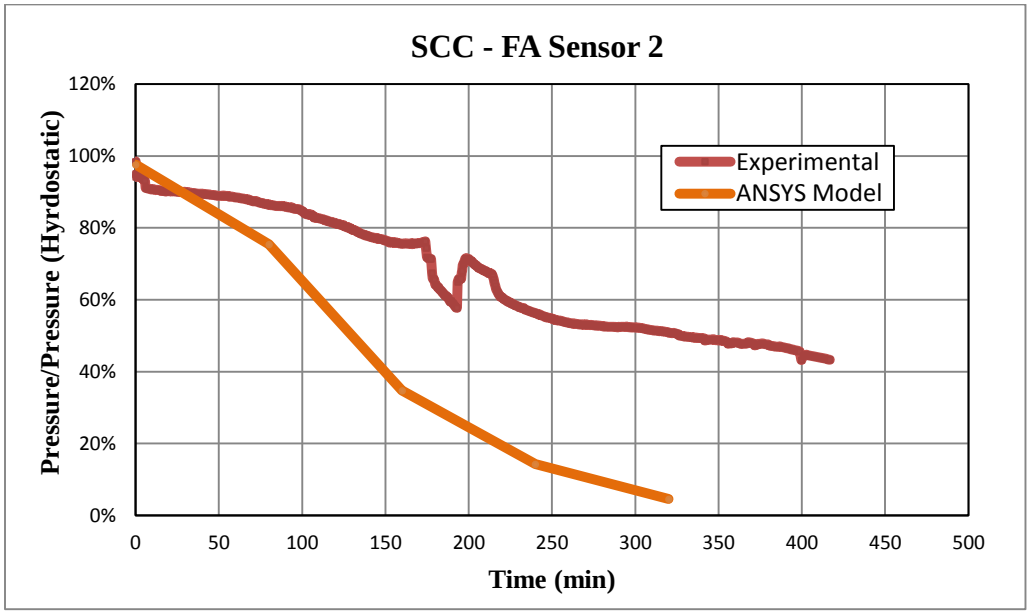

Figure 6.6: Experimental and Numerical Results for SCC – FA for Sensor 2 at 60 cm from Bottom Base

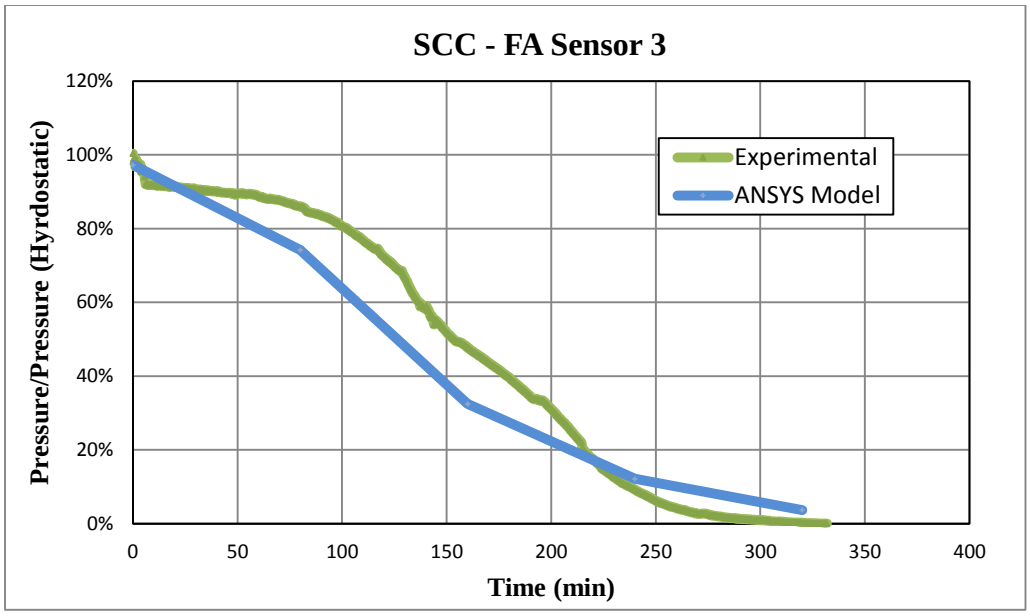

Figure 6.7: Experimental and Numerical Results for SCC – FA for Sensor 3 at 110 cm from Bottom Base

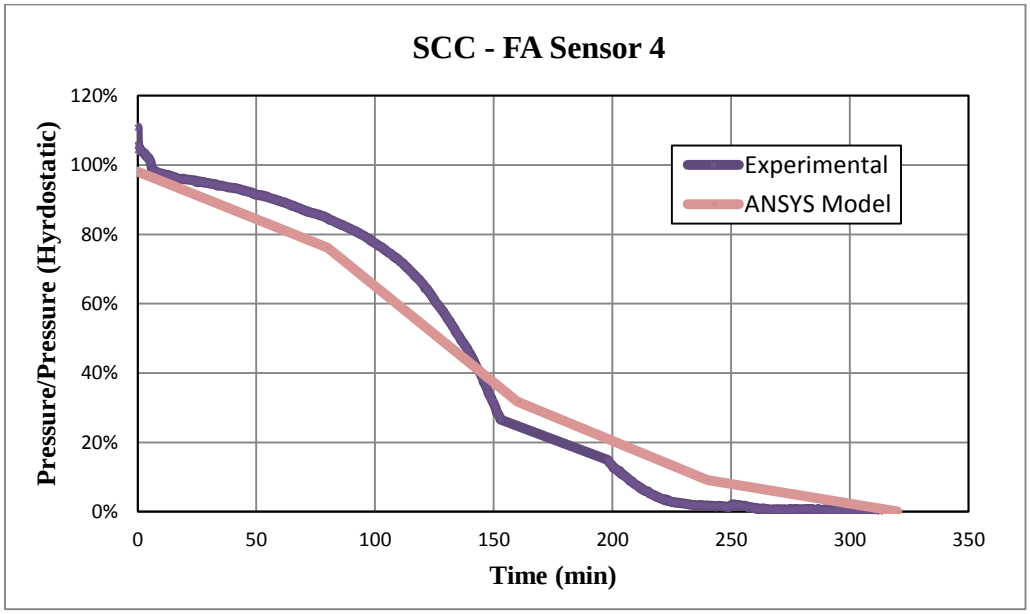

Figure 6.8: Experimental and Numerical Results for SCC – FA for Sensor 4 at 155 cm from Bottom Base

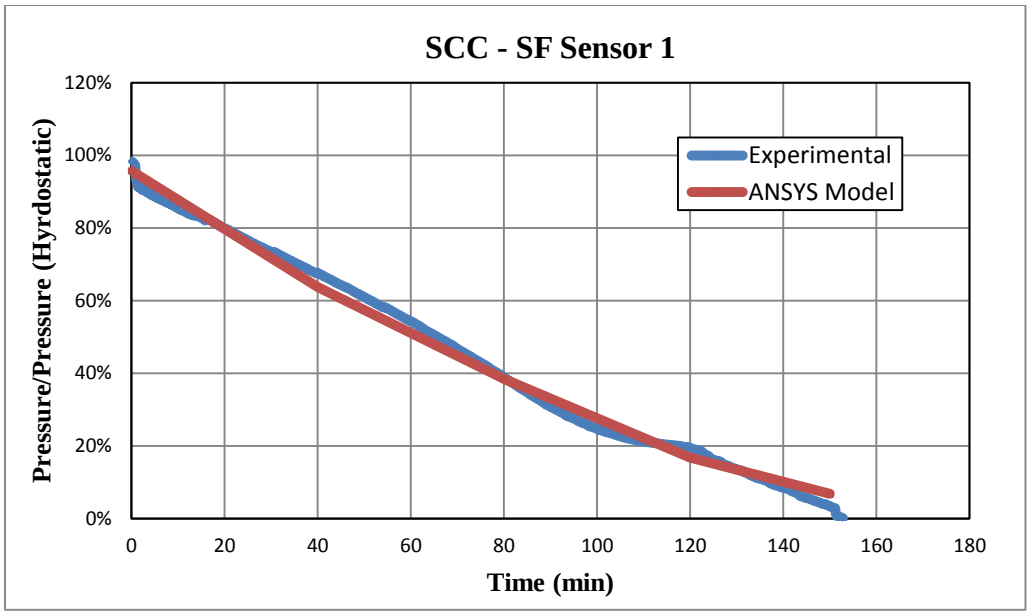

Figure 6.9: Experimental and Numerical Results for SCC – SF for Sensor 1 at 10 cm from Bottom Base

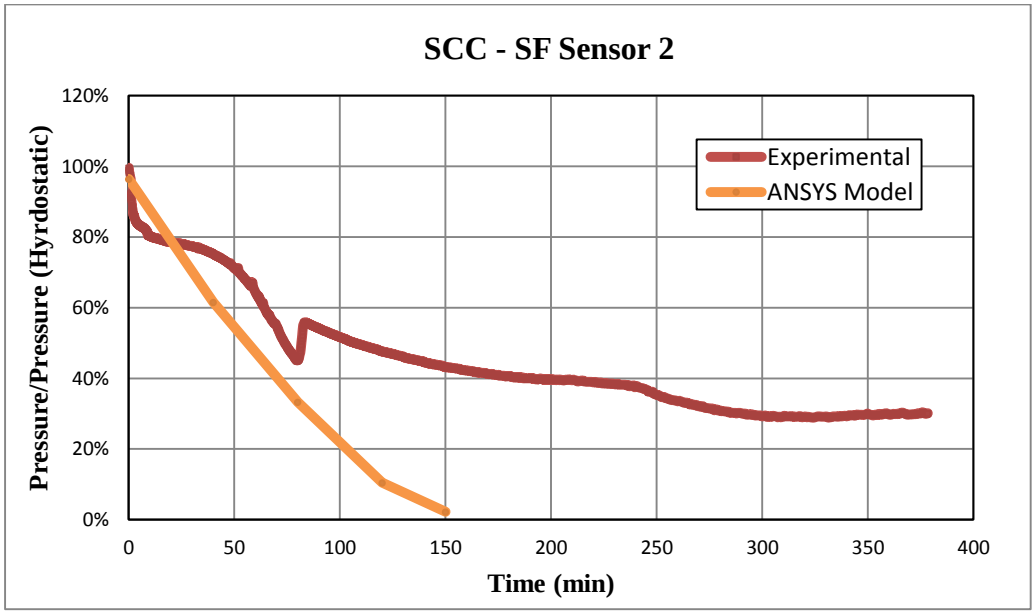

Figure 6.10: Experimental and Numerical Results for SCC – SF for Sensor 2 at 60 cm from Bottom Base

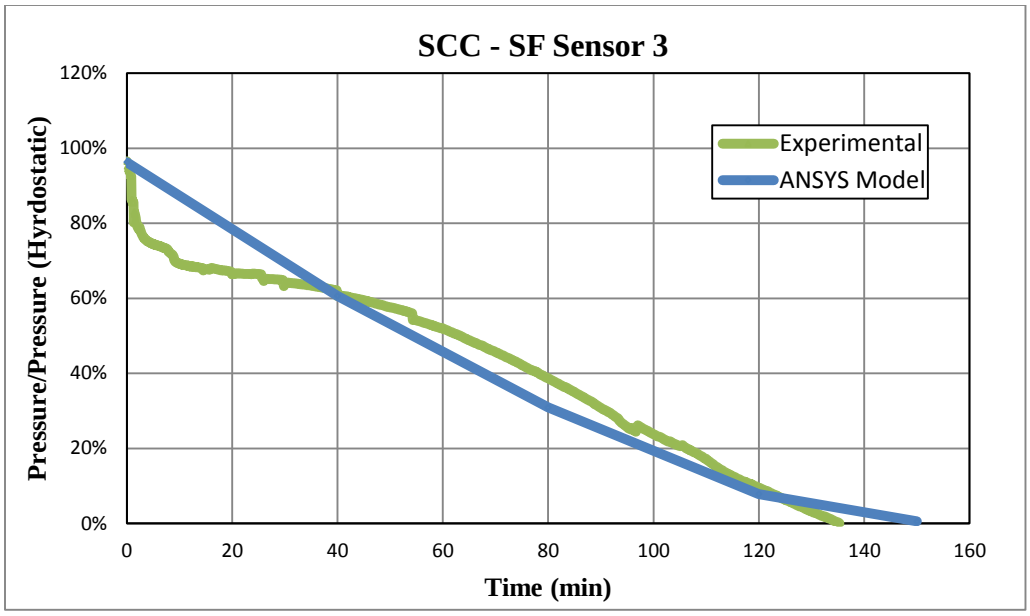

Figure 6.11: Experimental and Numerical Results for SCC – SF for Sensor 3 at 110 cm from Bottom Base

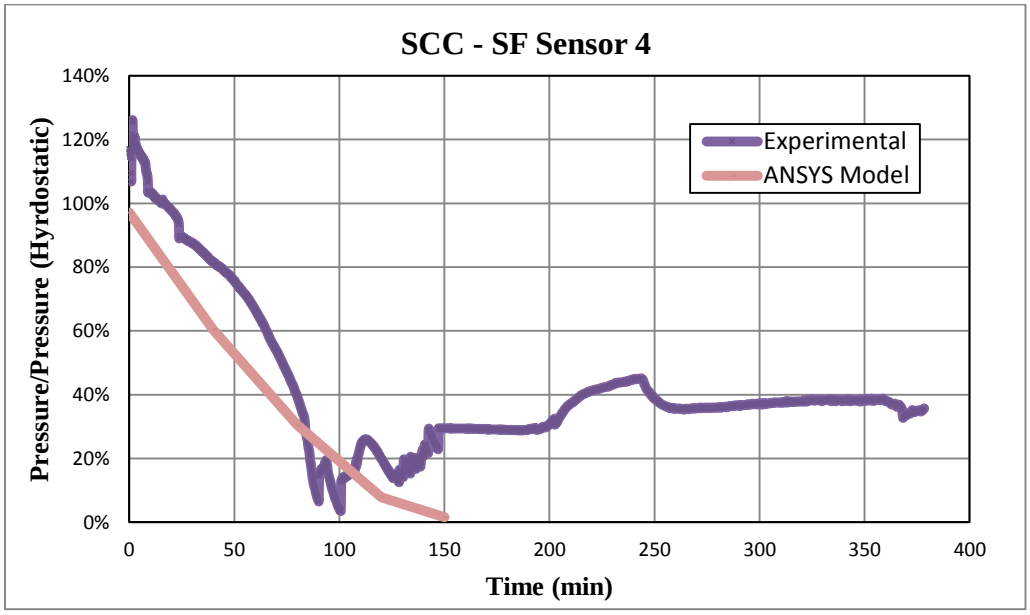

Figure 6.12: Experimental and Numerical Results for SCC – SF for Sensor 4 at 155 cm from Bottom Base

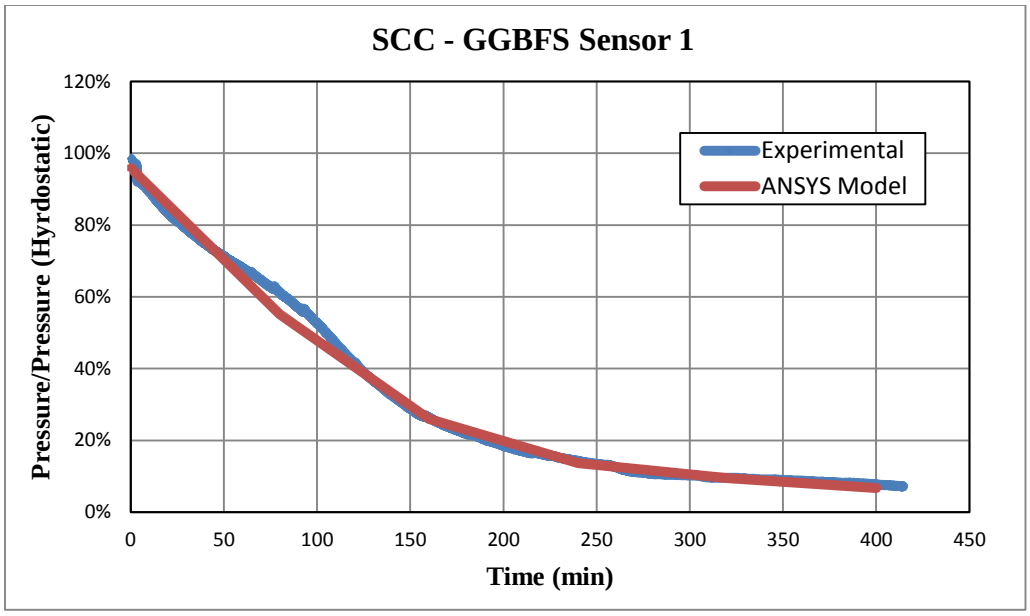

Figure 6.13: Experimental and Numerical Results for SCC – GGBFS for Sensor 1 at 10 cm from Bottom Base

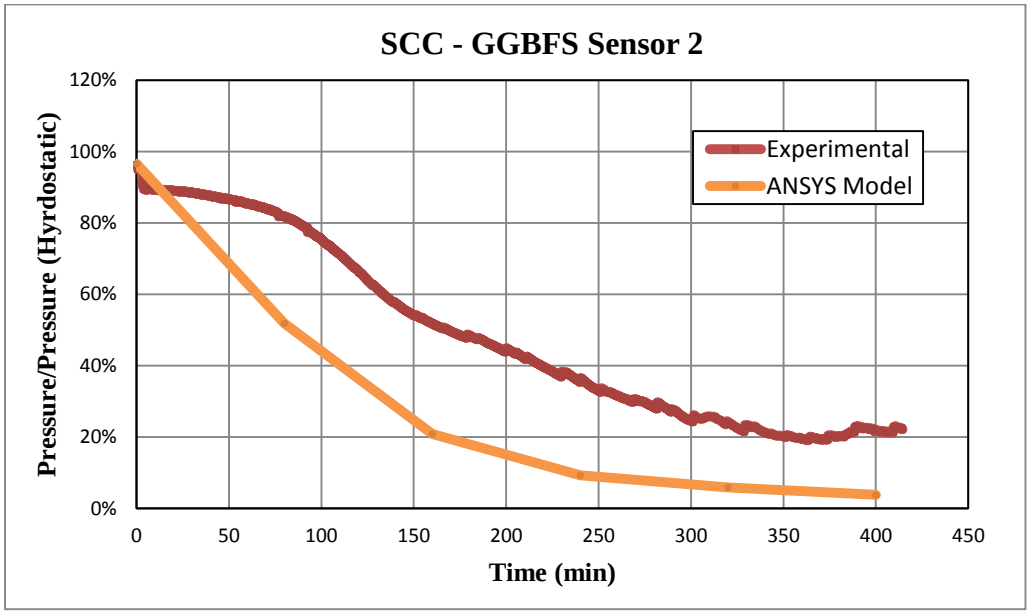

Figure 6.14: Experimental and Numerical Results for SCC – GGBFS for Sensor 2 at 60 cm from Bottom Base

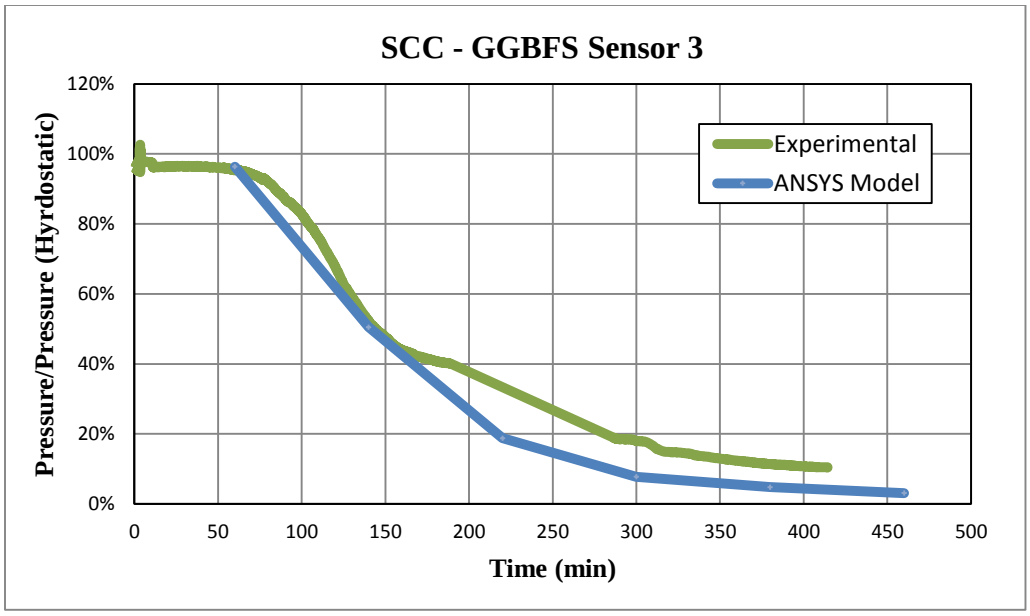

Figure 6.15: Experimental and Numerical Results for SCC – GGBFS for Sensor 3 at 110 cm from Bottom Base

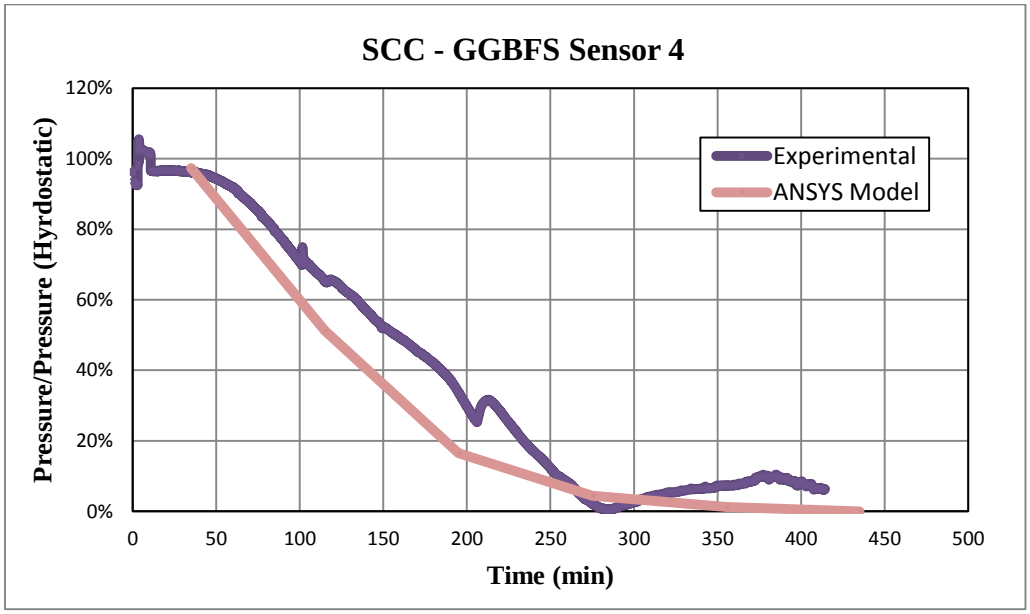

Figure 6.16: Experimental and Numerical Results for SCC – GGBFS for Sensor 4 at 155 cm from Bottom Base

6.3 Model Prediction versus Experimental Results from Literature

Expermental Results from literature were used to confirm the ability of the model to predict formwork pressure.

Figure 6.17 represents a comparison between the expermental results obtained Khayate et al. (2005) and a model created using based on the given data. Since A_{thix} was not given, a value of 0.2 Pa/s was suggested for such case based on the work reported by Roussel (2006). The wall was 2.1 m high and 0.2 m thick, two casting rates were used in this study; 25 m/hr and 10 m/hr. The comparison was made for the 25 m/hr casting rate. Good matching was found between the expermental data and the model results.

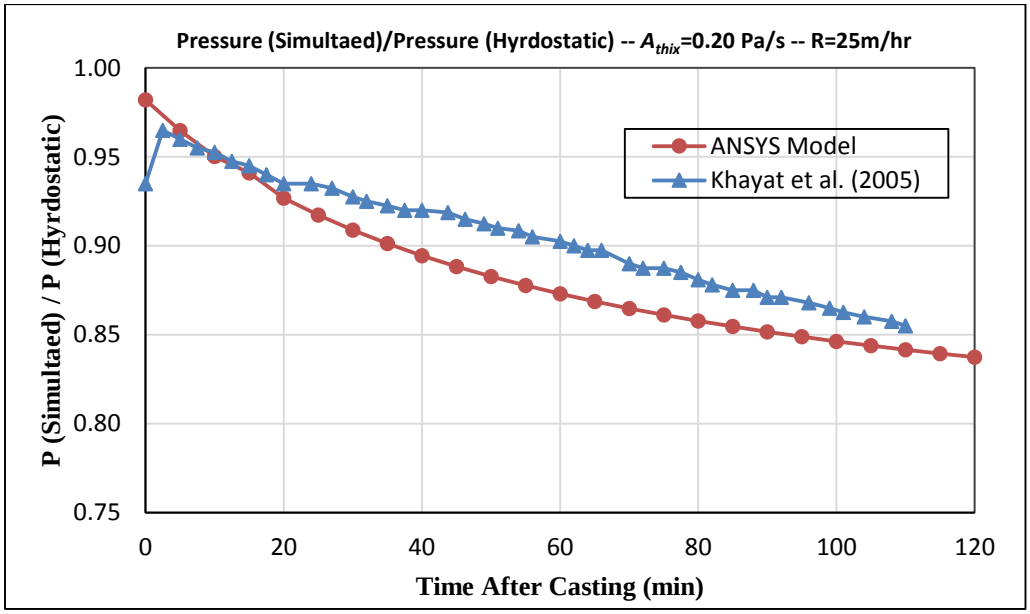

Figure 6.17: Experimental and Numerical Results from Khayat et al. (2005) and ANSYS Model

Vanhove et al. (2004) compared the results obtained from experimental data with a model that was reported in the same reference. The wall was 12 m high, concrete was poured from top in some cases and pumped from bottom in other cases, only the results of poured concrete were included in the comparison. Very good match can be seen between the numerical and experimental values (Figure 6.18).

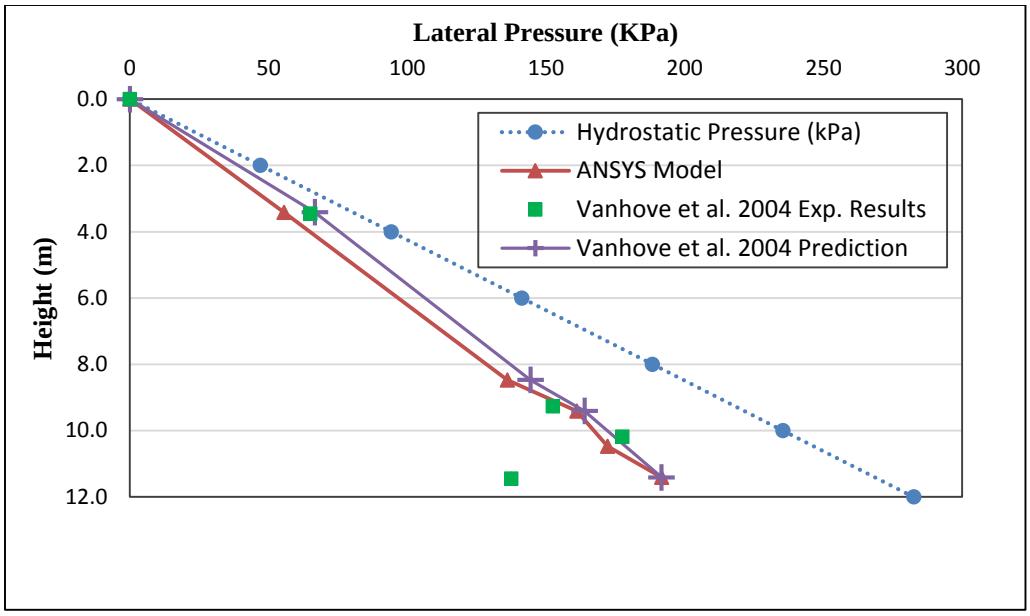

Figure 6.18: A Comparison between a set of Numerical and Experimental results.

In order to demonstrate the ability of the model to predict the pressure decay for longer periods of time and cooler temperatures, Figure 6.19 shows the relative formwork pressure in an actual wall of 2.8 m height as reported by Assad and Khayat (2006). The mix used ternary cement with 6% silica fume, 22% fly ash with the remaining being Portland cement. The experimental results were compared to two sets of models using ANSYS; one with A_{thix} value of 0.2 Pa/s and a second one with 0.1 Pa/s. The results obtained by using 0.1 Pa/s closely matches the experimental results. It should be highlighted that Poisson's ratio was essentially maintained as a constant $\upsilon = 0.498$. The apparent lack of sensitivity of the formwork pressure to the Poisson's ratio for this case may be attributed to the cooler ambient and concrete temperature conditions ($T = 20 \pm 2\ ^{o}C$) as reported in the reference.

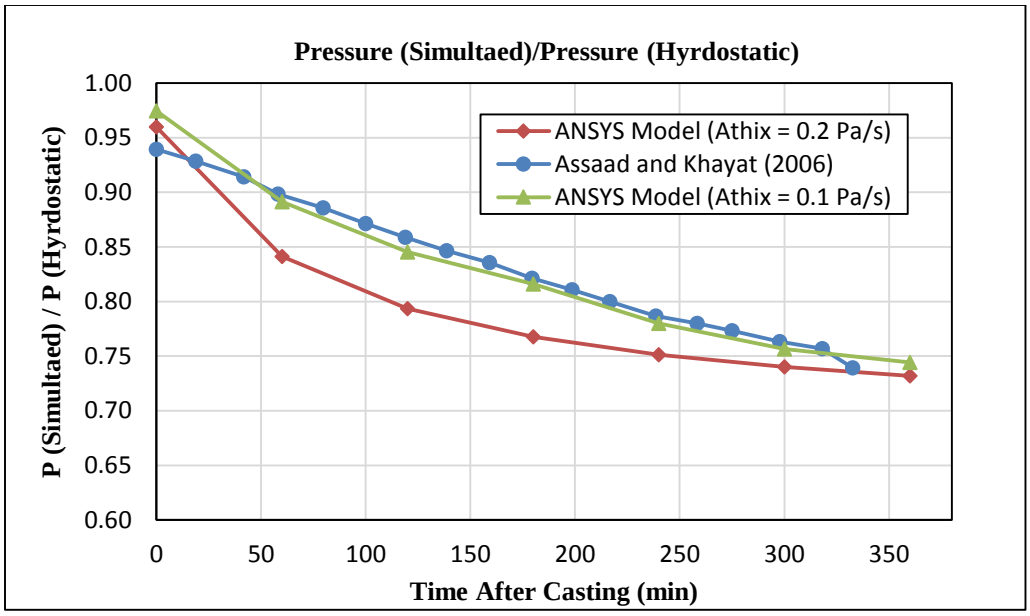

Figure 6.19: Validation of the ANSYS model using results from Assad and Khayat (2006)

6.4 Model Prediction for the Effect of A_{thix} and Casting Rate

The developed model was also utilized to study the effect A_{thix} and casting rate on the pressure decay. Using the data from Khayat et al. (2005) two comparisons were made for 2.1 m high wall.

The effect of A_{thix} on relative pressure decay is shown in Figure 6.20, three different value of A_{thix} were used at a constant casting rate of 25 m/hr. It is clear that a more thixotropic mix will result in higher reduction in relative pressure. On the contrary, Figure 6.21 illustrate effect of the casting rate on relative pressure, it is clear that higher casting rate will result higher initial pressure but not effect will be found in the decay behavior.

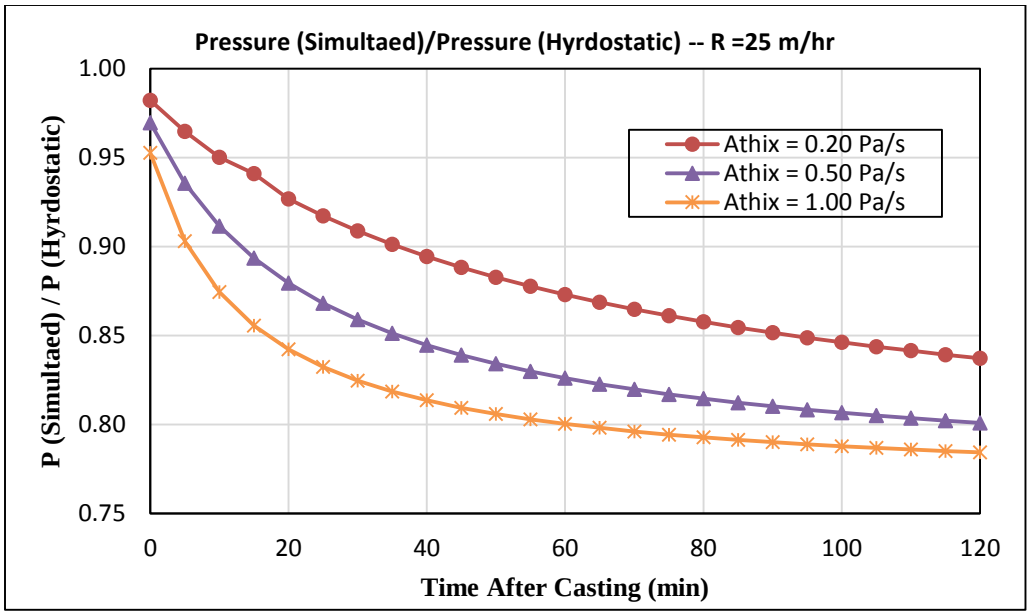

Figure 6.20: Effect of A_{thix} at Constant Casting Rate

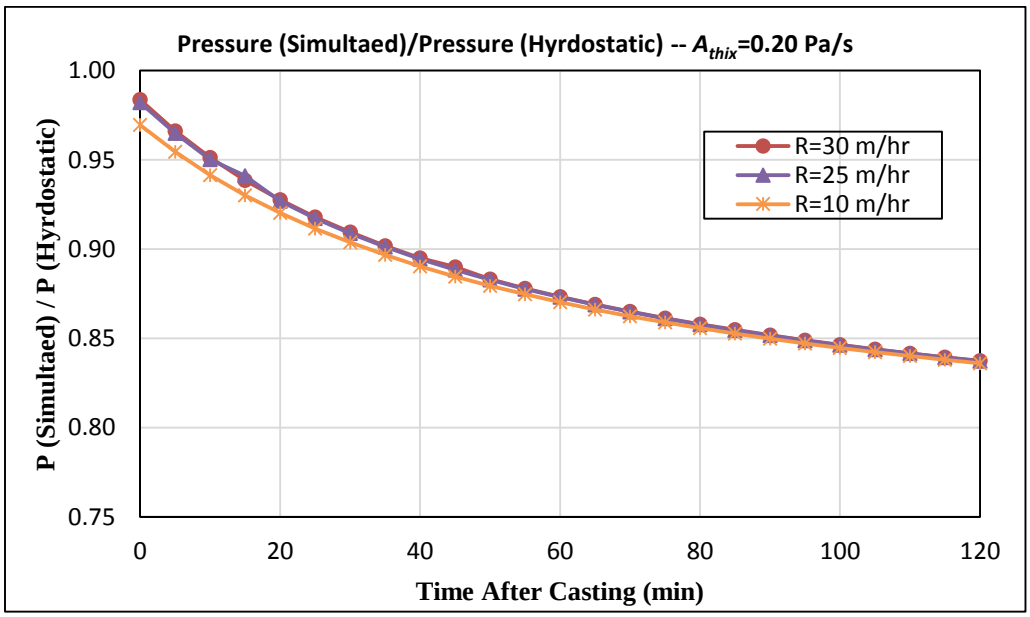

Figure 6.21: Effect of Casting Rate at Constant A_{thix}

6.5 Results for the Experimental Pumping Test

Table 6.3 summerizes the results obtained during the pumping test for a total of six mixtures, a typical pressure evolution as function of time is shown in Figure 6.22. Pressure drop per linear meter was measure for the straight horizontal sections and listed below.

Table 6.3: Test Results Obtained During Pumping Test

	Spread	τ_0 (Pa)	μ (Pa.s)	$\Delta P/\ \Delta X$ (kPa/m)	Q (m^3/h)
T1CO	705	253.3	96.1	36.6	27.69
T1FA	700	35.1	66.9	24.2	32.14
T1SF	675	45.0	81.9	26.8	29.27
T2CO	750	253.3	96.1	31.4	24.10
T2FA	655	42.1	85.4	26.1	35.71
T2SF	620	42.1	40.2	21.5	41.38
T1: Setup 1, T2: Setup 2, CO: Control Mixture, FA: Fly Ash Mixture, SF: Silica Fume Mixture					

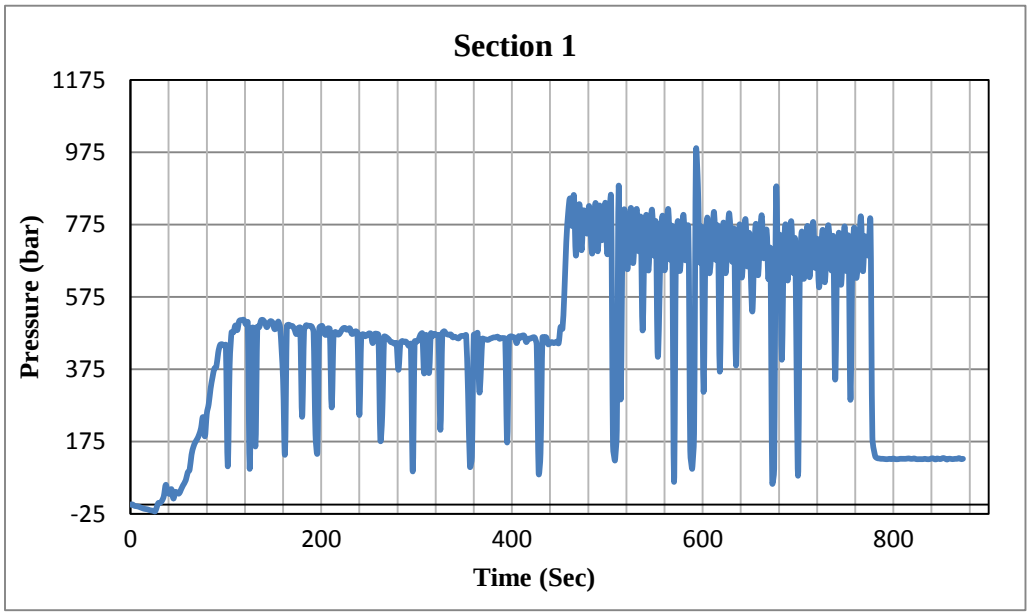

Figure 6.22: Typical Pressure Evolution for Mix T1CO at Section 1

Values for the drop in pressure was found to be between 21.5 to 36.6 kPa/m, this differnce was basically due to the different rheological properties and different flow rates. The pressure at different locations along the pipeline was measure by pressure sensors and strian gauges. These numbering of these location is illustrated in Figure 6.23 and Figure 6.24 for setup 1 and setup 2 respectively. Note that section 9 in setup 1 is on the vertical pipe at the discharge point and is at 1 m high starting from the previos bend. Similarly in setup 2, section 12 is on the vertical pipe at the discharge point and is at 1 m high strting from the previos bend.

Figure 6.25 to Figure 6.30 represent the pressure value in bar at different locations along the pipeline in comparison of pressure values obtained from the Abaqus model.Good matching was found between the expermental values and the ones obtained from the model, some of the expermental readings were higher and some were lower than the ones expected by the model due to some expermental errors. Contour plots obtained by Abaqus for the pressure drop in pipe for all mixtures are illustrated in Appendix B. Figure 6.31 shows the proposed constituve model used to estimate the pressure drop per linear meter using the values of the yield stress and viscosity of the concrete in question. This model can be utalized as a design tool to find how much would be the pressure drop based on the given values of viscosity and yield stress. The eqution obtained for this model confirms that pressure drop is affect by the value of viscosity with a minor effect of yield stress.

$$\frac{\Delta P}{\Delta X} = 15.78 + 0.1115\mu + 0.02965\tau_0 \qquad \text{Eq. 6. 1}$$

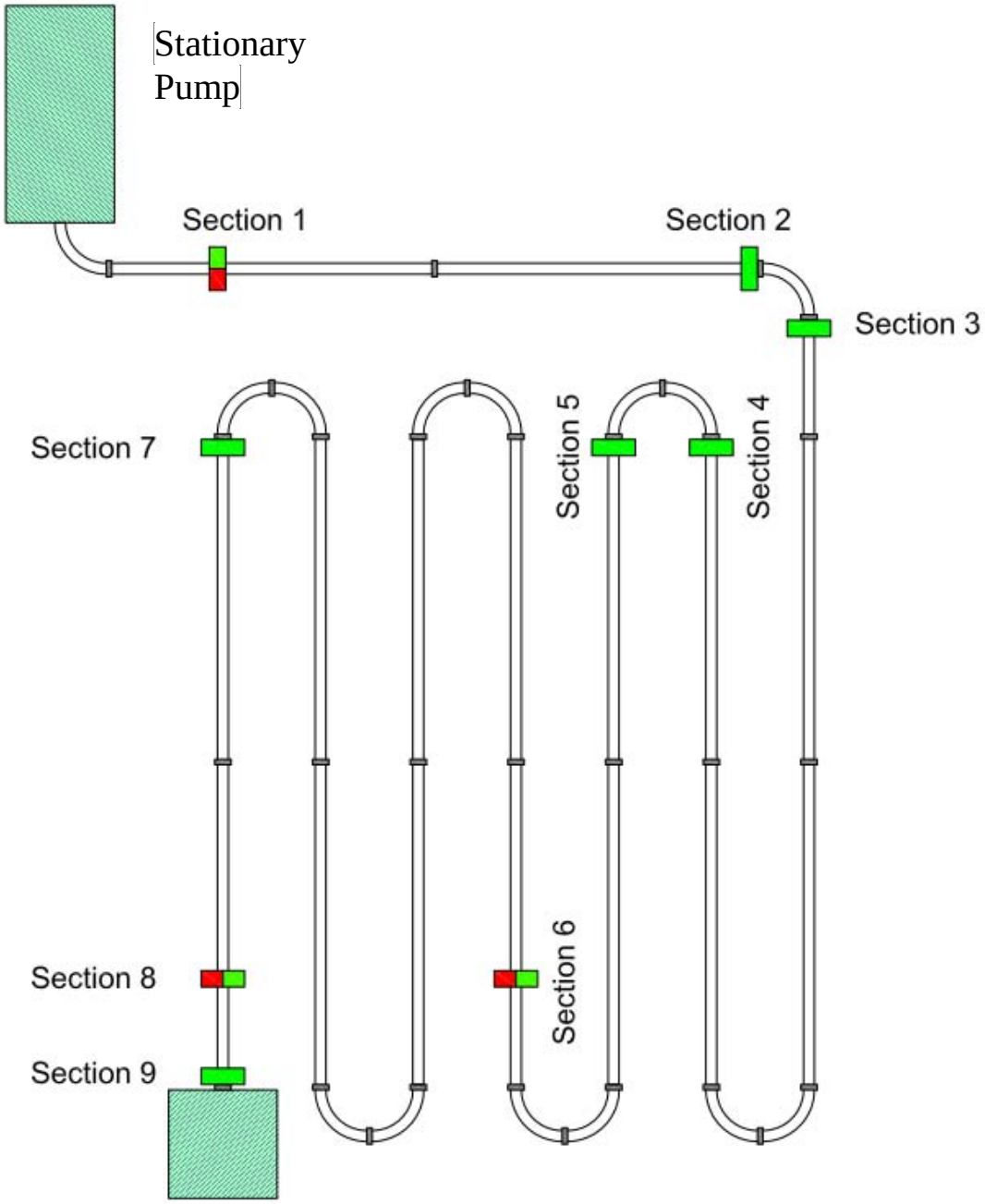

Figure 6.23: Sections for Setup 1

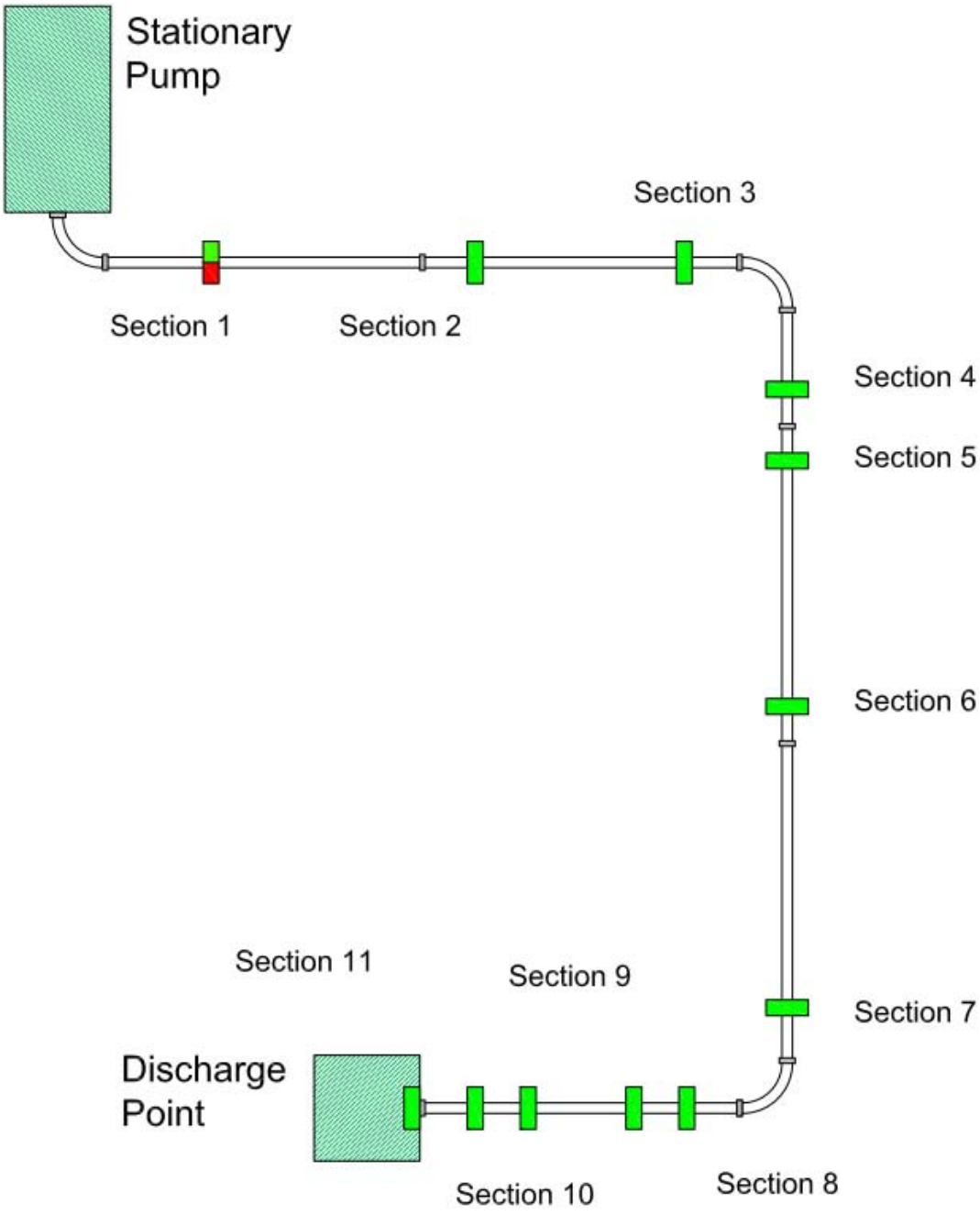

Figure 6.24: Sections for Setup 2

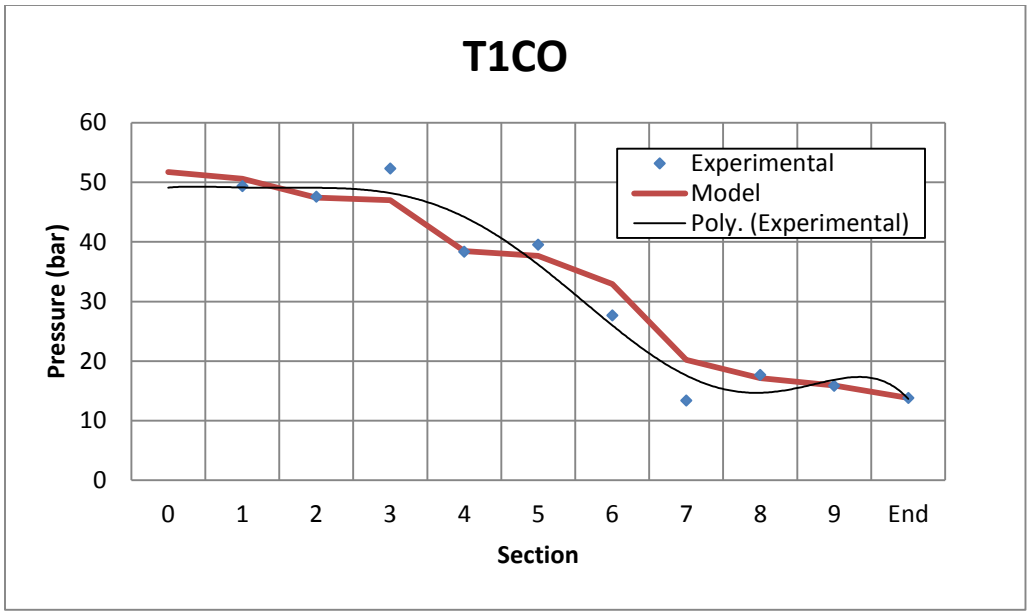

Figure 6.25: Pressure at Different Locations for T1CO

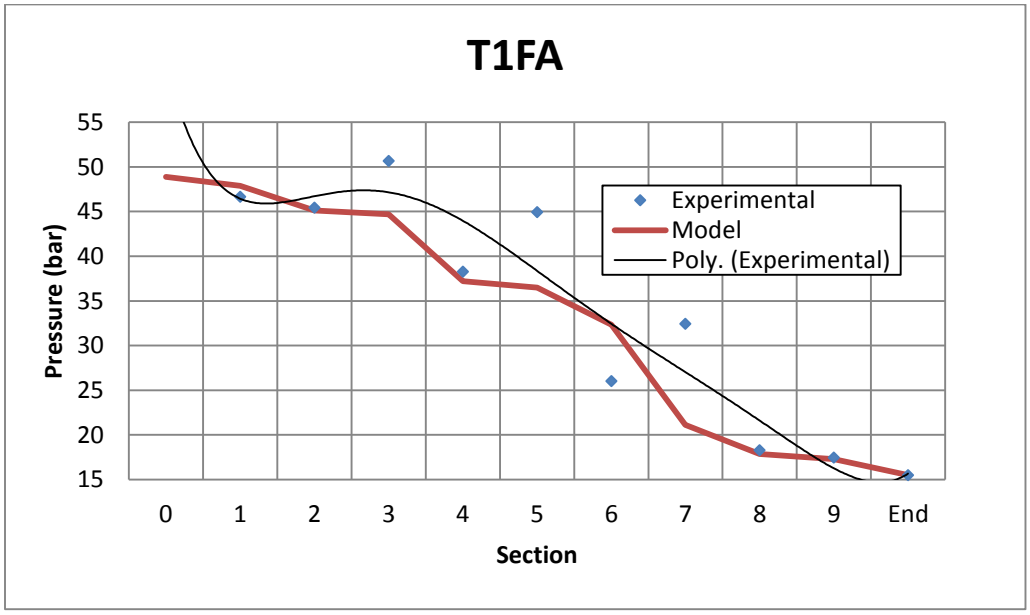

Figure 6.26: Pressure at Different Locations for T1FA

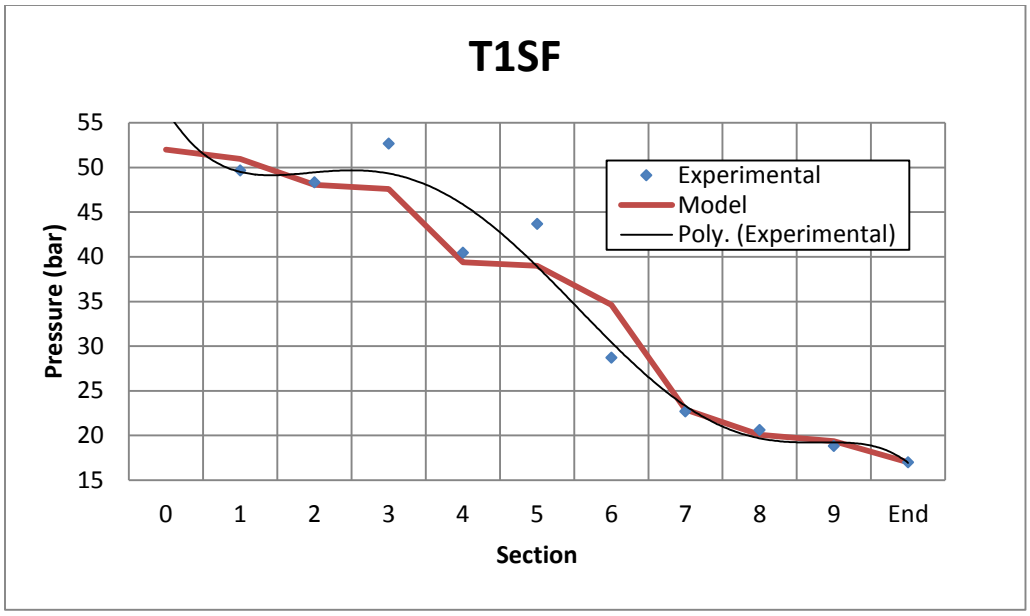

Figure 6.27: Pressure at Different Locations for T1SF

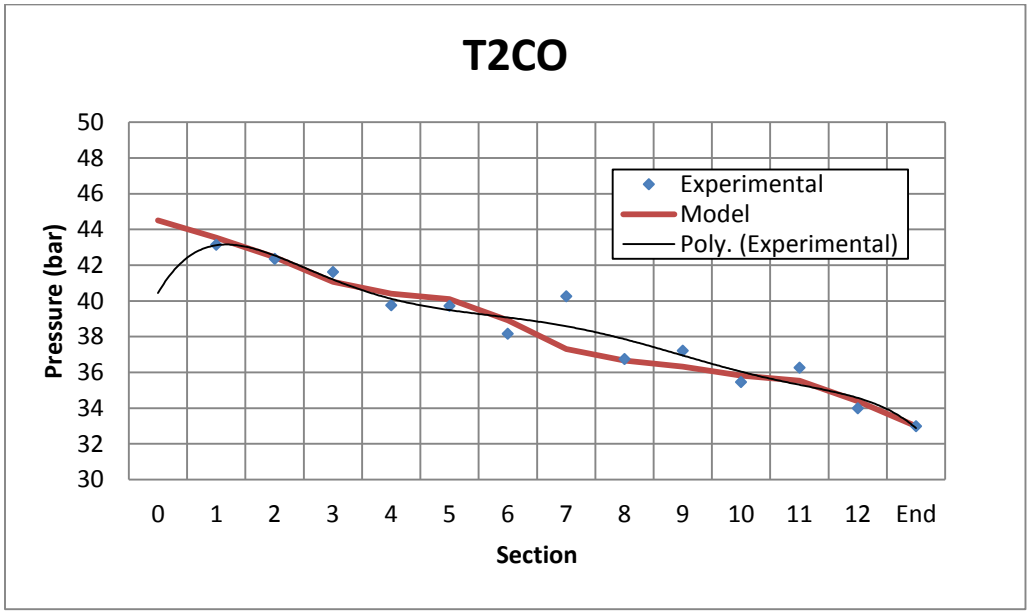

Figure 6.28: Pressure at Different Locations for T2CO

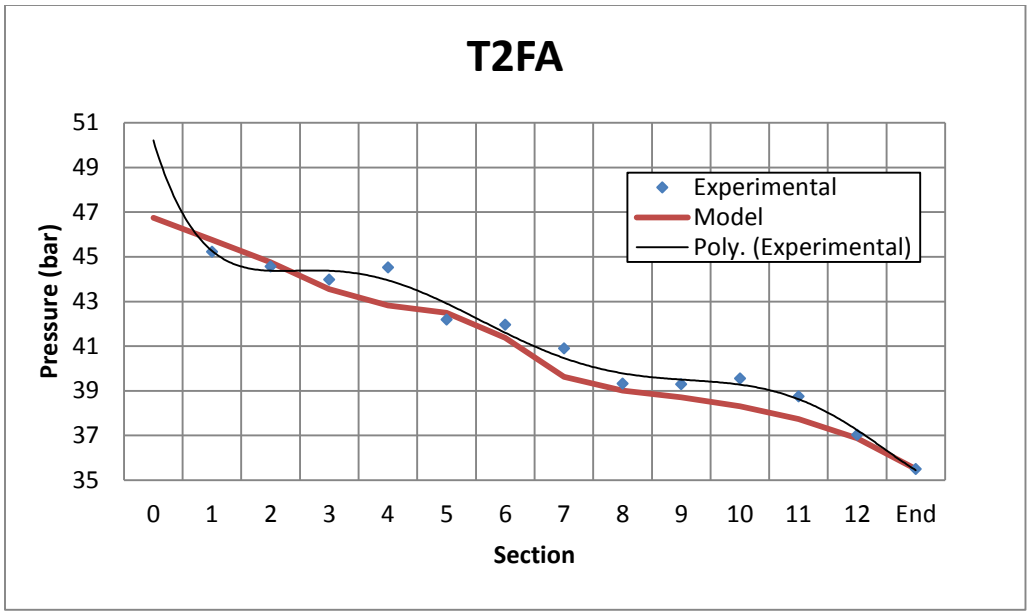

Figure 6.29: Pressure at Different Locations for T2FA

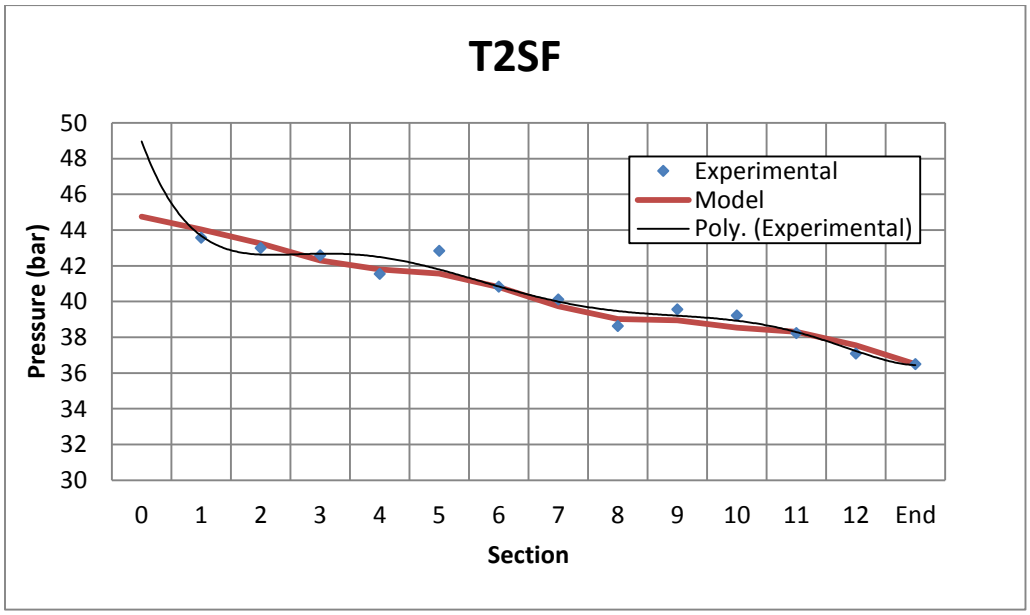

Figure 6.30: Pressure at Different Locations for T2SF

Pressure loss due to bends is summarized in Table 6.4.

Table 6.4: Pressure Loss due to Bends

	T1CO	T1FA	T1SF		T2CO	T2FA	T2SF	
Total Distance(m)	47.1	47.1	47.1		14.2	14.2	14.2	
# of Bends	13	13	13		2	2	2	
Pressure at Section 1	49.35	46.65	49.66		43.14	45.22	43.57	
Pressure at Section 8	17.67	18.30	20.64		36.26	38.76	38.23	
Total Drop (bar)	31.68	28.35	29.03		6.88	6.47	5.34	
Drop in Straight Sections (bar)	0.00	0.00	0.00		0.00	0.00	0.00	
Drop due to Bends (bar)	31.68	28.35	29.03	**Avg.**	6.88	6.47	5.34	**Avg.**
Loss per Bend (bar)	2.44	2.18	2.23	**2.28**	3.44	3.23	2.67	**3.12**

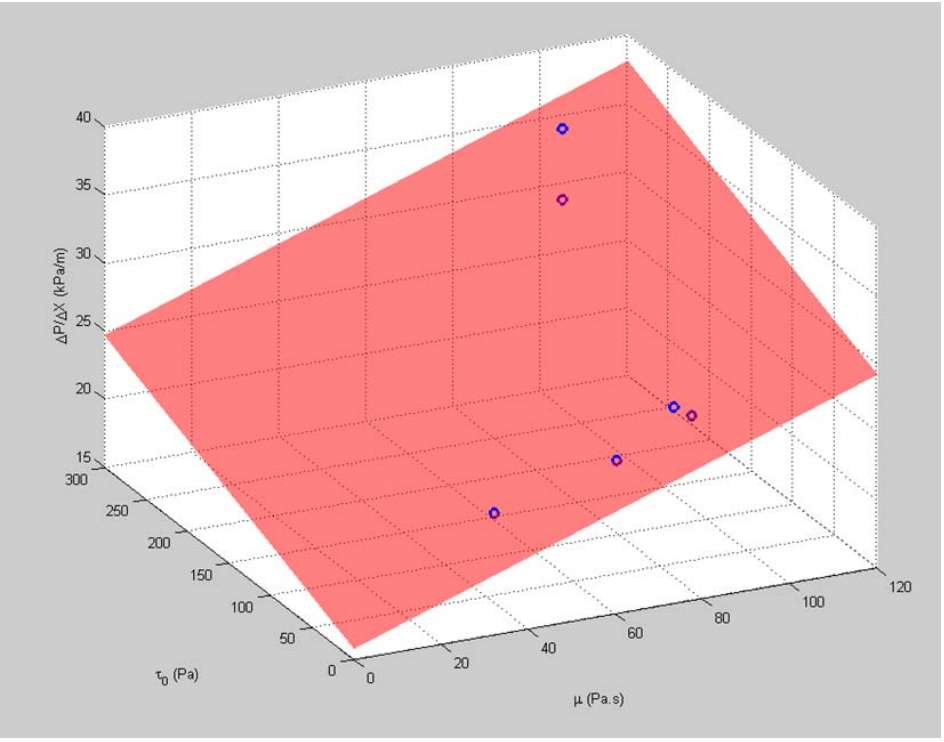

Figure 6.31: Proposed Constitutive Model to Estimate the Pressure drop using the Values of Yield Stress and Viscosity.

CHAPTER 7

CALCULATIONS FOR LUBRICATION LAYER AND PLUG FLOW MODEL

7.1 Introduction

The existence of the lubrication has been discussed in earlier chapters, in this chapter, derivation of the equation of velocity of concrete while pumping based on the work of Jacobsen et al. (2008) will be explained and the derived equation will be used to estimate the thickness of the lubrication layer and its rheological properties.

7.2 Plug Flow Behavior of Concrete

Jacobsen et al. (2008) discussed the differences between the flow of concrete and any other fluid. Basically the flow of concrete in pipes is considered as a plug flow where a very thin layer called the lubrication layer lubricate the movement of a plug of concrete moving as one unit and having a constant velocity all over the plug. Figure 7.1 and Figure 7.2 show velocity profile and the shape of the plug flow for Bingham fluids in circular pipes, it can be clearly seen that the thickness of the lubrication layer is very small compared to the size of the plug.

Newtonian fluids like water will have a parabolic velocity profile with a maximum velocity at the middle and zero velocity at the pipe surface.

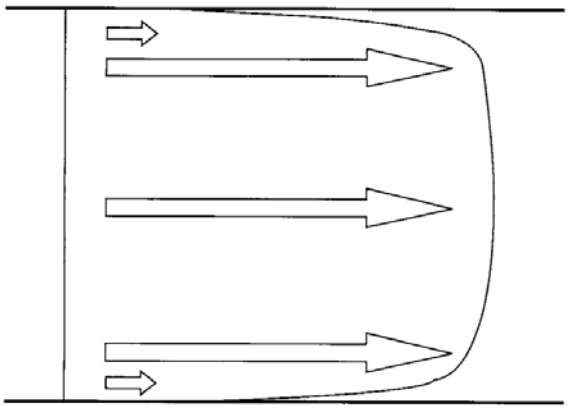

Figure 7.1: Velocity Profile for a Bingham Fluid in a Circular Pipe (Newman and Choo 2003)

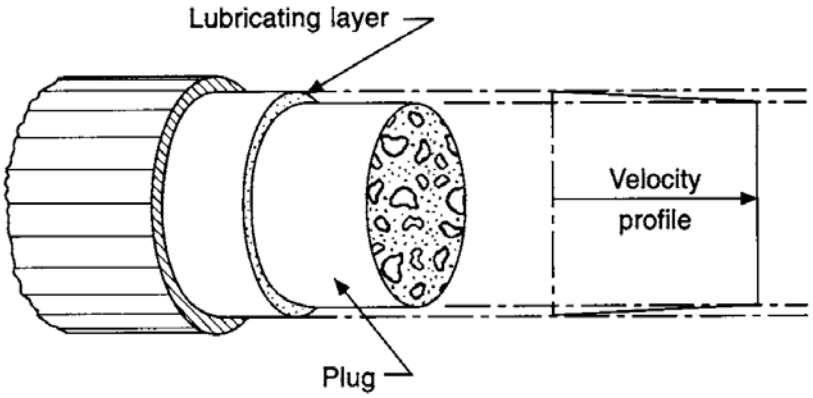

Figure 7.2: Plug Flow (Newman and Choo 2003)

Feys et al. (2013) reported that the entire velocity difference between the concrete the pipe wall is concentrated in the lubrication layer.

Although the properties of lubrication layer are not easy not measure, but still some researcher tried to evaluate the properties of the lubrication layer. Kaplan (2001) has reported that the thickness of the lubrication layer varies between few mm up to 1 cm. Ngo (2009) concluded in his study that the thickness of the lubrication layer increases with the volume of the cement paste, water-cement ratio and the superplasticizer content, and decreases if the fine sand content increase. Khatib (2013) reported that the rheological properties of the lubrication layer are well related to those of concrete; therefore, the

rheological properties of lubrication layer are affected by the rheological properties of the concrete.

Kaplan (2001) has established a relationship to relate the pumping pressure to the properties of the lubrication layer and he came up with the below expression. It should be highlighted that the rheological parameters were measured using tribometer rheometer.

$$\tau = \tau_{0,i} + \eta_i . \nu \qquad \text{Eq. 7.1}$$

where τ is the shear stress in the lubrication layer (Pa), $\tau_{0,i}$ is the yield stress of the lubrication layer (Pa), $\eta_i$is the viscous constant (Pa s/m), and ν is the velocity difference over the lubrication layer (m/s), determined from the rotational velocity of the tribometer cylinder.

Feys et al. (2013) reported the differences in the flow behavior represented by the velocity between normal slump concrete (denoted as conventionally vibrated concrete CVC) and SCC.

Figure 7.3 shows the velocity profile for both CVC and SCC. It can be clearly seen that due to low yield stress for SCC, the plug size in SCC is much smaller than CVC and a part of the concrete itself is sheared. Since the yield stress for CVC in most cases higher than the shear stress, concrete cannot flow unless the lubrication layer is available. On the opposite, for SCC the yield stress is lower than the shear stress, but still a lubrication layer is proven to be present.

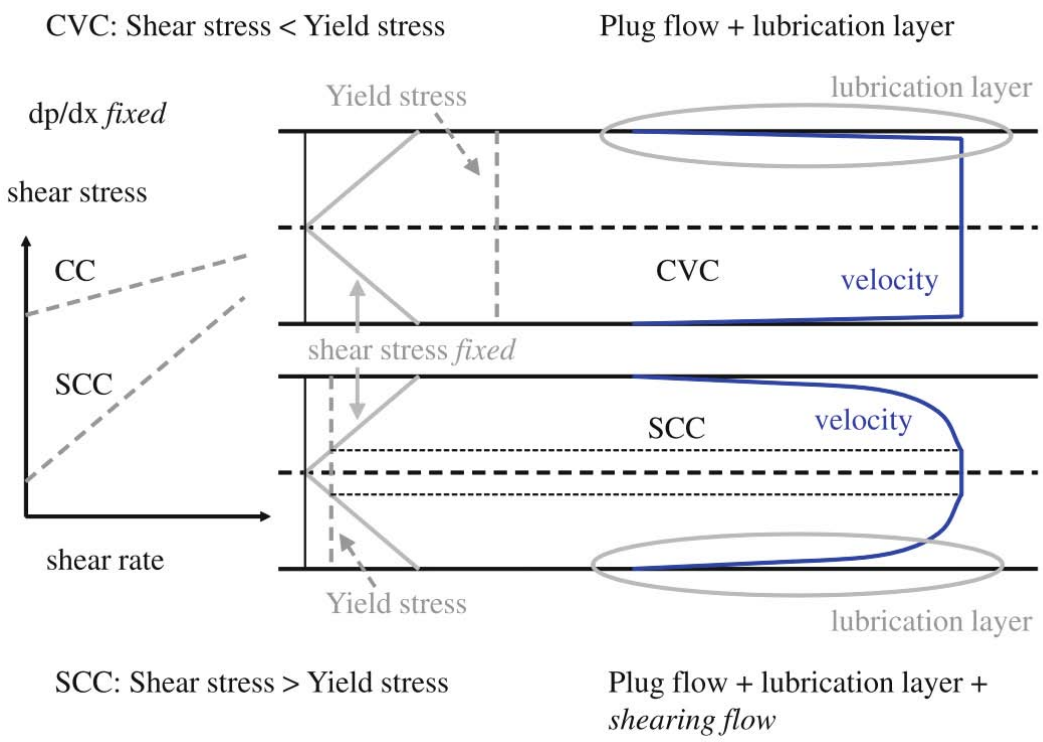

Figure 7.3: Theoretical Velocity Profiles for CVC and SCC (Feys 2013)

7.3 Velocity Distribution for Concrete Flowing in Pipes

Jacobsen et al. (2008) derived the velocity distribution of Bingham fluid flowing with or without plug.

7.3.1 No Slip Tube Flow of Bingham Fluid

Consider the simplified cylindrical element shown in Figure 7.4, where:

p: Pressure (Pa)
x: Length (m)
v_x: Total Concrete Flow (m/s)
v(r): Concrete Flow as Function of radius (m/s)
a: Radius of the Pipe
τ: shear in flowing concrete [Pa], τ assumed > τ_0 at infinitesimal distance from pipe wall and inwards

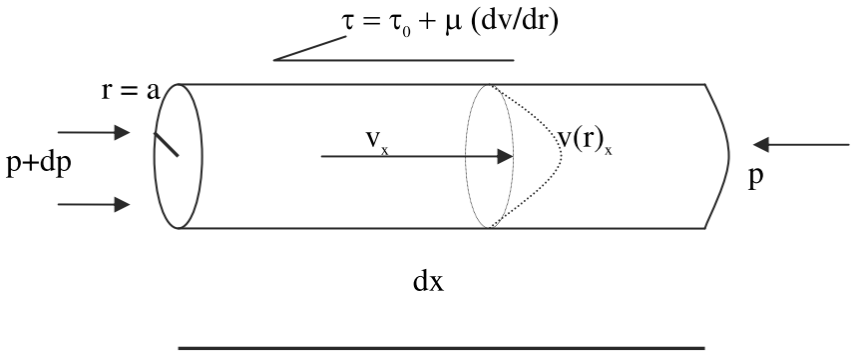

Figure 7.4: Simplified Cylindrical Element with Uni-Axial Pressure Difference (Jacobsen et al. 2008)

In order to maintain equilibrium, $\sum F_x = 0$, then

$$\pi r^2 dp - 2\pi r dx(\tau_0 + \mu \frac{dv}{dr}) = 0 \qquad \text{Eq. 7.2}$$

$$\frac{r}{2}\frac{dp}{dx} - \tau_0 - \mu \frac{dv}{dr} = 0 \qquad \text{Eq. 7.3}$$

By integrating the above equation with a boundary condition of no slip (*v(a) = 0*),

$$v(r) = \int dv = \frac{1}{2\mu}\frac{dp}{dx}\int r dr - \frac{\tau_0}{\mu}\int dr \qquad \text{Eq. 7.4}$$

7.3.2 Plug Flow with Bingham Slip Layer

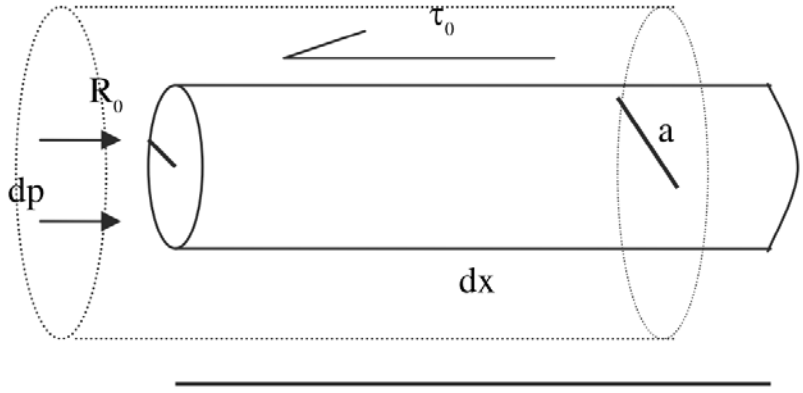

Figure 7.5: Plug with radius R_0 as shear load from pump pressure exceeds the yield τ_0 (Jacobsen et al. 2008)

In order to maintain equilibrium in Figure 7.5, $\sum F_x = 0$, then

$$\pi R_0^2 dp - 2\pi R_0 dx\tau_0 = 0 \;\Rightarrow R_0 = \frac{2\tau_0}{\left({}^{dp}/_{dx}\right)} \qquad \text{Eq. 7.5}$$

where: R_0: Plug Radius (m)

By completing the integration of Eq. 7.4 from r to a,

$$v(r) = \frac{(a^2 - r^2)}{4\mu}\frac{dp}{dx} - \frac{\tau_0}{\mu}(a - r) \qquad r \geq R_0 \qquad \text{Eq. 7.6}$$

$$v(r) = v(R_0) \qquad r < R_0 \qquad \text{Eq. 7.7}$$

As the flow equals velocity multiplied by the area of the pipe, the total flow of the plug and the slip layer can be written as:

$$G_x = v(R_0)\pi R_0^2 + \int_{R_0}^{a}\left[\frac{(a^2 - r^2)}{4\mu}\frac{dp}{dx} - \frac{\tau_0}{\mu}(a - r)\right]2\pi r dr \qquad \text{Eq. 7.8}$$

The resulting flow, so-called Buckingham-Reiner equation, can be written as (Kaplan 2010):

$$G_x = \frac{\pi a^4}{8\mu}\frac{dp}{dx}\left[1 - \frac{4}{3}\left(\frac{2\tau_0}{a\left({}^{dp}/_{dx}\right)}\right) + \frac{1}{3}\left(\frac{2\tau_0}{a({}^{dp}/_{dx})}\right)^4\right] = \frac{\pi a^4}{8\mu}\frac{dp}{dx}\left[1 - \frac{4R_0}{3a} + \left(\frac{R_0}{3a}\right)^4\right] \qquad \text{Eq. 7.9}$$

7.4 Estimation of the Lubrication Layer Thickness and Its Rheological Parameters

By using the above velocity equation, one can estimate the size of the lubrication layer and its rheological properties. Eq. 7.6 and Eq. 7.7 were used to estimate the lubrication layer

thickness and its rheological properties for the six mixtures used in the pumping test done earlier. The estimation is done by assuming a thickness for the lubrication layer (around 1.5% of the pipe diameter) along with an estimated relatively low value for the yield stress and viscosity.

By drawing a plug velocity profile of the flow the average velocity is found and is compared to the actual one (experimental value). Once the average velocity matches the actual one the required parameters are found. Summary of the estimated values of lubrication layer thickness and its rheological properties are shown in Table 7.1. It value assumed value of the lubrication layer thickness was assumed to be the same with the same yield stress value, and hence the only parameter left to change is the viscosity.

Table 7.1: Estimation of Lubrication Layer Properties

Mix ID	Thickness (mm)	τ_0 (Pa)	μ (Pa.s)
T1CO	2.75	0.5	4.600
T1FA	2.75	0.5	2.600
T1MS	2.75	0.5	2.880
T2CO	2.75	0.5	4.505
T2FA	2.75	0.5	2.525
T2MS	2.75	0.5	1.795

It can be clearly seen from Figure 7.6 and Figure 7.7 that if one assumes that velocity profile is parabolic instead of a plug using the estimated value for the thickness layer, the velocity will increase more than 10 times due to the low yield stress and viscosity. Excel sheet used for the estimation of the lubrication layer properties is illustrated in Appendix C.

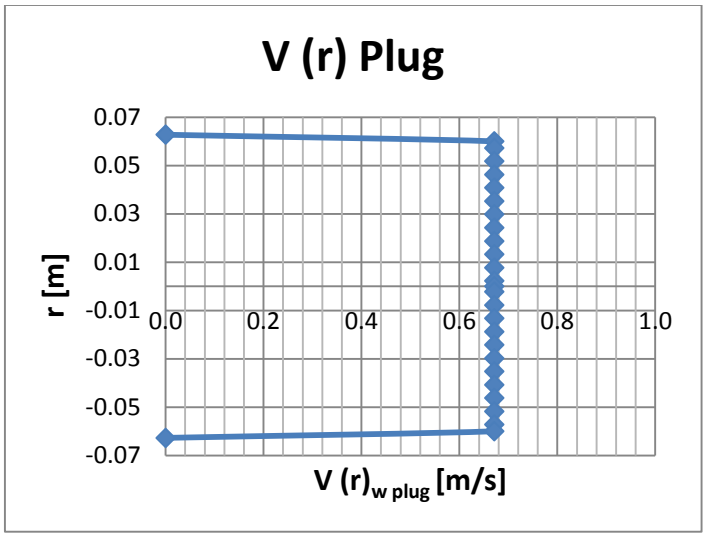

Figure 7.6: Velocity Profile Assuming Plug Flow for T1CO

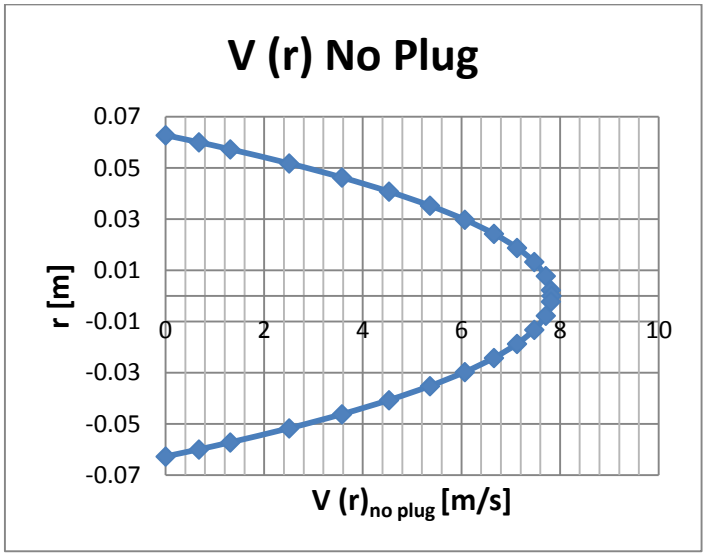

Figure 7.7: Velocity Profile Assuming No-Plug Flow for T1CO

CHAPTER 8

CONCLUSIONS AND RECOMMENDATIONS

8.1 Conclusions

The formwork lateral pressure exerted by fresh SCC was experimentally and numerically investigated for four mixes made with different mineral admixtures. The maximum formwork pressure recorded of SCC mixes was found to be given by hydrostatic pressure, followed by a decay which was governed by several variables. The type of mineral admixture used, the concrete and the ambient temperature and the Poisson's ratio played a major role in the pressure decay behavior of SCC mixes. The results obtained for SCC – SF showed the most quick pressure decay due to the high reactivity and surface area of silica fume. A model for the prediction of lateral formwork pressure exerted by SCC was presented and validated by the experimental data obtained from the full-scale test.

The variation of pressure while pumping SCC was experimentally investigated based on a full-scale pumping test for two arrangements of pipes. The pressure drop while pumping SCC was highly affected by mixture composition represented by the fresh properties like spread and by the rheological properties; including yield stress and viscosity. It was found that the pressure drop increases with the increase of viscosity and yield stress, and it decreases with the increase of spread. The average pressure drop due to bends obtained from all mixtures was found to be 1.226 and 1.245 bar per bend for the two setups respectively. The pressure drop due vertical pumping was close to 0.25 bar per linear meter.

Based on the values of viscosity and yield stress, a constitutive model was developed. The model proved the pressure drop is more sensitive to the change in the viscosity rather than the yield stress. The ABAQUS did not address the presence of the lubrication layer and plug flow. Instead, it only showed a traditional parabolic velocity profile for flow of pumped SCC. A mechanistic model has been utilized to estimate the slip layer thickness and was validated by comparing the actual flow with the calculated one.

8.2 Recommendations

1. Transporting of SCC was one of the major difficulties in obtaining the same results of the mix design that was obtained from lab trials, hence it recommended to keep the testing as close as possible to the concrete production unit.
2. Due to the higher accuracy of pressure sensors (transducers) as compared to strain gauges, it is advisable to use them in any pumping test and use the strain gauges as a backup measuring system.
3. Further studies are required to fully understand the flow behavior of SCC during pumping; SCC's should be tested for different flow rates, different pipe arrangements and large variety of mixture compositions.
4. Further studies are required to quantify the pressure loss due to vertical pumping and due to bends with different angles.
5. The pump should be capable of delivering different pressures or flow rates and these values should be given by the pump itself and then compared to the measured values.
6. It is recommended to use a data acquisition system that is capable of reading the signals in portion of second.

REFERENCES

[1]. **ACI Committee 304 (1995)**. *"Placing Concrete by Pumping Methods (ACI 304.2 R)"*. ACI Materials Journal, 92(4), 441-464.

[2]. **ACI Committee 304 (2000)**. *"Guide for Measuring, Mixing, Transporting, and Placing Concrete (ACI 304R)"*. American Concrete Institute (ACI), 28.

[3]. **ACI Committee 622 (1958)**. *"Pressures on Formwork"*, ACI Journal Proceedings, 55(2), 173-190.

[4]. **Adam, M., Bennasr, M., & Santos Delgado, H. (1963)**. *"Formwork Pressure of Fresh Concrete"*. Annales de l'Institut Technique du Bâtiment et des Travaux Publics, Série Béton (207-208), 403-423.

[5]. **ANSYS Inc. (2007)**. *"ANSYS Inc. Release Notes; Release 11.0"*. Global Headquaters, Suth Pointe, 275 Technology Drive, Canonsburg, PA.

[6]. **Arslan, M. (2002)**. *"Effects of Drainer Formworks on Concrete Lateral Pressure"*. Construction and Building Materials, 16(5), 253-259.

[7]. **Arslan, M., Simsek, O., & Subasi, S. (2005)**. *"Effects of Formwork Surface Materials on Concrete Lateral Pressure"*. Construction and Building Materials, 19(4), 319-325.

[8]. **Assaad, J., & Khayat, K.H. (2005A)**. *"Formwork Pressure of Self-Consolidating Concrete Made with Various Binder Types and Contents"*. ACI Materials Journal, 102(4), 215-223.

[9]. **Assaad, J., & Khayat, K.H. (2005B)**. *"Kinetics of Formwork Pressure Drop of Self-Consolidating Concrete Containing Various Types and Contents of Binder"*. Cement and Concrete Research, 35(8), 1522-1530.

[10]. **Assaad, J., & Khayat, K.H. (2005C)**. *"Effect of Coarse Aggregate Characteristics on Lateral Pressure Exerted by Self-Consolidating Concrete"*. ACI Materials Journal, 102(3), 145-153.

[11]. **Assaad, J.J., & Khayat, K.H. (2006)**. *"Effect of Viscosity-Enhancing Admixtures on Formwork Pressure and Thixotropy of Self-Consolidating Concrete"*. ACI Materials Journal, 103(4), 280-287.

[12]. **Barnes, H.A., & Hutton, J.F. (1989)**. *"An Introduction to Rheology"*. Elsevier.

[13]. **Bartos, P.J. (2000)**. *"Measurement of Key Properties of Self-Compacting Concrete"*. In CEN/STAR PNR Workshop, 6.

[14]. **Bianchi Technology for Precast (2014)**. *"Speedy 3-4 MC"*. Ireland, http://www.bianchicasseforme.it.

[15]. **Billberg, P. (2003)**. *"Form Pressure Generated by Self-Compacting Concrete"*. Proceeding of the 3rd International RILEM Symposium on Self-Compacting Concrete, 271-280.

[16]. **Brameshuber, W., Uebachs, S., Wallevik, O., & Nielsson, I. (2003)**. *"Investigations on the Formwork Pressure Using Self-Compacting Concrete"*. Proceedings of the 3rd International RILEM Symposium on Self-Compacting Concrete, 281-287.

[17]. **Browne, R.D., & Bamforth, P.B. (1977)**. *"Tests to Establish Concrete Pumpability"*. ACI Journal Proceedings 74(5), 193-203.

[18]. **Central Chemical Consulting (2014),** *"Rheology: Rheology and its Terminology"***.** http://www.chem.com.au/science/rheology/rheology2/.

[19]. **Civil Industries Research and Information Association (CIRIA) (1965)**. *"The Pressure of Concrete on Formwork"*. Research Report No. 1, London.

[20]. **Collepardi, M. (2005)**. *"Admixtures-Enhancing Concrete Performance"*. Proceedings of the 6th International Congress of Global Construction, 55-66.

[21]. **Daczko, J. A. (2012)**. *"Self-consolidating Concrete: Applying what We Know"*. Spon Press, 711 Third Avenue, New York, NY 10017.

[22]. **DIN 18218 (1980)**. *"Frishbeton Auf Lautrechte (Pressure of Fresh Concrete on Vertical Formwork)"*, (only available in German). Berlin.

[23]. **Djelal, C. (2001)**. *"Designing and Perfecting a Tribometer for the Study of Friction of a Concentrated Clay-Water Mixture against a Metallic Surface"*. Materials and Structures, 34(1), 51-58.

[24]. **Djelal, C., Vanhove, Y., & Magnin, A. (2004)**. *"Tribological Behavior of Self Compacting Concrete"*. Cement and Concrete Research, 34(5), 821-828.

[25]. **Dufour, F., & Pijaudier-Cabot, G. (2005)**. *"Numerical Modelling of Concrete Flow: Homogeneous Approach"*. International Journal for Numerical and Analytical Methods in Geomechanics, 29(4), 395-416.

[26]. **Feys, D. (2009)**. *"Interactions Between Rheological Properties and Pumping of Self-Compacting Concrete"*. PhD Dissertation, Ghent University, Belgium.

[27]. **Feys, D., De Schutter, G., & Verhoeven, R. (2013)**. *"Parameters Influencing Pressure during Pumping of Self-Compacting Concrete"*. Materials and Structures, 46(4), 533-555.

[28]. **Feys, D., De Schutter, G., Verhoeven, R., & Khayat, K.H. (2010)**. *"Similarities and Differences of Pumping Conventional and Self-Compacting Concrete"*. Design, Production and Placement of Self-Consolidating Concrete, Springer 153-162.

[29]. **Gallego, E., Fuentes, J.M., Ramirez, A., & Ayuga, F. (2009)**. *"Design of Tall Formworks by a Finite-Element Model"*. Journal of Construction Engineering and Management, 136(7), 803-810.

[30]. **Gallego, E., Fuentes, J.M., Ramirez, A., & Ayuga, F. (2011)**. *"Computer Simulation of Complex-Shaped Formworks using Three-Dimensional Numerical Models"*. Automation in Construction, 20(7), 830-836.

[31]. **Gardner, N.J. (1984)**. *"Formwork Pressures and Cement Replacement by Fly Ash"*. Concrete International, 6(10), 50-55.

[32]. **Gregori A., Ferron R.P., Sun Z., & Sha S.P. (2008)**. *"Experimental Simulation of Self-Consolidating Concrete Formwork Pressure"*. ACI Materials Journal, 150(1), 97-104.

[33]. **Hansen, J.K.B. (1988)**. *"Characterization of Concrete Pumpability using the Two-Point Apparatus"*. High Performance Concrete Materials Development Report, 3.2, Norway, Report No. Sintef STF65 F89046, 45.

[34]. **Hooke R. (1678)**. *"Lectures de Potentia Restitution"*. John Martin, London; reprinted by R.T. Gunter, Early Science in Oxford (1931), Oxford University Press, London, 8, 331-388.

[35]. **Hu, C., & De Larrard, F. (1996)**. *"The Rheology of Fresh High-Performance Concrete"*. Cement and Concrete Research, 26(2), 283-294.

[36]. **Hurd, M.K. (2002)**. *"Putting the Pressure on Formwork"*. Concrete International, 24(10).

[37]. **ICAR (2008)**. *"ICAR Rheometer User's Manual"*.

[38]. **Jacobsen, S., Mork, J. H., Lee, S. F., & Haugan, L. (2008)**. *"Pumping of Concrete and Mortar–State of the Art"*. COIN Project Report, 5, 45.

[39]. **Jolin, M., Burns, D., Bissonnette, B., Gagnon, F., & Bolduc, L. (2009)**. *"Understanding the Pumpability of Concrete"*. In Shotcrete for Underground Support XI, Switzerland.

[40]. **Jolin, M., Chapdelaine, F., Gagnon, F., & Beaupre, D. (2006)**. *"Pumping Concrete: a Fundamental and Practical Approach"*. In Shotcrete for Underground Support X, ASCE, 334-347.

[41]. **Kaplan, D. (2001)**. *"Pumping of Concretes"*. PhD Dissertation (In French), Laboratoire Central des Ponts et Chausées, Paris.

[42]. **Kaplan, D., De Larrard, F., & Sedran, T. (2005)**. *"Avoidance of blockages in concrete pumping process"*. ACI Materials Journal, 102(3).

[43]. **Khatib, R. (2013)**. *"Analysis and Prediction of Pumping Characteristics of High-Strength Self-Consolidating Concrete"*. PhD Dissertation, Sherbrooke University, Canada.

[44]. **Khayat, K., & Assaad, J. (2008)**. *"Measurement Systems for Determining Formwork Pressure of Highly-Flowable Concrete"*. Materials and Structures, 41(1), 37-46.

[45]. **Khayat, K., Assaad, J., Mesbah, H., & Lessard, M. (2005)**. *"Effect of Section Width and Casting Rate on Variations of Formwork Pressure of Self-Consolidating Concrete"*. Materials and Structures, 38(1), 73-78.

[46]. **Khayat, K.H., & Assaad, J.J. (2006)**. *"Effect of w/cm and High-Range Water-Reducing Admixture on Formwork Pressure and Thixotropy of Self-Consolidating Concrete"*. ACI Materials Journal, 103(3), 186-193.

[47]. **Khayat, K.H., Bonen, D., Shah, S., & Taylor, P. (2007)**. *"SCC Formwork Pressure – Task 1: Capturing Existing Knowledge on Formwork Pressure Exerted by SCC"*. The National Ready-Mix Concrete Research Foundation and the Strategic Development Council, American Concrete Institute, Sherbrooke.

[48]. **Kim, J.H., Beacraft, M.W., Kwon, S.H., & Shah, S.P. (2011)**. *"Simple Analytical Model for Formwork Design of Self-Consolidating Concrete"*. ACI Materials Journal, 108(1), 38-45.

[49]. **Kulasegaram, S., Karihaloo, B.L., & Ghanbari, A. (2011)**. *"Modelling the Flow of Self–Compacting Concrete"*. International Journal for Numerical and Analytical Methods in Geomechanics, 35(6), 713-723.

[50]. **Malik, M.A. (2011)**. *"Study on Segregation and Rheology of Self Compacting Concrete"*. MSc Thesis, King Fahd University of Petroleum and Minerals, Saudi Arabia.

[51]. **Mewis, J. (1979)**. *"Thixotropy - a General Review"*. Journal of Non-Newtonian Fluid Mechanics, 6(1), 1-20.

[52]. **Mukhtar, F. (2011)**. *"Computer-Aided Modeling and Simulation of Flow of Self Compacting Concrete"*. MSc Thesis, King Fahd University of Petroleum and Minerals, Saudi Arabia.

[53]. **Neville, A.M. (1995)**. *"Properties of Concrete"*. Pearson Prentice Hall, London.

[54]. **Newman, J., & Choo, B.S. (2003)**. *"Advanced Concrete Technology 3: Processes"*. Butterworth-Heinemann, Oxford.

[55]. **Ngo, T.T (2009)**. *"Influence of Concrete Compositions on the Pumpability Parameters"*. PhD Dissertation (In French), Cergy Pontoise, France.

[56]. **Nilson, A.H., Darwin, D., & Dolan, C.W. (2003)**. "*Design of Concrete Structures"*. McGraw Hill, New York.

[57]. **Omran, A.F. (2009)**. "*Formwork Pressure Exerted by Self-Consolidating Concrete"*. PhD Dissertation, Sherbrooke University, Canada.

[58]. **Ovarlez, G., & Roussel, N. (2006)**. *"A Physical Model for the Prediction of Lateral Stress Exerted by Self-Compacting Concrete on Formwork"*. Materials and Structures, 39(2), 269-279.

[59]. **Ozawa, K., Maekawa, K., Kunishima, M., & Okamura, H. (1989)**. *"Development of High Performance Concrete Based on the Durability Design of Concrete Structures"*. Proceedings of the second East-Asia and Pacific Conference on Structural Engineering and Construction (EASEC-2), 445-450.

[60]. **PMW Central Services (2011)**. *"Concrete Technology for Concrete Pumps"*. **Putzmeister AG, 46-53**

[61]. **Rahman, M.K., Baluch, M.H., & Malik, M.A. (2014)**. *"Thixotropic Behavior of Self Compacting Concrete with Different Mineral Admixtures"*. Construction and Building Materials, 50(0), 710-717.

[62]. **Roby, H.G. (1935)**. *"Pressure of Concrete on Forms"*. Civil Engineering, 5, 162.

[63]. **Rodin, S. (1952)**. *"Pressure of Concrete on Formwork"*. ICE Proceedings, Thomas Telford, London, 1(6), 709-746.

[64]. **Roussel, N. (2004)**. *"Three-Dimensional Numerical Simulations of Slump Tests"*. Annual Transactions of Nordic Rheology Society, Paris, 12, 55-62.

[65]. **Roussel, N. (2006)**. *"A Thixotropy Model for Fresh Fluid Concretes: Theory, Validation and Applications"*. Cement and Concrete Research, 36(10), 1797-1806.

[66]. **Roussel, N., Geiker, M.R., Dufour, F.d.r., Thrane, L.N., & Szabo, P. (2007)**. *"Computational Modeling of Concrete Flow: General Overview"*. Cement and Concrete Research, 37(9), 1298-1307.

[67]. **Roussel, N., Lemaître, A., Flatt, R.J., & Coussot, P. (2010)**. *"Steady State Flow of Cement Suspensions: a Micromechanical State of the Art"*. Cement and Concrete Research, 40(1), 77-84.

[68]. **Sakuta, M., Kasanu, I., Yamane, S., & Sakamoto, A. (1989)**. *"Pumpability of Fresh Concrete"*. Takenaka Technical Research Laboratory, Tokyo 125-133.

[69]. **Schjodt, R. (1955)**. *"Calculation of Pressure of Concrete on Forms"*. In Proceedings ASCE, 81, 1-16.

[70]. **Schwing (2014)**. *"In: Eckardstein KEV (ed) Pumping, Concrete and Concrete Pumps: a Concrete Placing Manual"*, 133.

[71]. **Shetty, M.S. (2005)**. *"Concrete Technology Theory and Practice"*. S. Chand, Delhi.

[72]. **Spiratos, N., Mailvaganam, N.P., Malhotra, V.M, & Jolicoeur, C (2003)**. *"Superplasticizers for Concrete: Fundamentals, Technology, and Practice"*. Supplementary Cementing Materials for Sustainable Development, Ottawa, Canada.

[73]. **Stephenson T.O. (1968)**. *"Concrete Pumping, Pumpable Concrete"*. Australian Civil Engineering, 24-27.

[74]. **Thrane, L.H. (2007)**. *"Form Filling with SCC"*. Concrete Centre DTI/DTU Denmark, 269.

[75]. **Vanhove, Y., Djelal, C. and Magnin, A. (2004)**, "*Prediction of the lateral pressure exerted by self-compacting concrete on formwork"* Magazine of Concrete Research, 56: 55–62.

[76]. **Vanhove, Y., Djelal, C., & Magnin, A. (2000)**. *"Friction Behaviour of a Fluid Concrete against a Metallic Surface"*. In International Conference on Advances in Mechanical Behaviour, Plasticity and Damage, 679-684.

APPENDIX A: ANSYS FLUENT RUNS

The below results were obtained by varying the components of Herschel–Bulkley equation namely, τ_0, μ and b using ANSYS Fluent.

$$\boldsymbol{\tau = \tau_0 + \mu\dot{\gamma}^b} \qquad \text{Eq. A.1}$$

Note: A1, B1 and C1 in the below table are experimental data obtained from Hu and De Larrard (1996)

A.1 Varying τ_0 while keeping μ Constant

	Concrete	A1*	A2	A3	A4	A5	A6	A7
Varying τ_0	τ_0 (Pa)	216	250	400	600	150	100	50
	μ (Pa.s)	262	262	262	262	262	262	262
	Actual Slump (cm)	25.00	NA	NA	NA	NA	NA	NA
	Model Slump (cm)	23.01	22.60	19.1	17.28	23.9	24.56	25.39
	Model Flow (cm)	38.04	36.63	33.81	30.81	40.67	43.92	47.11

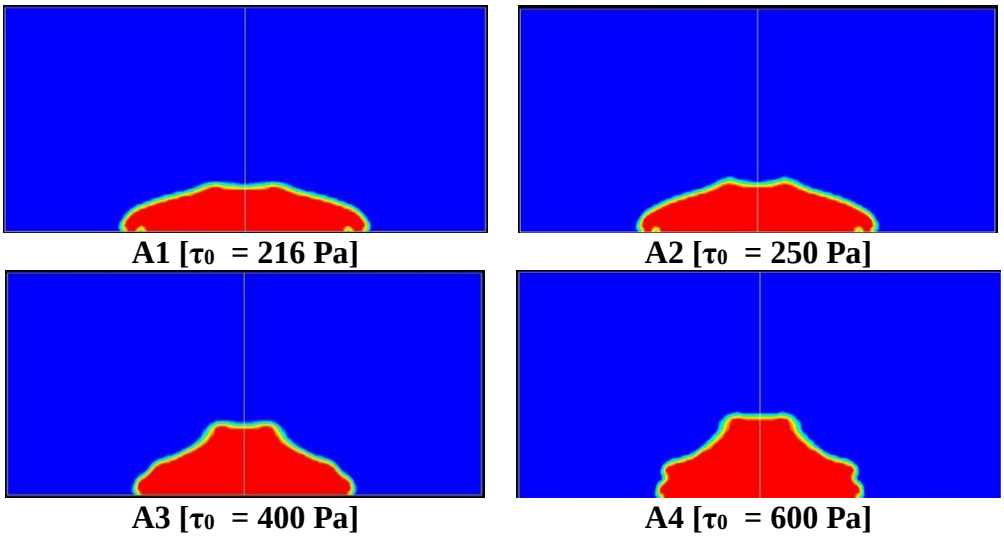

Figure A.1: Slump Cone Test Modeled by ANSYS Fluent for Increasing τ_0

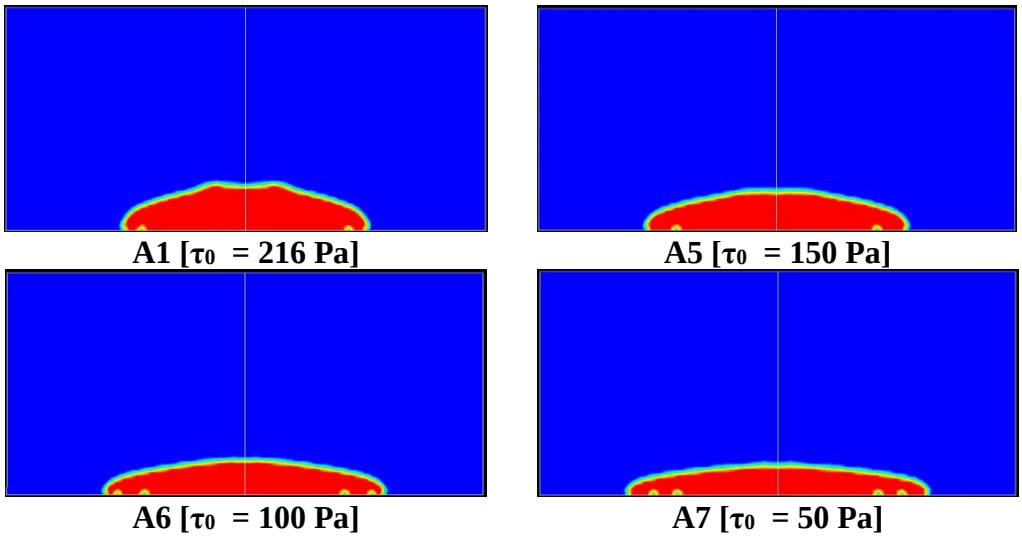

Figure A.2: Slump Cone Test Modeled by ANSYS Fluent for Decreasing τ_0

A.2 Varying μ while keeping τ_0 Constant

	Concrete	B1*	B2	B3	B4	B5	B6	B7
Varying μ	τ_0 (Pa)	216	216	216	216	216	216	216
	μ (Pa.s)	262	320	400	500	180	130	60
	Actual Slump (cm)	25.00	NA	NA	NA	NA	NA	NA
	Model Slump (cm)	23.01	22.95	22.88	22.64	23.04	23.21	23.57
	Model Flow (cm)	38.04	37.42	36.91	36.29	38.36	38.39	39.72

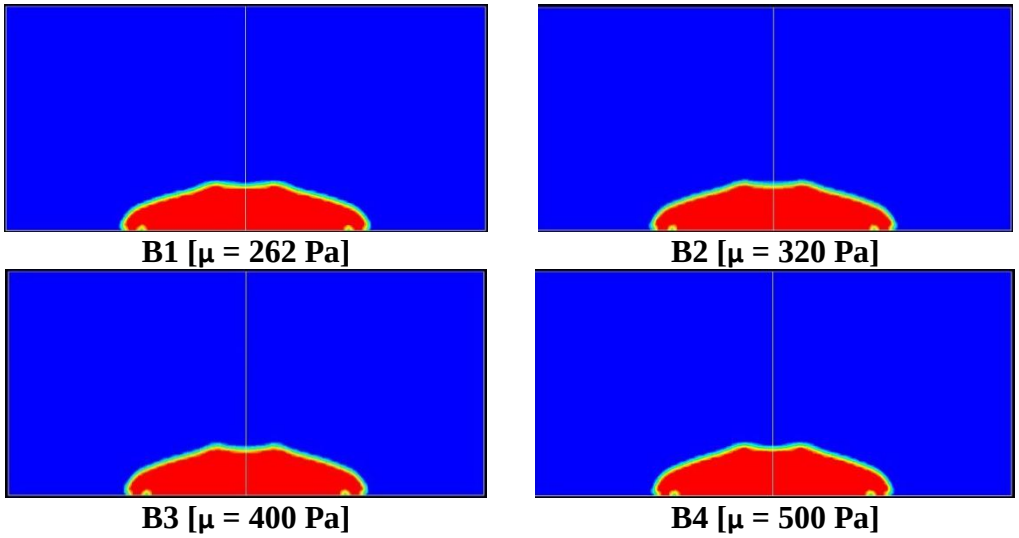

Figure A.3: Slump Cone Test Modeled by ANSYS Fluent for Increasing μ

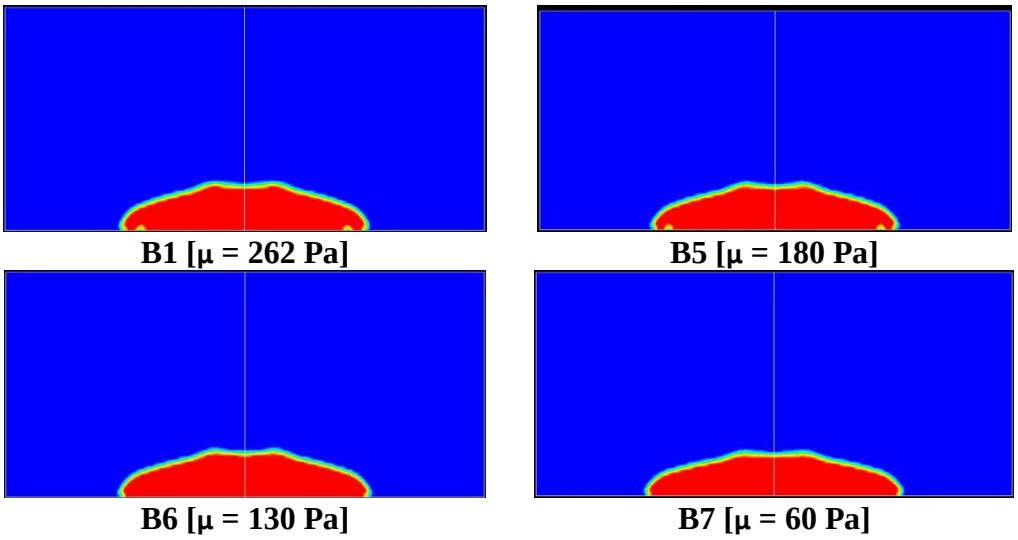

Figure A.4: **Slump Cone Test Modeled by ANSYS Fluent for Decreasing μ**

A.3 Varying b while keeping μ and τ_0 Constant

	Concrete	C1	C2	C3	C4	C5	C6	C7
Varying b	b	1	1.5	2	3	0.85	0.5	0.3
	τ_0 (Pa)	216	216	216	216	216	216	216
	μ (Pa.s)	262	262	262	262	262	262	262
	Actual Slump (cm)	25.00	NA	NA	NA	NA	NA	NA
	Model Slump (cm)	23.01	23.26	23.20	23.35	22.89	22.08	21.54
	Model Flow (cm)	38.04	39.14	39.42	40.21	37.17	36.49	36.04

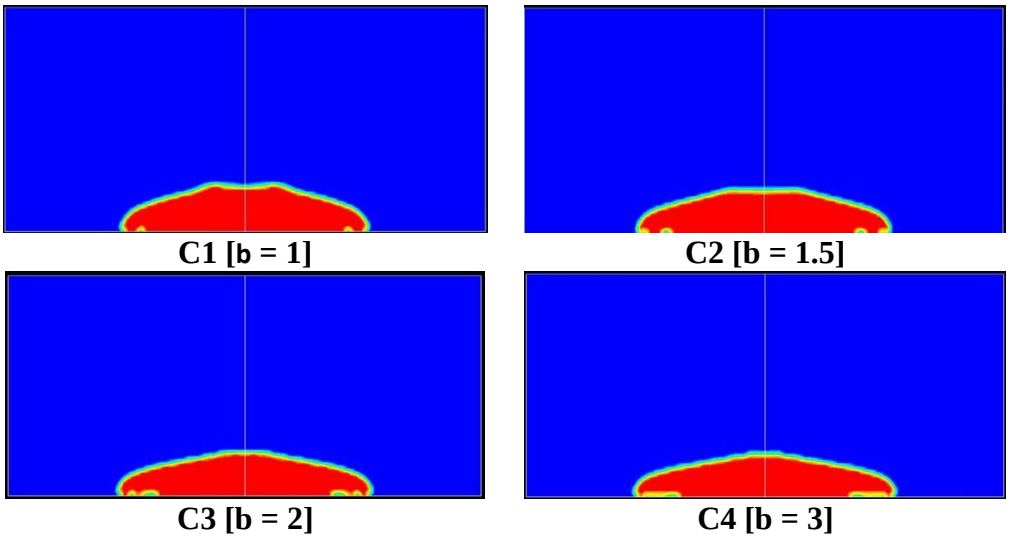

Figure A.5: Slump Cone Test Modeled by ANSYS Fluent for Increasing b

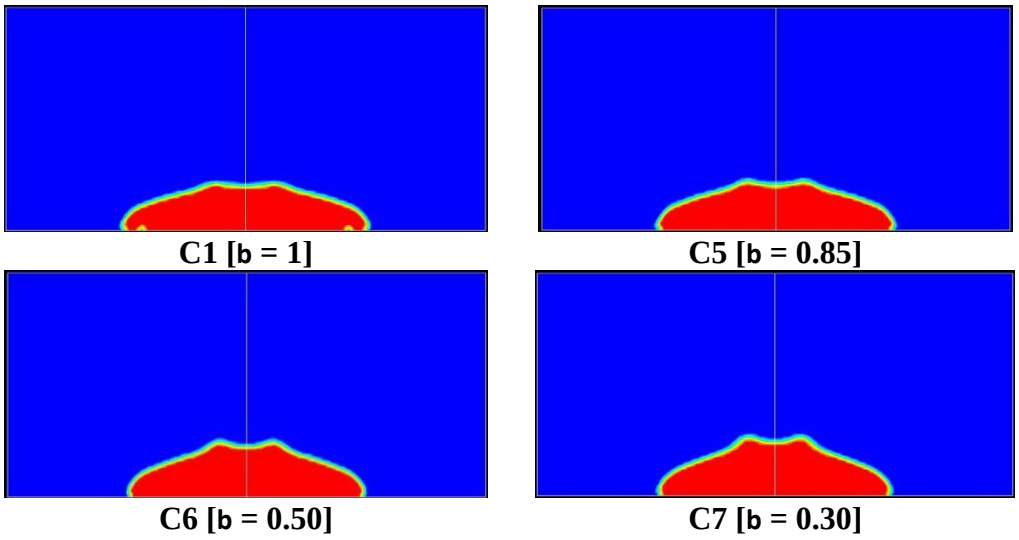

Figure A.6: Slump Cone Test Modeled by ANSYS Fluent for Decreasing b

APPENDIX B: ABAQUS RUNS

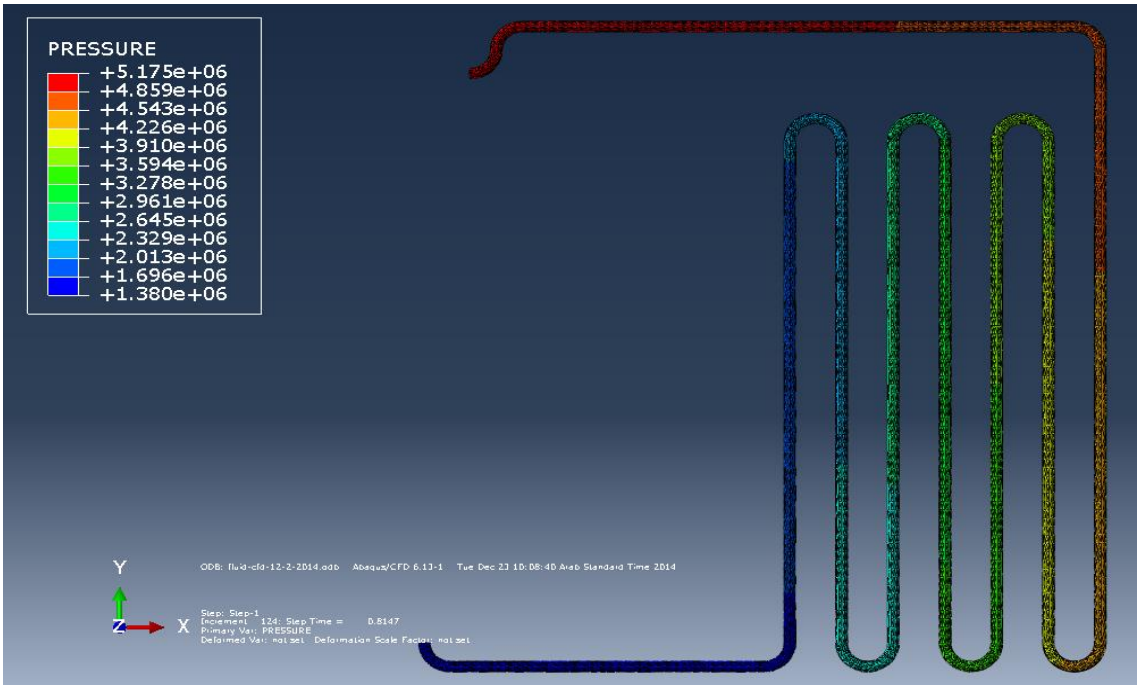

Figure B.1: Pressure Contour Obtained using ABAQUS for T1CO

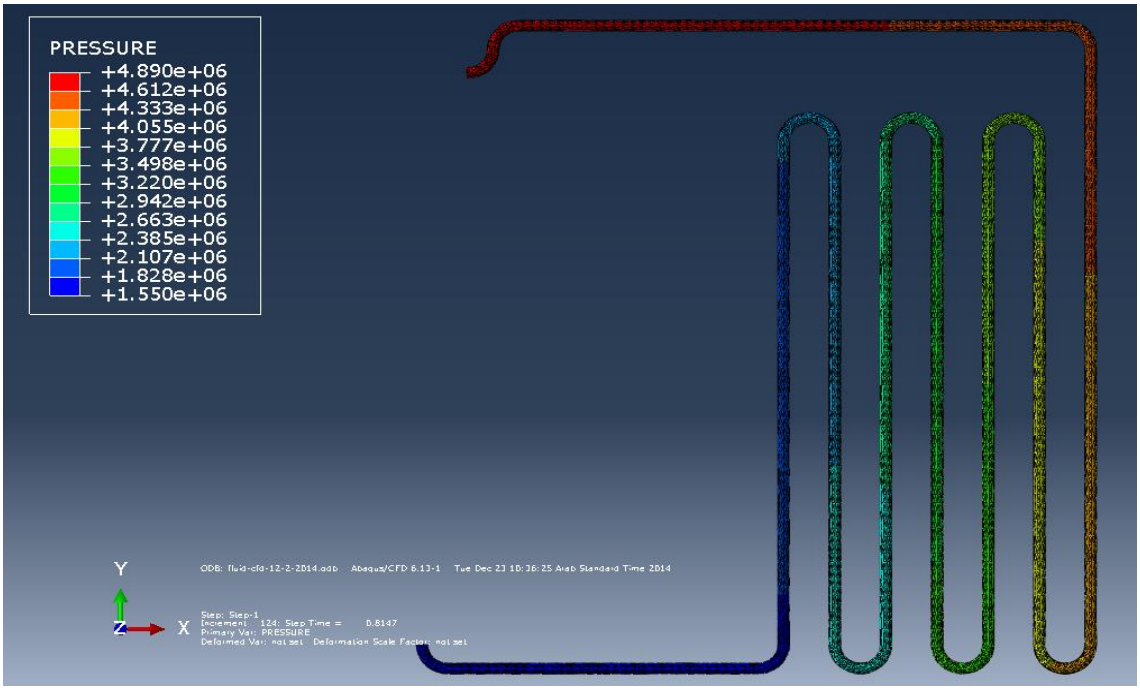

Figure B.2: Pressure Contour Obtained using ABAQUS for T1FA

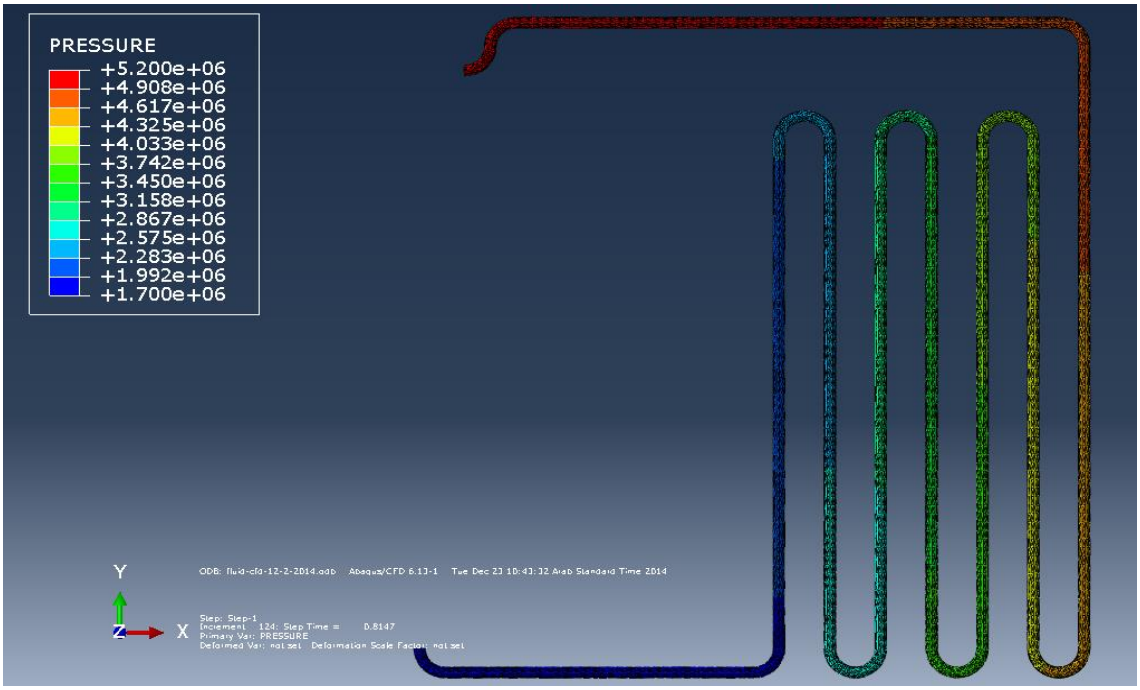

Figure B.3: Pressure Contour Obtained using ABAQUS for T1SF

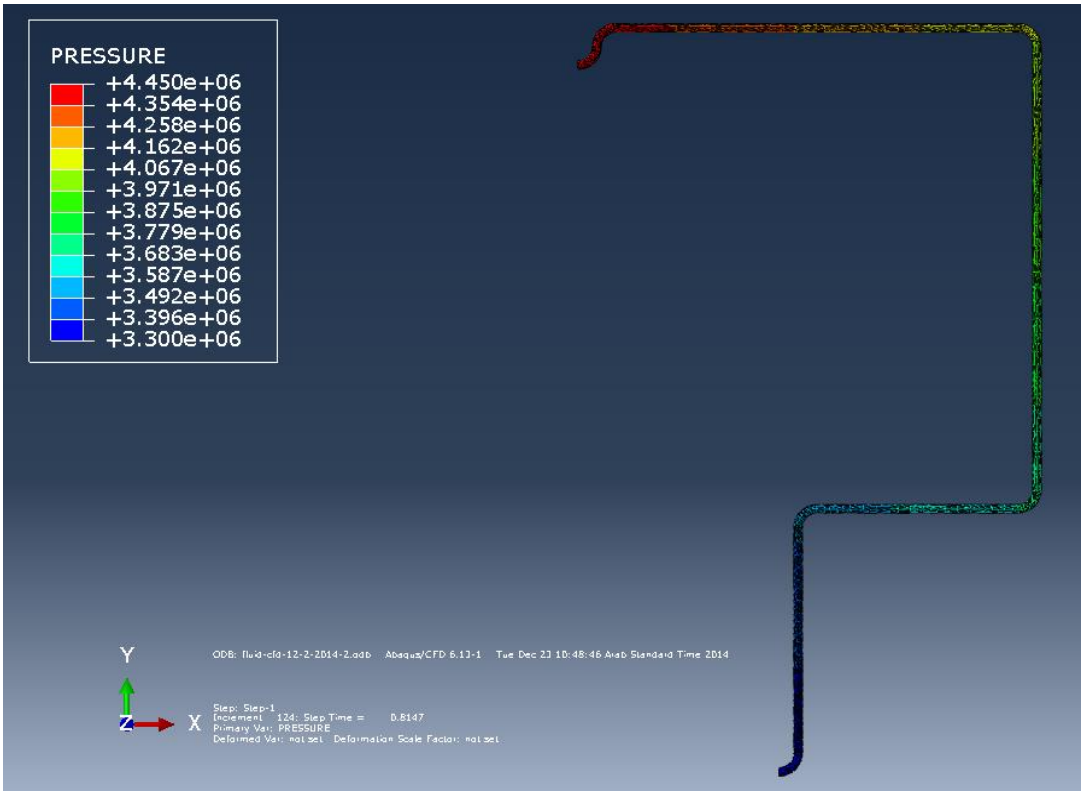

Figure B.4: Pressure Contour Obtained using ABAQUS for T2CO

Figure B.5: Pressure Contour Obtained using ABAQUS for T2FA

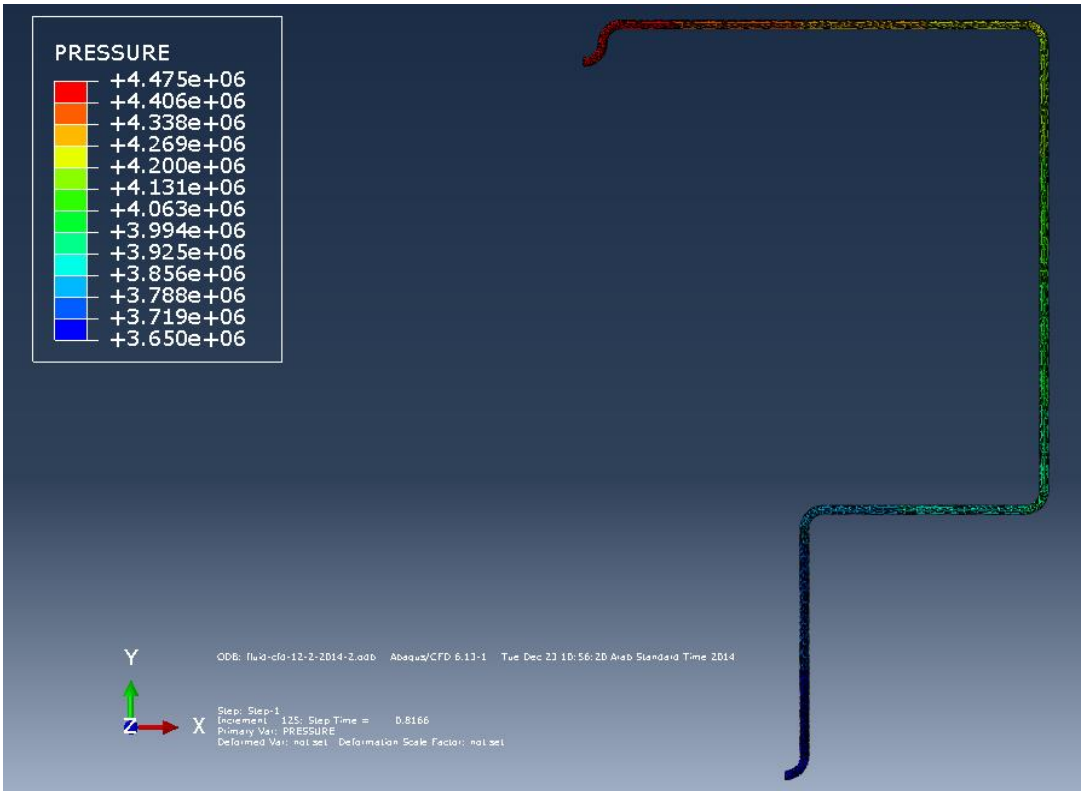

Figure B.6: Pressure Contour Obtained using ABAQUS for T2SF

APPENDIX C: EXCEL SHEET USED FOR THE ESTIMATION OF LUBRICATION PROPERTIES

V(r) No Plug (m/s)	V (r) Plug (m/s)		r (m)		
0.06275	0.000	0.000	0.06275	0.06275	62.75
0.06000	0.671	0.671	0.06000	0.06000	60.00
0.05725	1.312	0.671	0.05725	0.06000	57.25
0.05175	2.504	0.671	0.05175	0.06000	51.75
0.04625	3.576	0.671	0.04625	0.06000	46.25
0.04075	4.527	0.671	0.04075	0.06000	40.75
0.03525	5.358	0.671	0.03525	0.06000	35.25
0.02975	6.068	0.671	0.02975	0.06000	29.75
0.02425	6.658	0.671	0.02425	0.06000	24.25
0.01875	7.128	0.671	0.01875	0.06000	18.75
0.01325	7.478	0.671	0.01325	0.06000	13.25
0.00775	7.707	0.671	0.00775	0.06000	7.75
0.00225	7.816	0.671	0.00225	0.06000	2.25
0.00000	7.826	0.671	0.00000	0.06000	0.00
0.00225	7.816	0.671	-0.00225	0.06000	-2.25
0.00775	7.707	0.671	-0.00775	0.06000	-7.75
0.01325	7.478	0.671	-0.01325	0.06000	-13.25
0.01875	7.128	0.671	-0.01875	0.06000	-18.75
0.02425	6.658	0.671	-0.02425	0.06000	-24.25
0.02975	6.068	0.671	-0.02975	0.06000	-29.75
0.03525	5.358	0.671	-0.03525	0.06000	-35.25
0.04075	4.527	0.671	-0.04075	0.06000	-40.75
0.04625	3.576	0.671	-0.04625	0.06000	-46.25
0.05175	2.504	0.671	-0.05175	0.06000	-51.75
0.05725	1.312	0.671	-0.05725	0.06000	-57.25
0.06000	0.671	0.671	-0.06000	0.06000	-60.00
0.06275	0.000	0.000	-0.06275	0.06275	-62.75

dp/dx (Pa/m)	a (m)	τ_0 Pa	μ Pa.s	R_0 (mm)	LL (mm)
36600	0.06275	0.5	4.6	60.00	2.75
Q =	27.69	m³/r	=	7.69	l/s
V =	2238.44	m/hı	=	0.62	m/s
V = Graph				0.62	m/s
Q = Graph				7.69	l/s

$r < R_0$, hence r taken $r = R_0$

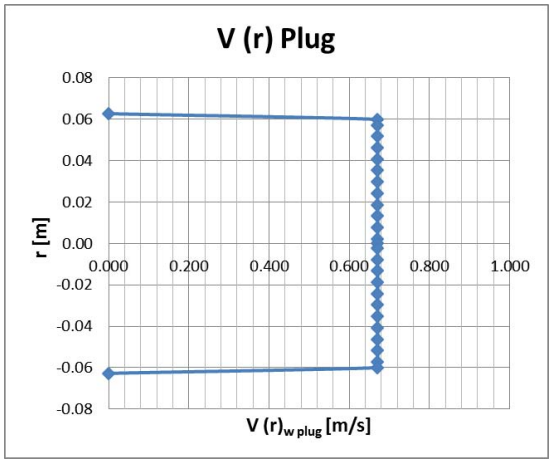

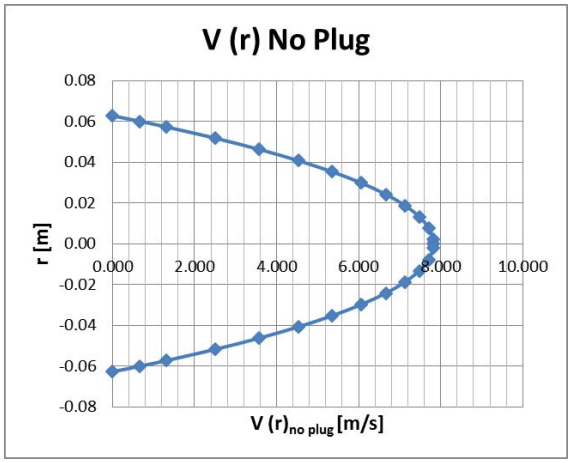

Figure C.1: Velocity Profile Assuming Plug Flow (Left) and No Plug Flow (Right)

VITAE

Name : Naeem Sohail Saleem Saleem

Nationality : Jordanian

Date of Birth : 11/07/1982

Email : Naeem.Saleem@Live.com

Address : Bandaria District, Al Khobar, Saudi Arabia

Academic Background :

PhD. in Civil Engineering (Structures)
King Fahd University for Petroleum and Minerals,
Dhahran, Saudi Arabia, **2015**
Thesis Title *"Modeling of Polymer-Based Self-Compacting Concrete Using Rheological Indexing"*

M.Sc. in Civil Engineering (Structures)
King Fahd University for Petroleum and Minerals,
Dhahran, Saudi Arabia, **2008**
Thesis Title *"Moisture Transport in Self-Sealing Concrete"*

B.Sc. in Civil Engineering (Structures)
University of Jordan,
Amman, Jordan, **2004**
Graduation Project *"Design of a Structural Steel Building"*

Publications :

Conference Papers:

N. S. Saleem, M. K. Rahman, and M. H. Baluch (2008), "*Moisture Transmissibility and Shrinkage of Waterproof Concretes".* Proceedings of Creep, Shrinkage and Durability Mechanics of Concrete and Concrete Structures (CONCREEP8), 793–798.

Baluch, M. H., Rahman, M. K., Mukhtar, F., Saleem, N., (2012). *"Finite Element Model for Predicting the Evolution of Formwork Pressure by Self Compacting Concrete"*. International Conference on Advanced Concrete Technology and its Applications (ACTA-2012), 6-7 November, Islamabad, Pakistan.

Saleem, N.S., Baluch, M. H., Rahman M. K., & Al-Osta, M. "*Formwork Pressure Exerted by Self-Compacting Concrete Made with Different Mineral Admixtures"*. The Fifth International Conference on Construction Materials: Performance, Innovations and Structural Implications, Canada (Conmat'15). (Accepted)

Presentations:

N. S. Saleem, I. A. Hussein, M. H. Baluch and M. K. Rahman, (2013), ***"Superplasticizers: State-of-The-Art ".*** The 9th International Concrete Conference and Exhibition, Bahrain, Feb 2013.